

Resource-Aware Hierarchical Federated Learning in Wireless Video Caching Networks

Md Ferdous Pervej, *Member, IEEE*, and Andreas F. Molisch, *Fellow, IEEE*

Abstract—Backhaul traffic congestion caused by the video traffic of a few popular files can be alleviated by storing the to-be-requested content at various levels in wireless video caching networks. Typically, content service providers (CSPs) own the content, and the users request their preferred content from the CSPs using their (wireless) internet service providers (ISPs). As these parties do not reveal their private information and business secrets, traditional techniques may not be readily used to predict the dynamic changes in users' future demands. Motivated by this, we propose a novel resource-aware hierarchical federated learning (RawHFL) solution for predicting user's future content requests. A practical data acquisition technique is used that allows the user to update its local training dataset based on its requested content. Besides, since networking and other computational resources are limited, considering that only a subset of the users participate in the model training, we derive the convergence bound of the proposed algorithm. Based on this bound, we minimize a weighted utility function for jointly configuring the controllable parameters to train the RawHFL energy efficiently under practical resource constraints. Our extensive simulation results validate the proposed algorithm's superiority, in terms of test accuracy and energy cost, over existing baselines.

Index Terms—Federated learning, resource-aware hierarchical federated learning, resource optimization, video caching.

I. INTRODUCTION

VIDEO streaming is the dominant source of data traffic in wireless networks: approximately 3 out of 5 video views are generated from wireless devices [2], accounting for some 70% of bits sent over the air. This traffic not only burdens the over-the-air transmission but also the backhaul: since the videos are owned by some content service providers (CSPs), e.g., YouTube, Netflix, Amazon Prime Video, HBO, Hulu, to name a few, and stored in the cloud servers used by the CSPs, the requested videos need to be obtained from the cloud by the (wireless) internet service provider (ISP) and transported over its backhaul in order to be delivered to the requester node. As such, continuous deliveries of the requested content can overwhelm the backhaul network due to large bandwidth requirements engendered by the combination of large data amount and latency constraints required for the quality of experience (QoE). These problems can be greatly mitigated by caching at (or near) the wireless edge [3], i.e., wireless networks can store the to-be-requested content at the base station (BS), reducing repetitive extractions and saving

considerable backhaul resources. Therefore, if the CSP and the ISP collaborate, they can design a practical solution to ameliorate the load for the backhaul.

Among many design parameters of a video caching network, two main elements are the content *placement* and *delivery* of the requested content [4]. Typically, the storage size required to store *all* content available from the CSPs far exceeds the capacity of a local cache. Consequently, it is critical to know the most likely to-be-requested content sets during the content placement phase. Unfortunately, determination of these to-be-requested content is challenging: they may deviate considerably from the most recently used ones and may also differ significantly from the global or even regional most-popular files. This is particularly true when the users have individual preferences and do not always request the most popular content. Thanks to machine learning (ML), such changes can be accurately captured by carefully designing the ML model and its training algorithm. Nonetheless, the need for large amounts of training data samples to accurately learn the ML model parameters remains a challenge.

Additionally, content caching becomes inevitably difficult due to the need to protect privacy and business secrets. In order to get the requested content from the CSP, the user must place the request using its serving BS. However, neither the user equipment (UE) nor the CSP wants to reveal the exact content ID to the serving BS: the UE as a matter of privacy, and the CSP because the user requests are business secrets that it does not disclose to the ISP, which often is a competitor. Conversely, while the UE can place an encrypted content request to the CSP via the serving BS, the BS does not wish to reveal the exact spatial information of the requester UE to the CSP, since that is *its* business secret. The above factors must be considered in designing any ML algorithm for wireless video caching networks. Fortunately, these challenges can be handled with federated learning (FL) [5], which enables distributed model training on users' devices, thus protecting the users' data privacy. While traditional FL follows a parameter server paradigm, where a central server (CS) coordinates the training process for the distributed clients¹, almost all practical wireless networks have hierarchical structures [6], [7]. Therefore, it is critical to devise an efficient hierarchical federated learning (HFL) considering the cooperation among the UE, ISP and CSP.

Part of this work was presented at the 2024 IEEE International Conference on Communications (ICC) [1].

This work was supported by NSF-IITP Project 2152646.

The authors are with the Ming Hsieh Department of Electrical and Computer Engineering, University of Southern California, Los Angeles, CA 90089 USA (e-mail: pervej@usc.edu; molisch@usc.edu).

¹A user is usually named by the terms *UE* and *client* in wireless networks and FL, respectively. We use these terms interchangeably in this paper.

A. State-of-the-Art

Content placement is widely investigated to maximize cache hit ratio (CHR) and/or minimize content delivery delay. Recently, Javedankherad *et al.* leveraged a weighted vertex graph coloring and a greedy algorithm for mobility-aware content placement to maximize the CHR [8]. Malak *et al.* optimized cache placement and transmission power to minimize transmission delays in multi-hop wireless heterogeneous networks [9]. Qian *et al.* first derived closed-form solutions for cache placement and transcoding, followed by designing trading contracts between a communication, caching and computing resource provider and mobile network operators in order to minimize personalized content delivery delay [10]. Considering users' long-term request patterns, Ning *et al.* jointly optimized cache placement and content recommendations in order to minimize content delivery costs [11]. While these studies show the benefits of content caching, dynamic changes in user preferences, leading to frequent changes in global/regional content popularity, still cause significant challenges in wireless video caching networks.

ML is widely used in literature [12]–[18] to apprehend the dynamic changes in content popularity. These works broadly fall into two ML domains, namely (1) supervised learning and (2) reinforcement learning (RL). In the supervised ML category, existing works [12]–[14] mainly used some variants of recurrent neural network (RNN) to predict future content popularity or cache placement. Besides, deep reinforcement learning (DRL) is also widely used [15]–[18] to learn long-term cache placement policy. However, these works mainly adopted a centralized ML strategy, considering training datasets are centrally available. This assumption differs in many practical cases where training data are only available to the end users who want to protect their data privacy.

Many recent studies [19]–[28] leveraged FL-based solutions for different content caching applications in order to protect users' data privacy. Qiang *et al.* proposed an adaptive FL-based proactive content caching solution [19], where two sets of DRL agents were used to learn two tasks: subset client selection and clients' local training rounds selection. They then leveraged FL to aggregate the models of these DRL agents. [20] also used two separate DRL agent sets — one at the user level for learning computation offloading policy and one at the edge server level for learning content placement policy — and applied federated aggregation of these DRL models. A similar strategy was also adopted by Wang *et al.*, where clients' mobility and preferences were first utilized to cluster the clients [21]. They then let each cluster head train a DRL model to learn the cache placement. In [22], users first learned their content preferences, followed by sharing their context information and learned preferences with their associated access points (APs). The APs then partitioned the users and derived popularity scores of the content that they leveraged to train stochastic variance reduced gradient models to predict the global content popularity. An attention-weighted FL algorithm was proposed by Li *et al.* for predicting content popularity in a device-to-device network, leveraging a similar user partitioning strategy based on mobility and social

behavior [23]. Khanal *et al.* also proposed a self-attention-based FL algorithm to predict cell-wise content popularity in vehicular networks [24].

Lin *et al.* proposed a proactive caching scheme using stacked autoencoders for global content popularity prediction [25]. Maale *et al.* considered a unmanned aerial vehicles (UAV)-assisted caching network [26], where popular content of the ground users was placed in the UAV's limited cache to ensure ground users' QoEs. Cao *et al.* proposed a similar mobility-aware content caching solution [27], where FL was used to predict users' trajectories and content popularity. These prediction results were then used to place the contents to minimize content delivery costs. Feng *et al.* also considered a similar approach [28], which first predicted the residence time of moving vehicles and then utilized that to predict content popularity in each BS.

It is worth noting that FL has many open problems (see [29] and the references therein). Efficient client sampling has recently emerged as one of the key solutions to resource constraints [30]–[32]. These works advocate for a subset of clients selection from the entire client pool in order to mitigate the straggler effect [33]. Owing to the limited resources in wireless communication, many recent works also suggest client scheduling based on the available resources of the clients and the BS that acts as the CS [34]–[37]. These works, however, deal with general wireless networks and do not consider a wireless video caching platform.

B. Our Contributions

While [12]–[18] showed ML improves caching performance, these centralized ML methods are not suitable due to privacy concerns. Besides, although some studies [19], [21]–[28] only considered users' data privacy, collaboration among the three entities involved, i.e., UE, BS and CSP, was not addressed. Furthermore, the above works do not consider sporadic content request patterns and the important fact that the users' training datasets are not readily available: they need to process their requested content's information to prepare their training datasets. Additionally, an HFL based solution is preferable due to the hierarchical architecture of practical networks. Moreover, while clients have limited computational power and energy resources, the ISP has limited radio resources. As such, coordination among these parties is needed to ensure an efficient video caching platform. Due to these reasons, we propose a novel resource-aware hierarchical federated learning (RawHFL) algorithm where the clients train their local model to predict their to-be-requested content. More specifically, our key contributions are summarized as follows:

- Considering a realistic multi-cell wireless network consisting of multiple BSs and clients, where clients request content from a CSP using encrypted tagged IDs, we leverage privacy-preserving collaboration among these three parties to bring an efficient FL solution for predicting users' to-be-requested content in wireless video caching networks.
- Due to resource scarcity, the proposed RawHFL only selects a subset of the clients for model training. Furthermore, acknowledging the well-known system and data

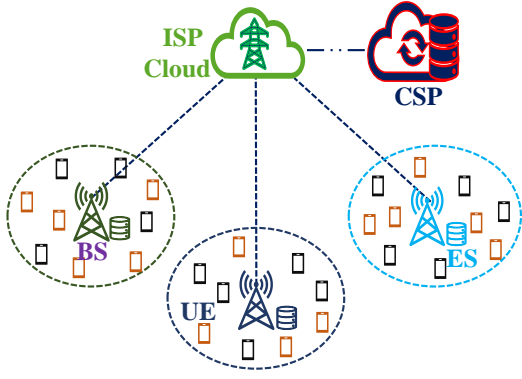


Fig. 1: Network system model: UEs are connected to their serving BSs, and these BSs are connected to their ISP cloud network, while the CSP has an agreement with the ISP that allows placing one edge server (ES) to each BS

heterogeneity, we derive RawHFL's convergence bound, which reveals that the global gradient norm depends on the successful reception of the selected clients' trained accumulated gradients and their local training rounds.

- To that end, we jointly optimize client selection and clients' (i) local training rounds, (ii) central processing unit (CPU) cycles and (iii) transmission power to minimize a weighted utility function that facilitates RawHFL's convergence and minimizes energy expense under delay, energy and radio resource constraints. As the original problem is non-convex, we transform it into a relaxed difference of convex programming problems and use a low-complexity iterative solution.
- Our extensive simulation results validate that the proposed solution outperforms existing baselines in terms of test accuracy and energy expense in a resource-constrained setting². Moreover, the proposed RawHFL performs nearly identically to the ideal case performance of hierarchical federated averaging (H-FedAvg) [38] in all examined scenarios.

The rest of the paper is organized as follows. Section II presents our system model, content request model and preliminaries of HFL. In Section III, we first summarize the proposed RawHFL and then present our detailed theoretical analysis. Besides, Section IV describes our joint problem formulation, followed by problem transformations and solutions. Section V presents our extensive simulation results, followed by the concluding remarks in Section VI. Moreover, Table I summarizes the important notations used in this paper.

II. SYSTEM MODEL

A. Network Model

This paper considers a video caching wireless network, where distributed UEs, denoted by $\mathcal{U} = \{u\}_{u=0}^{U-1}$, can request content

²Note that the predicted content information can be utilized to design content placement and evaluate other metrics, such as cache hit ratio, latency, revenue, etc., to name a few. However, the evaluation of such metrics depends on system parameters and is beyond the scope of this paper. These metrics are generally directly proportional to the prediction accuracy.

TABLE I: Summary of important variables

Parameter	Definitions
u, \mathcal{U}	User u , all user set
b, \mathcal{B}	base station b , all BS set
l, L	l^{th} SGD round, upper bound for local SGD round
e, E	e^{th} edge round, total edge round
k, K	k^{th} global round, total global round
t	t^{th} discrete slot at which UE may request content
$\mathcal{U}_b, \mathcal{U}_b^{k,e}$	BS b 's UE set; selected UE/client set of BS b during edge round e of global round k
$L_u^{k,e}$	UE/client u 's local SGD round during edge round e of global round k
g, G	Genre g ; total genres
$c_g, \mathcal{C}_g, \mathcal{C}$	c^{th} content of genre g ; all content set in genre g ; entire content catalog
$\bar{\mathcal{C}}_g, C$	Total content in genre g ; total content in the catalog
z, Z, \mathcal{Z}^e	z^{th} pRB; total pRBs; pRB set
$\mathcal{D}_{u,\text{raw}}^0$	UE u 's initial historical dataset
$p_{u,\text{ac}}$	UE u 's probability of being active (making a content request)
I_{u,c_g}^t	Binary indicator function that defines whether u requests content c_g during slot t
$p_{u,g}$	UE u 's preference to genre g
Υ	Dirichlet distribution's concentration parameter for the genre preference
$\mathcal{D}_{u,\text{proc}}^t, \mathcal{D}_{u,\text{proc}}^t$	UE u 's processed dataset; total samples in UE u 's processed dataset
$J_u(\cdot); f_b(\cdot), f(\cdot)$	UE u 's loss function; BS b 's loss function; global loss function
$\mathbf{w}_u^{k,e,l}, \mathbf{w}_b^{k,e}, \mathbf{w}^k$	UE/Client u 's local model during SGD round l of edge round e of global round k ; BS b 's edge model during edge round e of global round k ; global model during round k
$g_u(\mathbf{w}_u^{k,e,l})$	UE u 's gradient during l^{th} local round of e^{th} edge round of k^{th} global round
$\bar{g}_u^{k,e}$	UE u 's accumulated gradients during e^{th} edge round of k^{th} global round
η	Learning rate
α_u, α_b	UE u 's trained model/accumulated gradients' weight; BS b 's model/accumulated gradients' weight
$1_{u,sl}^{k,e}; P_{u,sl}^{k,e}$	Binary indicator function to define whether u is selected in edge round e of global round k ; success probability of $1_{u,sl}^{k,e}$
$t_{u,cp}^{k,e}; e_{u,cp}^{k,e}$	UE u 's local model training time and energy overheads during edge round e of global round k
$t_{u,up}^{k,e}; e_{u,up}^{k,e}$	UE u 's accumulated gradient offloading time and energy overheads during edge round e of global round k
t_{th}	Deadline threshold to finish one edge round
$P_{u,\text{tx}}^{k,e}; P_{u,\text{max}}$	Transmission power of u ; maximum allowable transmission power of u
$e_{u,\text{bud}}$	Energy budget of u for each edge round
$1_{u,sc}^{k,e}; P_{u,sc}^{k,e}$	Binary indicator function to define whether accumulated gradient of u is received by the BS; success probability of $1_{u,sc}^{k,e}$
$\phi; s$	Floating point precision; client's uplink payload size for the accumulated gradients
β	Smoothness of the loss function
σ^2	Bounded variance of the gradients
ε_0^2	Bounded divergence between the local and the edge loss functions
ε_1^2	Bounded divergence between the edge and the global loss functions
$\phi_b^{k,e}$	Utility function for the joint optimization problem

from a CSP using their serving BSs. Let us denote the BS set by $\mathcal{B} = \{b\}_{b=0}^{B-1}$ and the user set associated with BS b by \mathcal{U}_b . Besides, a UE is only associated with a single BS and $\mathcal{U} = \bigcup_{b=0}^{B-1} \mathcal{U}_b$. For simplicity, we assume that all BSs are operated and controlled by the same ISP. Denote the content catalog of the CSP by $\mathcal{C} = \{\mathcal{C}_g\}_{g=0}^{G-1}$, where $\mathcal{C}_g = \{c_g\}_{c=0}^{\bar{C}_g-1}$ represents the content set of genre g . Therefore, the content

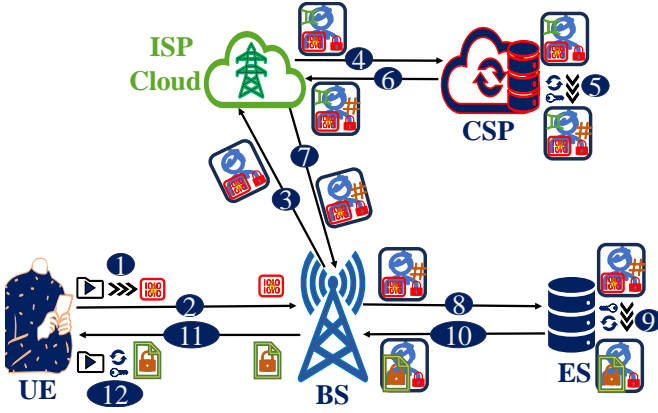


Fig. 2: Privacy protection in different nodes: (1) UE uses tag ID, (2) UE sends encrypted content request to the serving BS, (3) BS sends the encrypted content request to its cloud for charging/authentication, (4) ISP cloud sends encrypted content request information to CSP, (5) CSP decode actual content ID from the tagged ID, (6) CSP sends encrypted information for the ES to the ISP cloud, (7) ISP sends the encrypted information to serving BS, (8) serving BS forwards encrypted information to the ES, (9) ES decode the CSP's information, (10) ES sends encrypted video payload to serving BS, (11) BS sends the packet to the UE, and (12) UE decrypts the packet

catalog has a fixed set of $C = \sum_{g=0}^{G-1} \bar{C}_g$ content³. The CSP and the ISP have mutual agreements that enable the CSP to install one ES to every BS of the ISP. This lets the CSP leverage the ES' limited storage and computation power to devise an efficient FL-based caching solution. The considered system model is shown in Fig. 1. Furthermore, we assume that the CSP and the ISP are entirely different entities under two different business organizations and, therefore, always keep their operations secrets from each other. As such, the CSP neither reveals the information of the UE's requested content nor shares what content it stores in the ESs with the BSs. The UEs, on the other hand, know the exact content information and can place their content requests using encrypted temporal tag IDs via their associated BSs. Fig. 2 shows the privacy protection procedures at different nodes. Furthermore, the CSP can frequently change these encrypted tag IDs and their mapping with the original content to further enhance its operational secrets.

The network operates in discrete time slots, denoted by t , and the duration between two consecutive slots is κ seconds. The ISP dedicates \bar{Z} hertz (Hz) bandwidth to perform the FL training. More specifically, each BS of the ISP utilizes \bar{Z} Hz bandwidth, which they divide into Z orthogonal physical resource blocks (pRBs), for sharing the FL-related payloads with the participating UEs and the ESs. Denote the pRB set by $\mathcal{Z} = \{z\}_{z=0}^{Z-1}$. We assume that node association, radio resource allocations and channel state information (CSI) are known at the BS. Besides, the neighboring BSs can utilize \bar{Z} Hz bandwidth for the FL task from different portions of their en-

tire operating bandwidth to avoid inter-cell interference⁴ [39, Chap. 21]. Moreover, since orthogonal pRBs are used within each cell, there is no intra-tier interference. Furthermore, we consider that the wireless channel between the UE and the BS is dominated by large-scale fading since users are stationary in our system model, and practical networks can exploit enough diversity to mitigate small-scale fading. As such, we model the large-scale path loss and log-Normal shadowing following 3GPP's urban macro model [40, Section 7.4].

B. Content Request Model and Dataset Acquisition

1) *Content Request Model*: We assume that each UE's content request model follows two steps. Firstly, a UE may or may not request content during a slot t , depending on its need. Let $p_{u,ac}$ be the probability that the u^{th} UE makes a content request, which can also be interpreted as the *activity level* of the UE. In other words, the content request arrival is essentially modeled as a Bernoulli random variable with success probability $p_{u,ac}$, which is widely used in the literature [41]–[43]. Given that the UE is *active*, in the next step, we model *which* content it wants to request. To model this, we consider a popularity-preference tradeoff owing to the fact that both individual preference and global content popularity can influence the UE in choosing the content to request. In particular, we assume that each UE has a genre preference, denoted by $p_{u,g}$, such that $0 \leq p_{u,g} \leq 1$ and $\sum_{g=0}^{G-1} p_{u,g} = 1$. These genre preferences are modeled following a symmetric Dirichlet distribution $\text{Dir}(\Upsilon)$, where the Υ is the concentration parameter [34].

We assume that the UE requests the most popular content c_g from its preferred genre g when it makes the first content request. Let $1_{u,c_g}^t$ be a binary variable that takes value 1 if the UE requests content c_g in slot t and value 0 otherwise. In the subsequent content request, the UE can either exploit the most similar content⁵ from the same genre with probability v_u or explore the most popular content from a different genre, $g' \neq g$, with probability $(1 - v_u)$. It is worth noting that the genre preference $p_{u,g}$ does not influence $p_{u,ac}$ in the above content request model⁶.

2) *Dataset Acquisition Method*: We assume that each UE has a small initial historical raw dataset, denoted by $\mathcal{D}_{u,\text{raw}}^0$ that the client updates based on the information of its requested content. Following the above content request model, for $t > 0$, each UE updates its local raw dataset using the requested content's information as

$$\mathcal{D}_{u,\text{raw}}^t := \begin{cases} \mathcal{D}_{u,\text{raw}}^{t-1} \cup \{\mathbf{x}(1_{u,c_g}^t), y(1_{u,c_g}^t)\}, & \text{if } u \text{ is active,} \\ \mathcal{D}_{u,\text{raw}}^{t-1}, & \text{otherwise,} \end{cases} \quad (1)$$

where $\mathbf{x}(1_{u,c_g}^t)$ and $y(1_{u,c_g}^t)$ are the feature vector and label index of the requested content, respectively. Note that (1)

⁴If the BSs have to use the same portion of the bandwidth, they can coordinate and assign the pRBs in neighboring cells and/or use advanced beamforming techniques such as zero-forcing for interference-free communication.

⁵Each content has its own distinctive feature set that can be used to calculate its similarity with other content in the same genre.

⁶However, other content request strategies can also be easily incorporated, which will only change the clients' datasets. Our RawHFL solution is general, and our theoretical analysis in the sequel will still hold.

³While new content may arrive/generate at the CSP, given that the CSP has a limited storage capacity, following standard practice [26]–[28], we assume the number of content that the CSP can store remains fixed.

makes UE's dataset size time-varying and essentially captures natural data sensing methods in many practical applications [44], [45]. The UEs then process their local raw datasets acquired by (1) to train the ML model locally. Let us denote the processed dataset by $\mathcal{D}_{u,\text{proc}}^t = \{\mathbf{x}_u^a, y_u^a\}_{a=0}^{D_{u,\text{proc}}^t-1}$, where (\mathbf{x}_u^a, y_u^a) is the a^{th} (processed) training samples⁷, and $D_{u,\text{proc}}^t$ is the total training samples. Note that the probability that a UE is active, i.e., $p_{u,\text{ac}}$, directly governs its data acquisition policy in (1). Particularly, the UE receives a new training sample with probability $p_{u,\text{ac}}$. It is worth noting that while a larger $p_{u,\text{ac}}$ means the client has more training samples, the impact of $p_{u,\text{ac}}$ may not be directly measured in the theoretical analysis since all clients select n mini-batches (discussed in the sequel) from their respective datasets to perform the local model training.

C. Hierarchical Federated Learning: Preliminaries

In this paper, we consider that the CS, ESs, BSs and the distributed clients collaboratively train an ML model, parameterized by $\mathbf{w} \in \mathbb{R}^d$. The task is to predict the to-be-requested content of these UEs so that the video caching network can make the most out of the limited storage of the ESs⁸. We consider an HFL [38] framework consisting of two tiers: (1) client-ES and (2) ES-CS. The UEs/clients perform local rounds, while the ES and CS conduct *edge rounds* and *global rounds*, respectively. In each *local round*, the UEs train the ML model using their processed datasets $\mathcal{D}_{u,\text{proc}}^t$'s to minimize the following local loss function.

$$f_u(\mathbf{w}|\mathcal{D}_{u,\text{proc}}^t) := [1/D_{u,\text{proc}}^t] \sum_{(\mathbf{x}_u^a, y_u^a) \in \mathcal{D}_{u,\text{proc}}^t} l(\mathbf{w}|\mathbf{x}_u^a, y_u^a), \quad (2)$$

where $l(\mathbf{w}|\mathbf{x}_u^a, y_u^a)$ is the loss associated with the a^{th} data sample.

Besides, each ES minimizes the following loss function in each *edge round*.

$$f_b(\mathbf{w}|\mathcal{D}_b^t) := \sum_{u \in \mathcal{U}_b} \alpha_u f_u(\mathbf{w}|\mathcal{D}_{u,\text{proc}}^t), \quad (3)$$

where α_u is the weight of the u^{th} client in BS b and $\mathcal{D}_b^t := \bigcup_{u \in \mathcal{U}_b} \mathcal{D}_{u,\text{proc}}^t$. Note that we use the same notation b in the subscript to represent the ES of the b^{th} BS for brevity. Furthermore, the CS wants to minimize the following global loss function in each *global round*.

$$f(\mathbf{w}|\mathcal{D}^t) := \sum_{b=0}^{B-1} \alpha_b f_b(\mathbf{w}|\mathcal{D}_b^t), \quad (4)$$

where α_b is the weight of the ES of the b^{th} BS at the CS and $\mathcal{D}^t := \bigcup_{b=0}^{B-1} \mathcal{D}_b^t$. Recall that clients' datasets are not stationary and keep evolving following (1). Therefore, the global optimal model \mathbf{w}^* may not necessarily remain stationary [45]. The CS thus wants to find the optimal \mathbf{w}^* in each t as follows.

$$\mathbf{w}^* = \arg \min_{\mathbf{w}} f(\mathbf{w}|\mathcal{D}^t), \quad \forall t. \quad (5)$$

III. RESOURCE-AWARE HIERARCHICAL FEDERATED LEARNING: CONVERGENCE ANALYSIS

⁷The exact processing of the raw data samples shall depend on the application/simulation. More details are provided in the Section V.

⁸Our solution is general and can easily be extended for other tasks.

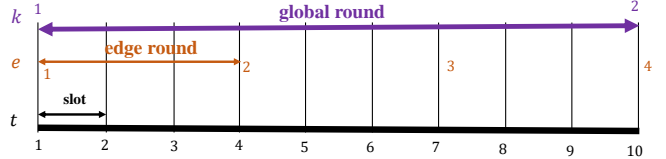


Fig. 3: Time flow in the proposed system model: each edge round can have multiple content request slots, while local training happens in between two consecutive edge rounds, and each global round consists of multiple edge rounds

A. Resource-Aware Hierarchical Federated Learning Model

The proposed RawHFL is designed on top of the general HFL [6], [7], [38] framework under explicit consideration of the available computational, radio and energy resources. In the proposed RawHFL, the clients perform local training that consists of taking multiple local stochastic gradient descent (SGD) steps within an edge round. Similarly, the ESs perform $E > 1$ edge rounds in each global round. Fig. 3 describes the flow of the local, edge, and global rounds. Besides, we consider a fully synchronous updating procedure at the upper tiers, i.e., in the ES and the CS, which leads to a deadline-constrained case. More specifically, this necessitates receiving the trained model parameters of the client at the ES during the ES' model update. Our proposed RawHFL has 6 key steps, which are summarized below.

Step 1 - Global Round k Initialization: At the beginning of each global round k , the CS broadcasts the latest available global model, denoted by \mathbf{w}^k , to all ESs via the ISP's infrastructure.

Step 2 - Edge Round e Initialization: Let us denote the edge round by e and the edge model of the b^{th} ES by $\mathbf{w}_b^{k,e}$. During the first edge round, i.e., $e = 0$, of every global round k , each ES synchronizes its edge model with the latest model received from the CS, i.e., $\mathbf{w}_b^{k,e} \leftarrow \mathbf{w}^k, \forall b \in \mathcal{B}$. Due to limited resources, RawHFL considers partial client participation by only selecting $\bar{\mathcal{U}}_b^{k,e} \subseteq \mathcal{U}_b$ clients for each ES (of each BS) in all edge rounds. It is worth noting that we assume the ESs and the BSs collaborate to optimize these subset client selections and selected clients' (1) local training rounds and (2) transmit powers jointly in the sequel. Let $1_{u,\text{sl}}^{k,e}$ denote client's participation during e^{th} edge round of the k^{th} global round, which is defined as

$$1_{u,\text{sl}}^{k,e} = \begin{cases} 1, & \text{with probability } p_{u,\text{sl}}^{k,e} \\ 0, & \text{otherwise,} \end{cases} \quad (6)$$

It is worth noting that the objective of each ES in RawHFL differs from (3) when $\bar{\mathcal{U}}_b^{k,e} \subset \mathcal{U}_b$. More specifically, each ES minimizes the following loss in RawHFL.

$$f_b(\mathbf{w}|\bigcup_{u \in \bar{\mathcal{U}}_b^{k,e}} \mathcal{D}_{u,\text{proc}}^t) := \sum_{u \in \bar{\mathcal{U}}_b^{k,e}} \alpha_u f_u(\mathbf{w}|\mathcal{D}_{u,\text{proc}}^t), \quad (7)$$

where $\sum_{u \in \bar{\mathcal{U}}_b^{k,e}} \alpha_u = 1$ and t is the time slot at which the e^{th} edge round starts. The ES then forwards its current local model to its BS, which broadcasts⁹ the model to the selected clients.

⁹Following existing literature [7], [34], [45], downlink communication overheads are ignored in this paper.

Step 3 - Local Model Training: Firstly, each $u \in \mathcal{U}_b^{k,e}$ synchronizes its local model as

$$\mathbf{w}_u^{k,e,0} \leftarrow \mathbf{w}_b^{k,e}. \quad (8)$$

The client then trains its local model $\mathbf{w}_u^{k,e,0}$ for $L_u^{k,e}$ SGD rounds to minimize the loss function defined in (2). As such, the local updated model is

$$\mathbf{w}_u^{k,e,L_u^{k,e}} = \mathbf{w}_u^{k,e,0} - \eta \sum_{l=0}^{L_u^{k,e}-1} g_u(\mathbf{w}_u^{k,e,l}), \quad (9)$$

where η is the learning rate and $g_u(\mathbf{w}_u^{k,e,l})$ is the stochastic gradient. Note that $1 \leq L_u^{k,e} \leq L$, where L is the maximum local SGD rounds. Besides, $L_u^{k,e}$ can be different for different clients because each client has a deadline of t_{th} seconds and an energy budget of $e_{u,bd}$ Joules during each edge round.

Note that, in each SGD step, we let each client randomly sample n mini-batches, which yields the following local computation time overhead

$$t_{u,cp}^{k,e} = L_u^{k,e} \times n \bar{n} c_u D_u / f_u^{k,e}, \quad (10)$$

where \bar{n} , c_u , D_u and $f_u^{k,e}$ are the batch size, number of CPU cycles to compute 1-bit data, data sample size in bits, and the CPU frequency. The corresponding energy expense is calculated as [7], [19], [45]

$$e_{u,cp}^{k,e} = L_u^{k,e} \times 0.5 \zeta n \bar{n} c_u D_u (f_u^{k,e})^2, \quad (11)$$

where 0.5ζ is the effective capacitance of the CPU chip.

Step 4 - Trained Accumulated Gradients Offloading: Once the local training is finished, each client sends its accumulated gradients $\tilde{g}_u^{k,e} := \sum_{l=0}^{L_u^{k,e}-1} g_u(\mathbf{w}_u^{k,e,l})$ to its associated BS as an encrypted payload. This uplink communication causes time and energy overheads for the clients. The required time to complete the uplink transmission is calculated as

$$t_{u,up}^{k,e} = s / (\omega \log_2 [1 + \gamma_u^{k,e}]), \quad (12)$$

where $s = d \times (\phi + 1)$ bits [34] is the payload size, ϕ is the floating point precision (FPP), ω is the bandwidth of a pRB and $\gamma_u^{k,e}$ is the signal-to-noise-ratio (SNR), which is derived as¹⁰

$$\gamma_u^{k,e} = \beta_u^{k,e} \zeta_u^{k,e} P_{u,tx}^{k,e} / (\omega \zeta^2), \quad (13)$$

where $P_{u,tx}^{k,e}$ is the uplink transmission power, $\beta_u^{k,e}$ is the large-scale path loss, $\zeta_u^{k,e}$ is the log-Normal shadowing and ζ^2 is the noise variance. Besides, we calculate the energy expense for the client's uplink transmission as

$$e_{u,up}^{k,e} = s P_{u,tx}^{k,e} / (\omega \log_2 [1 + \gamma_u^{k,e}]). \quad (14)$$

¹⁰The *small-scale* fading channel $h_u^{k,e}$ can also be accommodated in the SNR calculation by modifying (13) as $\gamma_u^{k,e} = \beta_u^{k,e} \zeta_u^{k,e} P_{u,tx}^{k,e} |h_u^{k,e}|^2 / (\omega \zeta^2)$. Moreover, when the CSI is imperfect, the UE can use a lower modulation and coding scheme (MCS) with proper automatic repeat request (ARQ) that may scale down the data rate.

Step 5 - Edge Round Completion and Aggregation: Once the BS receives client's $\tilde{g}_u^{k,e}$, it forwards the payload to its ES. Note that the overheads in forwarding the received $\tilde{g}_u^{k,e}$ to the ES are ignored since the ES is embedded in the same BS. When the deadline t_{th} expires, the ES aggregates the received gradients and updates its edge model as

$$\mathbf{w}_b^{k,e+1} = \mathbf{w}_b^{k,e} - \eta \sum_{u \in \mathcal{U}_b^{k,e}} \alpha_u [1_{u,sc}^{k,e} / P_{u,sc}^{k,e}] \tilde{g}_u^{k,e}, \quad (15)$$

where $\alpha_u := 1/|\mathcal{U}_b^{k,e}|$ and $1_{u,sc}^{k,e}$ is defined as

$$1_{u,sc}^{k,e} = \begin{cases} 1, & \text{with probability } p_{u,sc}^{k,e}, \\ 0, & \text{otherwise,} \end{cases} \quad (16)$$

We use $1_{u,sc}^{k,e}$ to capture whether $\tilde{g}_u^{k,e}$ is received by the BS successfully within the allowable deadline. It is worth noting that the client selection strategy can allow us to select similar computationally capable clients who can perform nearly identical local SGD rounds. Besides, we consider mini-batch SGD, and each client selects n mini-batches. As such, putting equal weight on the client's accumulated gradients is practical¹¹.

To that end, each ES checks whether they have completed E edge rounds, i.e., if $(e+1) = E$. If the ESs do not complete E edge rounds, they repeat **Step 2** to **Step 5**. Upon completing E edge rounds, each ES forwards its updated edge model to the CS¹² using the ISP's infrastructure.

Step 6 - Global Round Completion and Aggregation: Upon receiving the updated edge models, the CS performs global aggregation and updates the global model as

$$\mathbf{w}^{k+1} = \mathbf{w}^k - \eta \sum_{e=0}^{E-1} \sum_{b=0}^{B-1} \alpha_b \sum_{u \in \mathcal{U}_b^{k,e}} \alpha_u [1_{u,sc}^{k,e} / P_{u,sc}^{k,e}] \tilde{g}_u^{k,e}. \quad (17)$$

It is worth noting that the CS minimizes the following global loss function in our proposed RawHFL algorithm.

$$f(\mathbf{w}^k | \bigcup_{b=0}^{B-1} \bigcup_{u \in \mathcal{U}_b^{k,e}} \mathcal{D}_{u,proc}^t) := \sum_{b=0}^{B-1} \alpha_b f_b(\mathbf{w}^k | \bigcup_{u \in \mathcal{U}_b^{k,e}} \mathcal{D}_{u,proc}^t). \quad (18)$$

Step 1 to **Step 6** are repeated for K global rounds. These steps are summarized in Algorithm 1. Note that from hereon onward, we have used $f_u(\mathbf{w})$, $f_b(\mathbf{w})$ and $f(\mathbf{w})$ to represent $f_u(\mathbf{w} | \mathcal{D}_{u,proc}^t)$, $f_b(\mathbf{w} | \bigcup_{u \in \mathcal{U}_b^{k,e}} \mathcal{D}_{u,proc}^t)$ and $f(\mathbf{w} | \bigcup_{b=0}^{B-1} \bigcup_{u \in \mathcal{U}_b^{k,e}} \mathcal{D}_{u,proc}^t)$, respectively, for notational simplicity.

B. Convergence of RawHFL

We make the following assumptions for our theoretical analysis, which are standard in the literature [6], [7], [34], [45].

Assumption 1. β -smoothness: The loss functions in all nodes are β -smooth, i.e., $\|\nabla f(\mathbf{w}) - \nabla f(\mathbf{w}')\| \leq \beta \|\mathbf{w} - \mathbf{w}'\|$, where $\|\cdot\|$ is the L_2 norm.

Assumption 2. Unbiased SGD: mini-batch gradients are unbiased, i.e., $\mathbb{E}_{\xi \sim \mathcal{D}_{u,proc}} [g_u(\mathbf{w})] = \nabla f_u(\mathbf{w})$, where $\mathbb{E}[\cdot]$ is the expectation operator, and ξ is client's randomly sampled mini-batch.

¹¹Different weighting strategies can also be easily incorporated.

¹²The transmission between the ES and the CS happens in the network's backhaul, and the corresponding time and energy overheads incur on the ES and the BS. We kept our focus on the overheads for the clients and thus ignored these overheads.

Algorithm 1: RawHFL Algorithm

Input: Global model: \mathbf{w}^0 ; total global round K , number of edge rounds E

1 **for** $k = 0$ to $K - 1$ **do**

2 **for** $b = 1$ to B **in parallel do**

3 Receives updated global model $\mathbf{w}_b^{k,0} \leftarrow \mathbf{w}^k$

4 **for** $e = 0$ to $E - 1$ **do**

5 BS b receives optimized $l_{u,sl}^{k,e}, L_u^{k,e}$ and $f_u^{k,e}$

6 // c.f. (28)

7 **for** u in $\mathcal{Q}_b^{k,e}$ **in parallel do**

8 Get updated edge model $\mathbf{w}_u^{k,e,0} \leftarrow \mathbf{w}_b^{k,e}$

9 Perform $L_u^{k,e}$ mini-batch SGD rounds and get updated local model based on (9)

10 Offload accumulated gradients $g_u^{k,e}$ to the BS

11 **end**

12 Update edge model $\mathbf{w}_b^{k,e+1}$ using update rule in (15)

13 **end**

14 Update global model \mathbf{w}^{k+1} based on the update rule in (17)

15 **end**

Output: Trained global model \mathbf{w}^K

Assumption 3. Bounded variance: variance of the gradients is bounded, i.e., $\|g_u(\mathbf{w}) - \nabla f_u(\mathbf{w})\|^2 \leq \sigma^2$.

Assumption 4. Independence: a) the stochastic gradients are independent of each other in different episodes and b) accumulated gradient offloading is independent of client selection and each other in each edge round e .

Assumption 5. Bounded divergence: divergence between the a) local and edge and b) edge and global loss functions are bounded, i.e., for all u, b and \mathbf{w}

$$\sum_{u \in \mathcal{Q}_b^{k,e}} \alpha_u \|\nabla f_u(\mathbf{w}) - \nabla f_b(\mathbf{w})\|^2 \leq \varepsilon_0^2, \quad (19)$$

$$\sum_{b=0}^{B-1} \alpha_b \left\| \sum_{u \in \mathcal{Q}_b^{k,e}} \alpha_u \nabla \tilde{f}_u(\mathbf{w}) - \sum_{b'=0}^{B-1} \alpha_{b'} \sum_{u' \in \mathcal{Q}_{b'}^{k,e}} \alpha_{u'} \nabla \tilde{f}_{u'}(\mathbf{w}) \right\|^2 \leq \varepsilon_1^2, \quad (20)$$

where $\nabla \tilde{f}_u(\mathbf{w}) := \sum_{l=0}^{L_u^{k,e}-1} \nabla f_u(\mathbf{w})$.

Note that our proposed RawHFL algorithm acknowledges data and system heterogeneity. While partial client selection may handle the system heterogeneity, clients' data heterogeneity still exists¹³. Owing to these two types of heterogeneity, we derive the converge bound of the proposed RawHFL algorithm below.

Theorem 1. Suppose $\eta < \min \left\{ \frac{1}{2\sqrt{5}\beta L}, \frac{1}{\beta EL} \right\}$ and the above assumptions hold. Then, the average global gradient norm from K global rounds of RawHFL is upper-bounded as

$$\frac{1}{K} \sum_{k=0}^{K-1} \mathbb{E}[\|\nabla f(\mathbf{w}^k)\|^2] \leq \frac{2}{\eta K} \sum_{k=0}^{K-1} \frac{1}{\Omega^k} \left\{ \mathbb{E}[f(\mathbf{w}^k)] - \mathbb{E}[f(\mathbf{w}^{k+1})] \right\}$$

¹³Note that tackling heterogeneous data distributions requires special measures (see [46] and the references therein), which are beyond the scope of this paper.

$$+ \frac{2\beta\eta L\sigma^2}{K} \sum_{k=0}^{K-1} \frac{N_1^k}{\Omega^k} + \frac{18E\beta^2\varepsilon_0^2\eta^2L^3}{K} \sum_{k=0}^{K-1} \frac{N_2}{\Omega^k} + \frac{20L\beta^2\varepsilon_1^2\eta^2E^3}{K} \sum_{k=0}^{K-1} \frac{1}{\Omega^k} + \frac{2\beta\eta L}{K} \sum_{k=0}^{K-1} \frac{1}{\Omega^k} \sum_{e=0}^{E-1} \sum_{b=0}^{B-1} \alpha_b \times \sum_{u \in \mathcal{Q}_b^{k,e}} \alpha_u N_u \left[(1/p_{u,sc}^{k,e}) - 1 \right] \sum_{l=0}^{L_u^{k,e}-1} \mathbb{E}[\|g_u(\mathbf{w}_u^{k,e,l})\|^2], \quad (21)$$

where the expectations depend on clients' randomly selected mini-batches and $l_{u,sc}^{k,e}$'s. Besides, $\Omega^k := \sum_{e=0}^{E-1} \sum_{b=0}^{B-1} \alpha_b \sum_{u \in \mathcal{Q}_b^{k,e}} \alpha_u L_u^{k,e}$, $N_1^k := 60\beta^3\eta^3E^3L^3 + 3\beta\eta EL + \sum_{e=0}^{E-1} \sum_{b=0}^{B-1} \alpha_b (\alpha_b + 4EL\beta\eta) \sum_{u \in \mathcal{Q}_b^{k,e}} (\alpha_u)^2$, $N_2 := 1 + 20\beta^2\eta^2E^2L^2$ and $N_u := E + 3\beta\eta L + 4\beta\eta E (\alpha_u + 15E\beta^2\eta^2L^3)$.

Sketch of Proof. Using the aggregation rule defined in (17) and β -smoothness assumption, we start with

$$f(\mathbf{w}^{k+1}) \leq f(\mathbf{w}^k) - \eta \left\langle \nabla f(\mathbf{w}^k), \sum_{e=0}^{E-1} \sum_{b=0}^{B-1} \alpha_b \sum_{u \in \mathcal{Q}_b^{k,e}} \alpha_u \frac{1_{u,sc}^{k,e}}{p_{u,sc}^{k,e}} \sum_{l=0}^{L_u^{k,e}-1} g_u(\mathbf{w}_u^{k,e,l}) \right\rangle + \frac{\beta\eta^2}{2} \left\| \sum_{e=0}^{E-1} \sum_{b=0}^{B-1} \alpha_b \sum_{u \in \mathcal{Q}_b^{k,e}} \alpha_u \frac{1_{u,sc}^{k,e}}{p_{u,sc}^{k,e}} g_u^{k,e} \right\|^2, \quad (22)$$

where $\langle \mathbf{a}, \mathbf{b} \rangle$ is the inner product of the vectors \mathbf{a} and \mathbf{b} .

Then, we derive the upper bounds of the second and third terms. Plugging these results and assuming $\eta \leq \frac{1}{\beta EL}$, we get the following after doing some algebraic manipulations.

$$\frac{1}{K} \sum_{k=0}^{K-1} \mathbb{E} \left[\|\nabla f(\mathbf{w}^k)\|^2 \right] \leq \frac{2}{\eta K} \sum_{k=0}^{K-1} \left[\frac{\mathbb{E}[f(\mathbf{w}^k)] - \mathbb{E}[f(\mathbf{w}^{k+1})]}{\Omega^k} \right] + \frac{2\beta\eta\sigma^2}{K} \sum_{k=0}^{K-1} \left[\frac{\sum_{e=0}^{E-1} \sum_{b=0}^{B-1} (\alpha_b)^2 \sum_{u \in \mathcal{Q}_b^{k,e}} (\alpha_u)^2 L_u^{k,e}}{\Omega^k} \right] + \frac{2\beta\eta E}{K} \sum_{k=0}^{K-1} \frac{1}{\Omega^k} \sum_{e=0}^{E-1} \sum_{b=0}^{B-1} \alpha_b \sum_{u \in \mathcal{Q}_b^{k,e}} \alpha_u L_u^{k,e} \sum_{l=0}^{L_u^{k,e}-1} \left[\frac{1}{p_{u,sc}^{k,e}} - 1 \right] \times \mathbb{E}[\|g_u(\mathbf{w}_u^{k,e,l})\|^2] + \frac{2L\beta^2}{K} \sum_{k=0}^{K-1} \frac{1}{\Omega^k} \sum_{e=0}^{E-1} \sum_{b=0}^{B-1} \alpha_b \mathbb{E}[\|\mathbf{w}^k - \mathbf{w}_b^{k,e}\|^2] + \frac{2\beta^2}{K} \sum_{k=0}^{K-1} \frac{1}{\Omega^k} \sum_{e=0}^{E-1} \sum_{b=0}^{B-1} \alpha_b \sum_{u \in \mathcal{Q}_b^{k,e}} \alpha_u \sum_{l=0}^{L_u^{k,e}-1} \mathbb{E}[\|\mathbf{w}_b^{k,e} - \mathbf{w}_u^{k,e,l}\|^2]. \quad (23)$$

When learning rate $\eta \leq \min \left\{ \frac{1}{\beta EL}, \frac{1}{3\sqrt{2}\beta L} \right\}$, we can derive the difference between the client's model and the ES's model in (23) as

$$\frac{1}{K} \sum_{k=0}^{K-1} \frac{1}{\Omega^k} \sum_{e=0}^{E-1} \sum_{b=0}^{B-1} \alpha_b \sum_{u \in \mathcal{Q}_b^{k,e}} \alpha_u \sum_{l=0}^{L_u^{k,e}-1} \mathbb{E}[\|\mathbf{w}_b^{k,e} - \mathbf{w}_u^{k,e,l}\|^2] \leq \frac{3EL^2\eta^2\sigma^2K-1}{K} \sum_{k=0}^{K-1} \frac{1}{\Omega^k} + \frac{9E\varepsilon_0^2\eta^2L^3K-1}{K} \sum_{k=0}^{K-1} \frac{1}{\Omega^k} + \frac{3L^2\eta^2K-1}{K} \sum_{k=0}^{K-1} \frac{1}{\Omega^k} \times \sum_{e=0}^{E-1} \sum_{b=0}^{B-1} \alpha_b \sum_{u \in \mathcal{Q}_b^{k,e}} \alpha_u \left[\frac{1}{p_{u,sc}^{k,e}} - 1 \right] \sum_{l=0}^{L_u^{k,e}-1} \mathbb{E}[\|g_u(\mathbf{w}_u^{k,e,l})\|^2]. \quad (24)$$

Similarly, when $\eta < \min\left\{\frac{1}{2\sqrt{5}\beta L}, \frac{1}{\beta EL}\right\}$, we have

$$\begin{aligned}
& \frac{1}{K} \sum_{k=0}^{K-1} \frac{1}{\Omega^k} \sum_{e=0}^{E-1} \sum_{b=0}^{B-1} \alpha_b \mathbb{E} \left[\left\| \mathbf{w}^k - \mathbf{w}_b^{k,e} \right\|^2 \right] \\
& \leq \frac{4E\eta^2\sigma^2}{K} \sum_{k=0}^{K-1} \frac{1}{\Omega^k} \sum_{e=0}^{E-1} \sum_{b=0}^{B-1} \alpha_b \sum_{u \in \mathcal{U}_b^{k,e}} (\alpha_u)^2 L_u^{k,e} + \\
& \frac{60\beta^2\sigma^2 E^3 L^3 \eta^4}{K} \sum_{k=0}^{K-1} \frac{1}{\Omega^k} + \frac{180\beta^2 \varepsilon_0^2 E^3 L^4 \eta^4}{K} \sum_{k=0}^{K-1} \frac{1}{\Omega^k} + \\
& \frac{10\varepsilon_1^2 \eta^2 E^3}{K} \sum_{k=0}^{K-1} \frac{1}{\Omega^k} + \frac{4E\eta^2}{K} \sum_{k=0}^{K-1} \frac{1}{\Omega^k} \sum_{e=0}^{E-1} \sum_{b=0}^{B-1} \alpha_b \sum_{u \in \mathcal{U}_b^{k,e}} \alpha_u (\alpha_u + \\
& 15E\beta^2\eta^2 L^3) \left[\frac{1}{p_{u,sc}^{k,e}} - 1 \right] \sum_{l=0}^{L_u^{k,e}-1} \mathbb{E} \left[\left\| g_u(\mathbf{w}_u^{k,e,l}) \right\|^2 \right]. \quad (25)
\end{aligned}$$

Finally, we plug (24) and (25) into (23) to find the final bound in (21). The detailed proof is left to the supplementary material. ■

Remark 1. The first diminishing term with $\{\cdot\}$ on the right-hand side of (21) captures the change in the global loss function in two consecutive global rounds. The second term with σ^2 arises due to the bounded variance assumption of the stochastic gradients. The third term stems from the assumption that the divergence between the local loss function and ES' loss function due to statistical data heterogeneity is upper bounded by ε_0^2 . Similarly, the fourth term arises due to the bounded divergence assumption between the ES' loss function and the global loss function due to data heterogeneity. Moreover, the fifth term stems from the wireless links between the clients and their serving BSs.

Corollary 1. When all clients perform the same number of SGD rounds, i.e., $L_u^{k,e} = L$, $\forall u, k$ and e , the convergence bound in Theorem 1 boils down to

$$\begin{aligned}
& \frac{1}{K} \sum_{k=0}^{K-1} \mathbb{E} \left[\left\| \nabla f(\mathbf{w}^k) \right\|^2 \right] \leq \frac{2(\mathbb{E}[f(\mathbf{w}^0)] - \mathbb{E}[f(\mathbf{w}^K)])}{\eta EKL} + \\
& [2\beta\eta\sigma^2/(EK)] \sum_{k=0}^{K-1} N_1^k + 18\beta^2\varepsilon_0^2\eta^2 L^2 N_2 + 20\beta^2\varepsilon_1^2\eta^2 E^2 + \\
& \frac{2\beta\eta}{EK} \sum_{k=0}^{K-1} \sum_{e=0}^{E-1} \sum_{b=0}^{B-1} \alpha_b \sum_{u \in \mathcal{U}_b^{k,e}} \alpha_u N_u \sum_{l=0}^{L_u^{k,e}-1} \left[\frac{1}{p_{u,sc}^{k,e}} - 1 \right] \mathbb{E} \left[\left\| g_u(\mathbf{w}_u^{k,e,l}) \right\|^2 \right],
\end{aligned}$$

Moreover, when $p_{u,sc}^{k,e}$'s are 1's, i.e., all selected clients' accumulated gradients are received successfully, we have

$$\begin{aligned}
& \frac{1}{K} \sum_{k=0}^{K-1} \mathbb{E} \left[\left\| \nabla f(\mathbf{w}^k) \right\|^2 \right] \leq \frac{2(\mathbb{E}[f(\mathbf{w}^0)] - \mathbb{E}[f(\mathbf{w}^K)])}{\eta EKL} + \\
& \frac{2\beta\eta\sigma^2}{EK} \sum_{k=0}^{K-1} N_1^k + 18\beta^2\varepsilon_0^2\eta^2 L^2 N_2 + 20\beta^2\varepsilon_1^2\eta^2 E^2, \quad (26)
\end{aligned}$$

which is analogous to existing studies [6], [7].

Remark 2. The second, third and fourth terms of (26) have some constant terms that may not depend on the global round k . However, the learning rate η is typically significantly smaller than 1. Since these terms are multiplied by the higher-order terms of η , they are negligible. Therefore, the global

gradient may converge to a neighborhood of the optimal solution.

Remark 3 (Choice of the learning rate η). Based on the above analysis, we write the dominating terms of the bound from Corollary 1 as follows by further assuming $\mathcal{U}_b^{k,e} = \mathcal{U}_b$.

$$\varpi := \frac{2F^{inf}}{\eta EKL} + 2\beta\eta\sigma^2 \sum_{b=0}^{B-1} (\alpha_b)^2 \sum_{u \in \mathcal{U}_b} (\alpha_u)^2, \quad (27)$$

where $F^{inf} := \mathbb{E}[f(\mathbf{w}^0)] - \mathbb{E}[f(\mathbf{w}^K)]$. This indicates that the optimal learning rate $\eta^* = \sqrt{\frac{F^{inf}}{EKL \times \beta \sigma^2 \sum_{b=0}^{B-1} (\alpha_b)^2 \sum_{u \in \mathcal{U}_b} (\alpha_u)^2}}$. Besides, using equal weights and equal number of clients in each ES, i.e., $\alpha_u = \frac{1}{|\mathcal{U}_b|} = \frac{1}{U}$ and $\alpha_b = \frac{1}{B}$, we have $\eta^* = \sqrt{\frac{F^{inf}}{EKL \times \beta \sigma^2 \sum_{b=0}^{B-1} (\frac{1}{B})^2 \sum_{u \in \mathcal{U}_b} (\frac{1}{U})^2}} = \sqrt{\frac{BU}{EKL} \times \frac{F^{inf}}{\beta \sigma^2}}$. Plugging η^* into (27) gives the convergence rate $\mathcal{O}\left(\frac{1}{\sqrt{EKL \times BU}}\right)$, which indicates that we achieve linear speed-up with respect to the number of clients in all ESs when $T := EKL$ is sufficiently large. This is due to the fact that we need $\mathcal{O}\left(\frac{1}{\tilde{\varepsilon}^2 \times BU}\right)$ steps as opposed to $\mathcal{O}\left(\frac{1}{\tilde{\varepsilon}^2}\right)$ steps to achieve $\tilde{\varepsilon}$ accuracy with algorithms that have the convergence rates of $\mathcal{O}\left(\frac{1}{\sqrt{T \times BU}}\right)$ and $\mathcal{O}\left(\frac{1}{\sqrt{T}}\right)$, respectively.

Remark 4. From the above Theorem and Corollary, it is quite evident that the convergence bound depends on $\mathcal{U}_b^{k,e}$'s, Ω^k 's and $p_{u,sc}^{k,e}$'s. Besides, since the client's local loss function depends on the local dataset $\mathcal{D}_{u,proc}^l$ by definition, the theoretical bounds also rely on the evolution of the dataset, which is governed by the activation probability $p_{u,ac}$. However, given the fact that the servers have no control over the data distribution of the clients, we cannot govern clients' data acquisitions. As such, in the sequel, we optimize the intertwined FL and wireless networking parameters jointly in order to facilitate RawHFL's convergence.

IV. RAWHFL: JOINT PROBLEM FORMULATION AND SOLUTIONS

A. Joint Problem Formulation

Based on the theoretical analysis in Section III-B, we want to focus on the controllable terms of the convergence bound in (21), which are $\mathcal{U}_b^{k,e}$'s, Ω^k 's and $p_{u,sc}^{k,e}$'s, such that the average global gradient norm after K global rounds is minimized. Intuitively, some clients may have some predicaments in performing local model training due to multifarious factors, such as residing at the cell edge, poor wireless channel quality, limited energy budget and low computational resources, to name a few. Besides, while a large $L_u^{k,e}$ may increase Ω^k , which improves the convergence rate, this is more complex in a constrained wireless network for the following reasons. More SGD rounds mean more local training overheads, leaving less time and energy for the uplink transmission once the local training is over. Therefore, if the clients do not have sufficient time and energy left to transmit their trained accumulated gradients, the BS and, hence, the ES cannot utilize these clients' contributions in the edge model aggregation.

Moreover, if $p_{u,sc}^{k,e} = 0$, the last term of (21) can blow up, making the theoretical bound ∞ . As such, it is critical to jointly optimize client selection and clients' local SGD rounds, CPU frequencies and transmission powers to make the convergence rate faster.

Remark 5. *In order to minimize the right-hand side of (21), we need to optimize the controllable parameters for all edge rounds in every global round before RawHFL training begins. However, since the wireless links between the clients and the BSs vary and are unknown beforehand, it is impossible to know the optimal parameters for all edge rounds of all global rounds at the beginning of model training. Owing to these complexities, a myopic perspective is necessary to sub-optimally minimize the right-hand side of (21).*

Concretely, we want to optimize the controllable parameters in every edge round so that the weighted summation of the local SGD steps $L_u^{k,e}$'s of the selected clients in $\mathcal{U}_b^{k,e}$ is maximized. In other words, we want to maximize $\sum_{b=0}^{B-1} \alpha_b \sum_{u \in \mathcal{U}_b^{k,e}} \alpha_u L_u^{k,e} \equiv \sum_{b=0}^{B-1} \alpha_b \sum_{u \in \mathcal{U}_b^{k,e}} 1_u^{k,e} \cdot [\alpha_u L_u^{k,e}]$. To that end, each client transmits its accumulated gradients $\bar{g}_u^{k,e}$ as a single wireless packet. Besides, as modern wireless networks have countermeasures for packet loss¹⁴, we assume that the transmitted packet can be decoded error-free if received during the aggregation time. In particular, we define $p_{u,sc}^{k,e} = \Pr\{[t_{u,cp}^{k,e} + t_{u,up}^{k,e} \leq t_{th}]\}$, which is also a common practice in the literature [7], [47]. Then, we enforce $t_{u,cp}^{k,e} + t_{u,up}^{k,e} \leq t_{th}$ as a constraint to ensure $p_{u,sc}^{k,e} \approx 1$ so that the last term in (21) becomes 0. Moreover, from (10) and (12), it is evident that $p_{u,sc}^{k,e}$ depends on $L_u^{k,e}$, $f_u^{k,e}$ and $P_{u,tx}^{k,e}$. Due to these facts, we pose the following optimization problem that can be solved in each edge round to jointly configure the intertwined optimization variables.

$$\min_{\mathbf{1}_{sl}^{k,e}, \mathbf{1}_{b,sl}^{k,e}, \mathbf{f}^{k,e}, \mathbf{P}_{tx}^{k,e}} \quad \phi_b^{k,e} := \frac{1}{\sum_{b=0}^{B-1} \alpha_b \sum_{u \in \mathcal{U}_b^{k,e}} 1_{u,sl}^{k,e} \cdot [\alpha_u L_u^{k,e}]} \quad (28)$$

$$\text{s.t. } C_1: \quad 1_{u,sl}^{k,e} \in \{0, 1\}, \quad \forall u, k, e \quad (28a)$$

$$C_2: \quad \sum_{u \in \mathcal{U}_b} 1_{u,sl}^{k,e} = Z, \quad \forall b, k, e \quad (28b)$$

$$C_3: \quad \begin{cases} \left(\mathbf{1}_{b,sl}^{k,e} \right)^T \mathbf{1}_{b,sl}^{k,e-1} \leq \Psi, & \text{if } k=0 \text{ \& } 1 \leq e \leq E-1, \\ \left(\mathbf{1}_{b,sl}^{k,e} \right)^T \mathbf{1}_{b,sl}^{k-1, E-1} \leq \Psi, & \text{if } k \neq 0 \text{ \& } (e+1) = E, \end{cases} \quad (28c)$$

$$C_4: \quad 1 \leq L_u^{k,e} \leq L, \quad L_u^{k,e} \in \mathbb{Z}^+, \quad \forall u, k, e \quad (28d)$$

$$C_5: \quad f_u^{k,e} \leq f_{u,max}, \quad \forall u, k, e \quad (28e)$$

$$C_6: \quad 0 \leq P_{u,tx}^{k,e} \leq P_{u,max}, \quad \forall u, k, e \quad (28f)$$

$$C_7: \quad 1_{u,sl}^{k,e} \cdot [t_{u,cp}^{k,e} + t_{u,up}^{k,e}] \leq 1_{u,sl}^{k,e} \cdot t_{th}, \quad \forall u, k, e \quad (28g)$$

$$C_8: \quad 1_{u,sl}^{k,e} \cdot [e_{u,cp}^{k,e} + e_{u,up}^{k,e}] \leq 1_{u,sl}^{k,e} \cdot e_{u,bd}, \quad \forall u, k, e \quad (28h)$$

where $\mathbf{1}_{b,sl}^{k,e} = \{1_{u,sl}^{k,e}\}_{u \in \mathcal{U}_b}$, $\mathbf{1}_{sl}^{k,e} = \{\mathbf{1}_{b,sl}^{k,e}\}_{b=0}^{B-1}$, $\mathbf{L}^{k,e} = \{\{L_u^{k,e}\}_{u \in \mathcal{U}_b}\}_{b=0}^{B-1}$, $\mathbf{f}^{k,e} = \{\{f_u^{k,e}\}_{u \in \mathcal{U}_b}\}_{b=0}^{B-1}$, $\mathbf{P}_{tx}^{k,e} = \{\{P_{u,tx}^{k,e}\}_{u \in \mathcal{U}_b}\}_{b=0}^{B-1}$ and Ψ is a positive constant.

¹⁴Almost all practical wireless networks have cyclic redundancy check, error correction coding, and (hybrid) ARQ in place [39, Chap. 13].

Note that C_1 is the binary client selection constraint, while C_2 ensures only Z clients are selected in each BS. Besides, C_3 ensures that at least Ψ new clients are selected in two consecutive edge rounds. Furthermore, constraints C_4 , C_5 and C_6 confirm that the client selects its local iteration, CPU frequency and transmission power within the upper bounds, respectively. Finally, constraints C_7 and C_8 satisfy the deadline and energy constraints, respectively.

Remark 6. *The clients can share their $P_{u,max}$'s, $f_{u,max}$'s and $e_{u,bd}$'s with their associated BS. Then, the BSs can collaborate since they are under the same ISP, which allows the ISP to solve (28) centrally. Once the problem is solved, each BS can broadcast the optimized parameters to the selected clients. However, (28) is a binary mixed-integer non-linear optimization problem and is NP-hard. Therefore, in the following, we first transform this complex problem into a weighted utility minimization problem, followed by approximating the non-convex constraints and solving the transformed problem using an iterative solution. It is worth noting that as artificial intelligence (AI)/ML is deemed a potential solution to many problems in wireless communication (see [48] and the reference therein), problem (28) may also be solved using AI/ML. However, since the problem is NP-hard, an AI/ML-based solution may also only lead to a sub-optimal solution.*

B. Problem Transformations and Solution

Intuitively, one may equivalently choose $\phi_b^{k,e} := -\sum_{b=0}^{B-1} \alpha_b \sum_{u \in \mathcal{U}_b} 1_{u,sl}^{k,e} \cdot [\alpha_u L_u^{k,e}]$ as the objective function in (28), which should be minimized if the clients are selected to maximize the weighted summation of their $L_u^{k,e}$'s. However, neither the equivalent objective nor the original one in (28) seeks an energy-efficient solution, as the clients with the maximum possible $L_u^{k,e}$'s are likely to be selected with these two objective functions. Besides, it is practical to consider that clients may request new content only after watching the previously requested video content. As such, a new training sample may only be available at the client's local dataset after a while. Due to these factors, we consider that the interval between two edge rounds, i.e., t_{th} , is at least as long as the duration of the video. Therefore, we concentrate on the energy costs. More specifically, we revise $\phi_b^{k,e}$ to balance the weight between $L_u^{k,e}$'s and the corresponding energy expenses of the clients as

$$\phi_b^{k,e} := -\theta \sum_{b=0}^{B-1} \alpha_b \sum_{u \in \mathcal{U}_b} 1_{u,sl}^{k,e} \cdot [\alpha_u L_u^{k,e}] + (1-\theta) \sum_{b=0}^{B-1} \alpha_b \sum_{u \in \mathcal{U}_b} 1_{u,sl}^{k,e} \cdot [\alpha_u e_{u,tot}^{k,e}], \quad (29)$$

where $e_{u,tot}^{k,e} = e_{u,cp}^{k,e} + e_{u,up}^{k,e}$ and $\theta \in [0, 1]$.

Since the problem is still non-convex and NP-hard, we introduce relaxations that allow the problem to be solved more efficiently. At first, we drop the integer constraint on $L_u^{k,e}$. Let $\bar{L}_u^{k,e} := 1_{u,sl}^{k,e} \cdot L_u^{k,e}$ be a new variable. Then, we introduce the following constraints to replace the multiplication of the binary and continuous variables.

$$1 \cdot 1_{u,sl}^{k,e} \leq \bar{L}_u^{k,e} \leq L \cdot 1_{u,sl}^{k,e}; \quad 0 \leq \bar{L}_u^{k,e} \leq L. \quad (30)$$

$$1 \cdot (1 - 1_{u,sl}^{k,e}) \leq L_u^{k,e} - \bar{L}_u^{k,e} \leq L \cdot (1 - 1_{u,sl}^{k,e}). \quad (31)$$

$$\bar{L}_u^{k,e} \leq L_u^{k,e} + (1 - 1_{u,sl}^{k,e})L. \quad (32)$$

After this, we equivalently transform the binary client selection constraint as

$$\sum_{b=0}^{B-1} \sum_{u \in \mathcal{U}_b} 1_{u,sl}^{k,e} - \sum_{b=0}^{B-1} \sum_{u \in \mathcal{U}_b} (1_{u,sl}^{k,e})^2 \leq 0, \quad (33)$$

$$0 \leq 1_{u,sl}^{k,e} \leq 1. \quad (34)$$

We then use (33) in objective function (29) to add a penalty when the client selection decision is not 0 or 1 as

$$\begin{aligned} \bar{\phi}_b^{k,e} := & -\beta \sum_{b=0}^{B-1} \alpha_b \sum_{u \in \mathcal{U}_b} \alpha_u \bar{L}_u^{k,e} + (1 - \beta) \sum_{b=0}^{B-1} \alpha_b \sum_{u \in \mathcal{U}_b} \alpha_u [\bar{e}_{u,cp}^{k,e} + \\ & \bar{e}_{u,up}^{k,e}] + \rho \left(\sum_{b=0}^{B-1} \sum_{u \in \mathcal{U}_b} 1_{u,sl}^{k,e} - \sum_{b=0}^{B-1} \sum_{u \in \mathcal{U}_b} (1_{u,sl}^{k,e})^2 \right), \end{aligned} \quad (35)$$

where $\bar{e}_{u,cp}^{k,e} = \bar{L}_u^{k,e} \times 0.5 \zeta \text{nnc}_u D_u (f_u^{k,e})^2$, $\bar{e}_{u,up}^{k,e} = s P_{u,tx}^{k,e} 1_{u,sl}^{k,e} / (\omega \log_2 [1 + \gamma_u^{k,e}])$ and $\rho > 0$ is a positive constant. However, the last quadratic term in (35) is still a problem and is thus approximated using a first-order Taylor series, resulting in the following modified objective function.

$$\begin{aligned} \bar{\phi}_b^{k,e} := & -\beta \sum_{b=0}^{B-1} \alpha_b \sum_{u \in \mathcal{U}_b} \alpha_u \bar{L}_u^{k,e} + (1 - \beta) \sum_{b=0}^{B-1} \alpha_b \sum_{u \in \mathcal{U}_b} \alpha_u [\bar{e}_{u,cp}^{k,e} + \bar{e}_{u,up}^{k,e}] + \\ & \rho \left(\sum_{b=0}^{B-1} \sum_{u \in \mathcal{U}_b} [1 - 2 \cdot 1_{u,sl}^{k,e,(i)}] 1_{u,sl}^{k,e} + \sum_{b=0}^{B-1} \sum_{u \in \mathcal{U}_b} (1_{u,sl}^{k,e,(i)})^2 \right), \end{aligned} \quad (36)$$

where $\bar{e}_{u,cp}^{k,e} = \zeta \text{nnc}_u D_u f_u^{k,e,(i)} [0.5 f_u^{k,e,(i)} \bar{L}_u^{k,e} + \bar{L}_u^{k,e,(i)} f_u^{k,e} - f_u^{k,e,(i)} \bar{L}_u^{k,e,(i)}]$ and $1_{u,sl}^{k,e,(i)}$, $\bar{L}_u^{k,e,(i)}$ and $f_u^{k,e,(i)}$ are some initial feasible points.

We now turn the focus on the non-convex constraints. First, we approximate the energy requirement for the accumulated gradient offloading as

$$\begin{aligned} \bar{e}_{u,up}^{k,e} \approx & \frac{s \log(2)}{\omega} \left[P_{u,tx}^{k,e,(i)} 1_{u,sl}^{k,e} / \log \left[1 + \frac{\beta_u^{k,e} \zeta_u^{k,e} P_{u,tx}^{k,e,(i)}}{\omega \zeta^2} \right] + \right. \\ & \left. 1_{u,sl}^{k,e,(i)} \log \left[1 + \frac{\beta_u^{k,e} \zeta_u^{k,e} P_{u,tx}^{k,e,(i)}}{\omega \zeta^2} \right] - \frac{\beta_u^{k,e} \zeta_u^{k,e} P_{u,tx}^{k,e,(i)} 1_{u,sl}^{k,e,(i)}}{\omega \zeta^2 + \beta_u^{k,e} \zeta_u^{k,e} P_{u,tx}^{k,e,(i)}} \right] \times \\ & \frac{\left(\log \left[1 + \frac{\beta_u^{k,e} \zeta_u^{k,e} P_{u,tx}^{k,e,(i)}}{\omega \zeta^2} \right] \right)^2}{\left(P_{u,tx}^{k,e} - P_{u,tx}^{k,e,(i)} \right)} := \bar{e}_{u,up}^{k,e} \end{aligned} \quad (37)$$

Similarly, we approximate the non-convex local computation time as

$$\bar{t}_{u,cp}^{k,e} \approx [\text{nnc}_u D_u / f_u^{k,e,(i)}] (\bar{L}_u^{k,e,(i)} - \bar{L}_u^{k,e,(i)} f_u^{k,e} / f_u^{k,e,(i)} + \bar{L}_u^{k,e}), \quad (38)$$

Furthermore, the non-convex offloading time constraint is approximated as follows:

$$\begin{aligned} \bar{t}_{u,up}^{k,e} := & 1_{u,sl}^{k,e} \cdot s / \left(\omega \log_2 \left[1 + \frac{\beta_u^{k,e} \zeta_u^{k,e} P_{u,tx}^{k,e}}{\omega \zeta^2} \right] \right) \\ \approx & \frac{s \log(2)}{\omega} \left[1_{u,sl}^{k,e} / \log \left[1 + \frac{\beta_u^{k,e} \zeta_u^{k,e} P_{u,tx}^{k,e,(i)}}{\omega \zeta^2} \right] - \right. \\ & \left. \frac{1_{u,sl}^{k,e,(i)} \beta_u^{k,e} \zeta_u^{k,e}}{\left(\omega \zeta^2 + \beta_u^{k,e} \zeta_u^{k,e} P_{u,tx}^{k,e,(i)} \right)} \left(\log \left[1 + \frac{\beta_u^{k,e} \zeta_u^{k,e} P_{u,tx}^{k,e,(i)}}{\omega \zeta^2} \right] \right)^2 \times \right. \end{aligned}$$

Algorithm 2: Iterative Solution for (40)

Input: Initial points $1_{u,sl}^{k,e,(i)}$, $\bar{L}_u^{k,e,(i)}$, $L_u^{k,e,(i)}$, $f_u^{k,e,(i)}$, s , $P_{u,tx}^{k,e,(i)}$, s , $i = 0$, total iteration I , precision level $\bar{\epsilon}$ and ρ

2 Repeat:

3 $i \leftarrow i + 1$

4 Solve (40) using $1_{u,sl}^{k,e,(i-1)}$, $L_u^{k,e,(i-1)}$, $\bar{L}_u^{k,e,(i-1)}$, $f_u^{k,e,(i-1)}$, s , $P_{u,tx}^{k,e,(i-1)}$, s and ρ , and get optimized $1_{u,sl}^{k,e}$, $L_u^{k,e}$, $\bar{L}_u^{k,e}$, s , $f_u^{k,e}$, s and $P_{u,tx}^{k,e}$, s

5 $1_{u,sl}^{k,e,(i)} \leftarrow 1_{u,sl}^{k,e}$, $L_u^{k,e,(i)} \leftarrow L_u^{k,e}$, $\bar{L}_u^{k,e,(i)} \leftarrow \bar{L}_u^{k,e}$, $f_u^{k,e,(i)} \leftarrow f_u^{k,e}$; $P_{u,tx}^{k,e,(i)} \leftarrow P_{u,tx}^{k,e}$

6 Until converge with precision $\bar{\epsilon}$ or $i = I$

Output: Optimal $1_{u,sl}^{k,e}$, $L_u^{k,e}$, $\bar{L}_u^{k,e}$, s , $f_u^{k,e}$, s and $P_{u,tx}^{k,e}$, s

$$\left(P_{u,tx}^{k,e} - P_{u,tx}^{k,e,(i)} \right) := \bar{t}_{u,up}^{k,e} \quad (39)$$

To that end, we pose the transformed problem as

$$\min_{1_{u,sl}^{k,e}, \bar{L}_u^{k,e}, L_u^{k,e}, f_u^{k,e}, P_{u,tx}^{k,e}} \bar{\phi}_b^{k,e} \quad (40)$$

$$\text{s.t.} \quad 0 \leq 1_{u,sl}^{k,e} \leq 1, \quad \forall u, k, e \quad (40a)$$

$$C_2, C_3, 1 \leq L_u^{k,e} \leq L, \quad (30), (31), (32), C_5, C_6 \quad (40b)$$

$$\bar{t}_{u,cp}^{k,e} + \bar{t}_{u,up}^{k,e} \leq 1_{u,sl}^{k,e} \cdot t_{th}, \quad \forall u, k, e \quad (40c)$$

$$\bar{e}_{u,cp}^{k,e} + \bar{e}_{u,up}^{k,e} \leq 1_{u,sl}^{k,e} \cdot e_{u,bd}, \quad \forall u, k, e \quad (40d)$$

where the constraints are similar as in (28).

This transformed problem (40) now belongs to the class of ‘‘difference of convex programming’’ problems. Starting with some initial feasible points, we can iteratively solve the problem using existing tools such as CVX [49]. In particular, we use Algorithm 2 to solve this problem. Note that the above iterative solution is well known to converge to a local stationary point of the original problem in polynomial time [50]. Problem (40) has $5U$ decision variables and $(2B + 12U)$ constraints. As such, the worst-case time complexity of running Algorithm 2 for I iterations is $\mathcal{O}(I \times 125U^3 [12U + 2B])$ [34]. It is worth noting that while the proposed algorithm yields a sub-optimal solution, the empirical performance of the proposed RawHFL is nearly identical to the performance of the ideal case H-FedAvg [38].

V. SIMULATION RESULTS AND DISCUSSIONS

A. Simulation Setting

We perform extensive simulations with different parameter settings to show the performance of the proposed solution. We consider a total $B = 4$ BSs, each serving $|\mathcal{U}_b| = 12$ UEs with a coverage radius of 400 meters, as shown in Fig. 4. Therefore, there are total $U = 48$ clients. The ISP’s carrier frequency is 2.4 GHz. The pRB size is $\omega = 3 \times 180$ kHz, while we vary the number of pRBs based on $|\mathcal{Z}_b^{k,e}|$ ’s. We model the path loss and line-of-sight probabilities following the 3GPP urban macro model [40, Section 7.4]. Besides, $G = 8$, $\bar{C}_g = 32$, $\forall g$, $C = 256$, $I = 50$, $\rho = 1$, $\theta = 0.4$, $\phi = 32$ [7], $\zeta = 2 \times 10^{-28}$ [38] and $\kappa = t_{th} = 150$ seconds. The c_u ’s, $f_{u,max}$ ’s, $e_{u,bd}$ ’s and

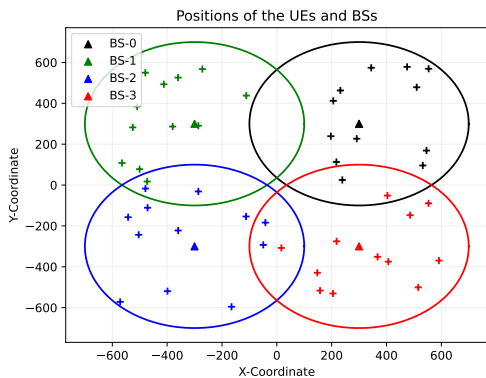


Fig. 4: Locations of the UEs and BSs in one realization

$P_{u,\max}$'s are uniformly randomly drawn from $[25, 40]$ cycles, $[1.2, 2.0]$ GHz, $[0.8, 1.5]$ Joules and $[20, 30]$ dBm, respectively. Furthermore, we uniformly randomly select the activity levels $p_{u,\text{ac}}$'s and the probability of exploiting similar content in the same genre v_u 's from $[0.2, 0.8]$ and $[0.1, 0.8]$, respectively. Moreover, for the genre preferences $p_{u,g}$'s, we use $\text{Dir}(\mathbf{0.3})$.

To our best knowledge, there exists no extensive real-world video-caching-related dataset containing spatial and temporal information about the users and their requested content set that is suitable for RawHFL. As such, we use the procedures described in Section II-B to let the UEs make content requests and acquire their (synthetic) dataset. Given that the UE requests content c_g during slot t , the extracted features for this content, i.e., $\mathbf{x}(1_{u,c_g}^t)$ contains the following information:

$\left\{ v_u, \{p_{u,g}\}_{g=0}^{G-1}, \frac{g}{G}, \mathbf{sim}(c_g), \frac{c_g}{C_g} \right\}$, where $\mathbf{sim}(c_g)$ is a vector of *cosine* similarities between the features of the requested content c_g and the features of the rest of the content in genre g . Besides, the label $y(1_{u,c_g}^t)$ is the index of the requested content ID¹⁵.

We use a simple fully connected (FC) neural network¹⁶ with rectified linear (ReLU) activation functions. More specifically, the model has the following architecture: $\text{FC}(\text{input_shape}, 512) \rightarrow \text{ReLU}() \rightarrow \text{FC}(512, 256) \rightarrow \text{ReLU}() \rightarrow \text{FC}(256, \text{output_shape})$. This model has $d = 219648$ trainable parameters in our implementation, which makes the wireless payload size $s = 7248384$ bits. Moreover, a sliding window technique is used to prepare the processed datasets $\mathcal{D}_{u,\text{proc}}^t$'s for model training. Particularly, we consider that each client processes its raw dataset such that the *previous* slot's requested content's feature set and the *current* slot's requested content ID are used as the feature and label, respectively. The clients use batch size $\bar{n} = 32$, $n = 10$ mini-batches, at max $L = 50$ local rounds and SGD optimizer with a learning rate of 0.01 for model training. Besides, cross-entropy loss function¹⁷ is used for model training. The accuracy is determined by calculating the fraction of total correctly predicted labels over the total

¹⁵The number of labels equals the number of total files. We can stack the files from each genre one after another to prepare the label indices.

¹⁶Our proposed RawHFL solution is general. Other ML models, e.g., RNNs or transformers, can also be used.

¹⁷<https://pytorch.org/docs/stable/generated/torch.nn.CrossEntropyLoss.html>

labels. Furthermore, we use $E = 4$ edge rounds in every global round and train for a total of $K = 100$ global rounds¹⁸.

Finally, as the clients are randomly dropped, and their system configurations are generated randomly, we completely repeat our simulations 10 times in order to get an average performance. In the following, unless mentioned otherwise, the average performance from these 10 trials is reported. It is worth noting that although the wireless channel between a client and the serving BS can vary significantly, the choice of the ISP's pRB size should generally impact the accumulated gradient offloading time when the model has a large number of trainable parameters. As such, the CSP and ISP should collaborate to choose the model size and pRB size accordingly in order to facilitate the FL process in video caching networks under deadline and resource constraints.

B. Performance Analysis

In a resource-constrained environment, client selection is necessary due to the following factors. Firstly, the wireless network has limited radio resources. In many cases, $Z < |\mathcal{U}_b|$ is realistic as a practical network has many other tasks to perform simultaneously. Secondly, since wireless channels vary, some clients may have poor link quality that can prolong the accumulated gradient offloading. Thirdly, some clients may not have sufficient energy budgets to offload their accumulated gradients. Finally, depending on the system configurations, some clients may need extended time to complete the local training even though the link quality is good. As such, appropriate client selection based on the available resources is essential. Moreover, since we have a constrained environment, some clients may not even be eligible to participate in model training when their required time and/or energy overheads are beyond their budgets.

We observe a similar trend in our simulation results. In Fig. 5a, we show the eligible clients, i.e., the clients who can perform at least one local SGD round, for $K = 100$ global rounds in 1 of the 10 simulation runs. Recall that client selection happens in each edge round, and each global round has $E = 4$ edge rounds, leading to a total 4×100 edge rounds in Fig. 5a. As expected, some clients are only eligible to be selected in a few edge rounds. For example, client 11 is eligible to be selected only in 28 edge rounds. Moreover, we plotted the client selection frequency with our proposed solution of (40) in Fig. 5b for different $|\mathcal{U}_b|$'s. It is worth pointing out that since Algorithm 2 yields a sub-optimal solution, the client selection strategies may not be optimal. Our results in Fig. 5b validate that Algorithm 2 finds the subset client set (and other decision variables) to minimize the objective function to satisfy all constraints. As such, in the following, we utilize Algorithm 2 and report the average performance of the 10 simulation repeats.

Now, we investigate how the convergence performance of RawHFL varies with different $|\mathcal{U}_b^{k,e}|$'s. Intuitively, the number of available training data should affect the model performance.

¹⁸We only performed computer simulations, which were run on our HPC cluster (<https://www.carc.usc.edu/>) with different 32 gigabytes RAM and GPU-enabled compute nodes.

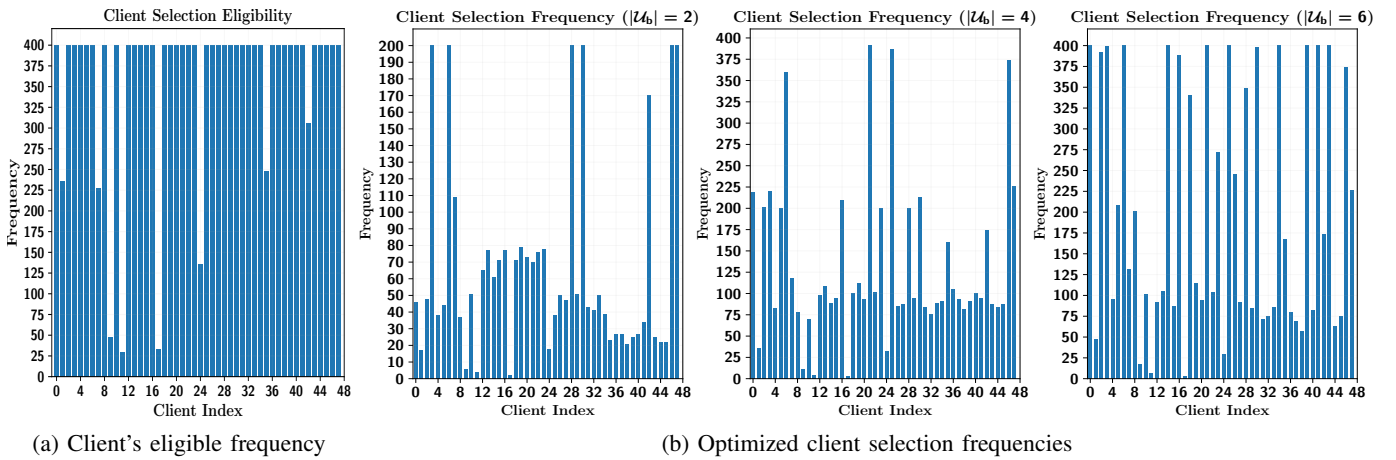


Fig. 5: Clients' participation eligibility and number of selections in 400 edge rounds

When only a few clients are selected, the model is trained on the few samples of these clients. This can be detrimental if appropriate clients are not selected, especially when data heterogeneity is severe. As such, RawHFL may require more training to achieve a certain level of accuracy when $|\mathcal{U}_b^{k,e}|$ is small. Moreover, a client's content request probability from the same genre, v_u , determines how frequently the client requests similar content from the same genre. A high v_u means less exploration, i.e., more exploitation from the same genre. As such, a high v_u is expected to yield better prediction performance since the client has fewer variations in its content requests.

Our simulation results also show similar trends in Figs. 6a - 6c. Note that these test results are the average of all clients' individual test datasets. We observe that the value of v_u governs the test accuracy and test loss. For example, when all clients randomly select their respective v_u from 0.1 to 0.8, the test accuracy after $K = 100$ global rounds is around 45%. When all clients have the same v_u , in Fig. 6b and Fig. 6c, we also observe that a large v_u leads to faster convergence. Moreover, the test loss and test accuracy performances improve when $|\mathcal{U}_b^{k,e}|$ increases regardless of the value of v_u 's. For example, with $|\mathcal{U}_b^{k,e}| = 2$, the test accuracy fluctuates, even for $v_u = 0.7$. However, the test accuracy reaches a plateau after about $K = 14$ global rounds with $|\mathcal{U}_b| \geq 4$ selected clients per BS when $v_u = 0.7$.

However, while more clients, i.e., large $|\mathcal{U}_b^{k,e}|$, may help RawHFL converge faster, that comes with higher bandwidth and energy overheads. On the one hand, the ISP will require more pRBs to schedule the clients for wireless transmission. On the other hand, the total energy cost per edge round also increases since more clients participate in the training process. However, regardless of the number of participating clients, the per-client energy cost in each edge round can be non-trivial. More specifically, when $|\mathcal{U}_b^{k,e}|$ increases, (40) must choose the defined number of clients so that the utility function is minimized. In doing so, it may select some clients with higher energy expenses that can be a byproduct of poor wireless links. However, the total energy costs per client can still be similar due to varying wireless links, different local SGD rounds and

sub-optimal solutions of (40) in different edge rounds. Our simulation results in Fig. 7 and Fig. 8 also validate these claims. Note that Fig. 7 shows the cumulative distribution function (CDF) of the total energy expenses per BS during each edge round e for different client set sizes. Besides, Fig. 8 shows the CDF of per client total energy expense during each edge round for different $|\mathcal{U}_b|$'s. For example, the probability of total energy expense of 50% of BSs are more than 3.7 Joules, 7.1 Joules, and 10.3 Joules for $|\mathcal{U}_b^{k,e}| = 2$, $|\mathcal{U}_b^{k,e}| = 4$ and $|\mathcal{U}_b^{k,e}| = 6$, respectively. Moreover, per client energy expense per edge round is quite similar in Fig. 8.

C. Performance Comparisons

To the best of our knowledge, no previous studies exactly considered our system design and used HFL for video caching. Therefore, we use the traditional H-FedAvg algorithm [38] and modify it to accommodate our system model for comparison. We consider two modifications. The first one calculates the smallest SGD rounds that all clients can perform without violating any constraints. We call this modified baseline H-FedAvg-M1. There are few clients who cannot even perform a single SGD round. These clients are dropped, and then the minimum SGD rounds that the retained clients can all perform without violating any constraints are calculated in the second modification. We call this baseline H-FedAvg-M2. Furthermore, we also consider the ideal case, where no constraints are enforced. This one is termed H-FedAvg-UB and is indeed the upper bound of H-FedAvg [38]. Finally, we also consider the traditional single server-based FL, namely, federated averaging (FedAvg) [5]. Concretely, in this baseline, the BSs merely act as relays between the central server and the clients. That is in every global round, the clients receive the same global model from the central server via their respective serving BSs. Upon finishing the local SGD steps, the clients offload the accumulated gradients to the central server via their serving BSs. Similar to H-FedAvg-UB, we do not enforce any constraints in this baseline, and this baseline is termed as FedAvg-UB. Note that these baselines require $Z = |\mathcal{U}_b|$ pRBs for clients' gradient sharing. Besides, FedAvg-UB causes $s \times |\mathcal{U}_b|$ bits payloads in the BS-CS backhaul in

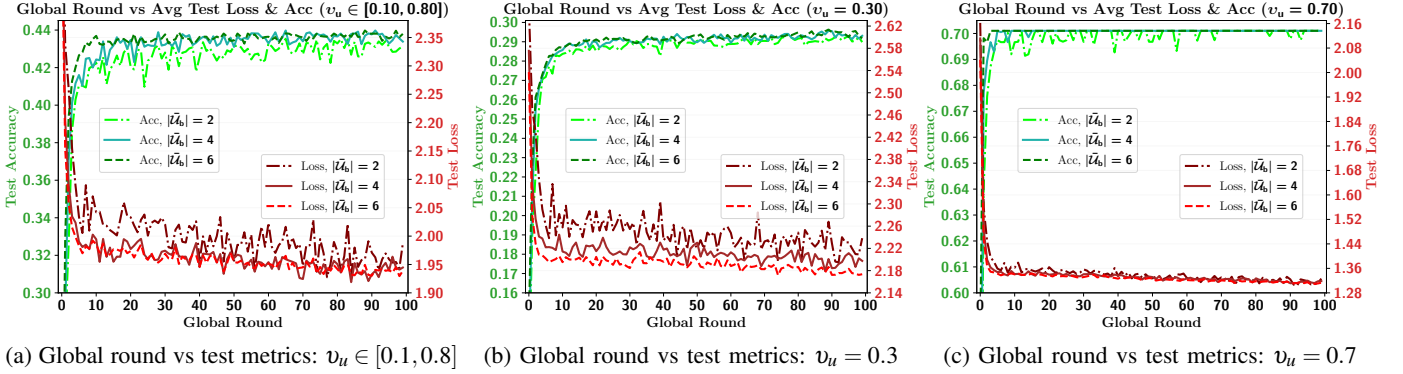


Fig. 6: Global round vs. test accuracy and test loss in RawHFL

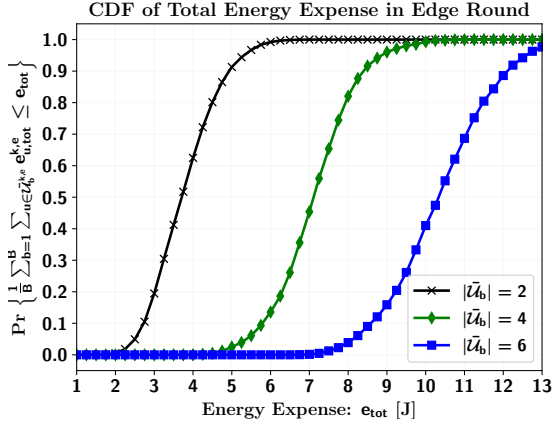


Fig. 7: CDF of total energy expense in the BS

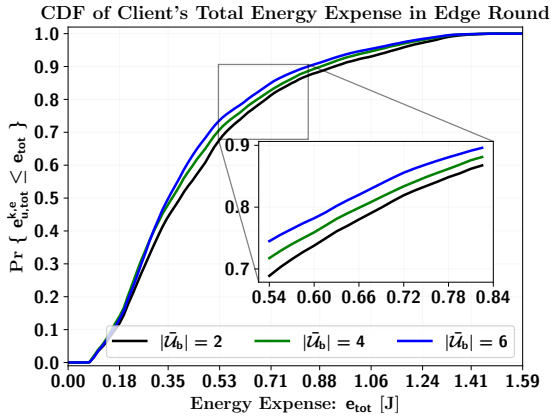


Fig. 8: CDF of client's total energy expense

every global round. Note that the HFL algorithm has only s bits of payload for the BS-CS backhaul.

H-FedAvg should work poorly in constrained cases, since some clients may be unable to participate in the training process due to time or energy overheads beyond the allowable budgets. This is particularly an impediment for the H-FedAvg-M1 baseline, as all clients are required to train the same number of local SGD rounds. Therefore, if any clients fail to participate in model training during an edge round, we discard performing model training during that edge round. This extreme case is alleviated in the H-FedAvg-M2

baseline, where we first drop the stragglers. As such, it is expected that H-FedAvg-M1 will perform poorly compared to the H-FedAvg-M2 baseline. Furthermore, the H-FedAvg-UB baseline should provide the best possible performance, as all clients would train their local models for the maximum allowable number of SGD rounds in a perfect environment. Moreover, FedAvg-UB is expected to take additional rounds to catch up on the performance of H-FedAvg-UB since it does not have any intermediate edge aggregations. However, in reality, the corresponding energy overheads can be much higher than some clients' energy budgets, which we ignore to obtain the upper-bounded performances of FedAvg-UB and H-FedAvg-UB. Compared to these baselines, the proposed RawHFL selects a subset of the clients and minimizes the energy expense, since our joint objective function is designed as the weighted combination of energy expense and total local iterations of the clients.

Our simulation results in Fig. 9 also reflect these trends. More specifically, we observe that the test accuracies of H-FedAvg baselines in the constrained case lag significantly compared to the H-FedAvg-UB. Besides, H-FedAvg-M1 and H-FedAvg-M2 baselines do not reach a plateau even after $K = 100$ global rounds. The FedAvg-UB baseline, on the other hand, reaches the H-FedAvg-UB's test accuracy after around 60 global rounds. Furthermore, the proposed RawHFL—with $|\mathcal{L}_b^{k,e}| = 4$ clients selected per BS—performs nearly identically to the H-FedAvg-UB baselines in terms of test accuracy. However, it is evident that the proposed RawHFL requires significantly lower energy to finish $K = 100$ global rounds. Particularly, the energy expense grows linearly as the global round increases with significantly steep slopes for the H-FedAvg-M2 and H-FedAvg-UB baselines. Besides, it is expected that H-FedAvg-M1 has the lowest energy expense since there are many stragglers due to extreme resource constraints that lead to no model training in many edge rounds. Furthermore, the energy expense of FedAvg-UB is also significantly lower than the H-FedAvg-UB since FedAvg-UB does not have any edge aggregations. However, recall that the FedAvg-UB causes additional communication burdens for the BS-CS backhaul. For example, when $K = 50$, the test accuracies of H-FedAvg-M1, H-FedAvg-M1, H-FedAvg-UB, FedAvg-UB and RawHFL are about 7.3%, 17.3%, 44.55%, 44.55% and 44.30%, respectively, with energy overheads of 283, 6845, 8439, 2109 and

TABLE II: Performance comparison: $K=400$, $E=4$, $t_{th}=150$ s, $v_u=0.3$

FL Algorithm	Test Accuracy	Energy Expense [J]
RawHFL- $ \mathcal{Z}_b =2$	0.2994 ± 0.0143	1508.33 ± 205.47
RawHFL- $ \mathcal{Z}_b =4$	0.2998 ± 0.0146	2848.16 ± 273.85
RawHFL- $ \mathcal{Z}_b =6$	0.2991 ± 0.0155	4137.94 ± 401.28
Central-SGD	0.3947 ± 0.0856	N/A
H-FedAvg-M1	0.0663 ± 0.0352	490.23 ± 1391.70
H-FedAvg-M2	0.1591 ± 0.0906	11226.51 ± 413.97
H-FedAvg-UB [38]	0.2977 ± 0.0161	13836.46 ± 519.91
FedAvg-UB [5]	0.2964 ± 0.0170	3455.56 ± 131.95
Top-Popular	0.0978 ± 0.0395	N/A

1741 Joules. Moreover, the proposed RawHFL delivers nearly identical test accuracy as of the H-FedAvg-UB after $K=100$ global rounds with about 4.85 times lower energy overheads of H-FedAvg-UB.

We now also compare the results with centralized SGD and naive popularity-based Top-popular baselines. Note that in centralized SGD, we assume all datasets are available centrally to show the performance gap with RawHFL. In particular, we consider the Top- M accuracy metric, which we define as the probability that the true requested content is within the Top- M predicted content. Intuitively, the Top- M accuracy should improve with the increase of M , as the actual requested content has a higher chance of being one of the Top- M predicted content. Moreover, while the FL algorithms are expected to exhibit the performances as observed in the above discussions, the centralized SGD is the ideal performance since the ML model gets exposed to the datasets of all clients. Furthermore, since the clients request content following a popularity-preference tradeoff, the Top-Popular baseline is expected to perform worse.

Our simulation results in Fig. 10 also validate the above claims. Note that the solid lines show the mean Top- M accuracy while the shaded areas show the standard deviations of the test accuracies across all $U=48$ clients in Fig. 10. Particularly, our solution yields about 36.94%, 25.67% and 35.69% higher (Top-1) test accuracies than H-FedAvg-M1, H-FedAvg-M2 and Top-Popular baselines, respectively. Besides, RawHFL, H-FedAvg-UB and FedAvg-UB have nearly identical test accuracies for all M 's. Furthermore, centralized SGD has about 6.95% higher (Top-1) test accuracy than RawHFL. Moreover, for $M \leq 7$, we see the superior performance of the centralized SGD as expected. The RawHFL, H-FedAvg-UB and FedAvg-UB baselines can catch up with the performance of the centralized SGD when $M \geq 8$. The results also reveal that the actual content is almost surely within the Top-8 predicted contents, which can significantly help in designing the cache placement. Moreover, for all M 's, the other H-FedAvg baselines perform poorly as those are not suitable for a resource-constrained environment. Finally, naive popularity-based prediction does not work since the content requests are modeled following an exploration-exploitation tradeoff.

To that end, we examine how these baselines perform for different v_u . As such, we list the test accuracy and energy expense of these baselines in Tables II - IV. These results reveal that while RawHFL achieves nearly identical test accuracies

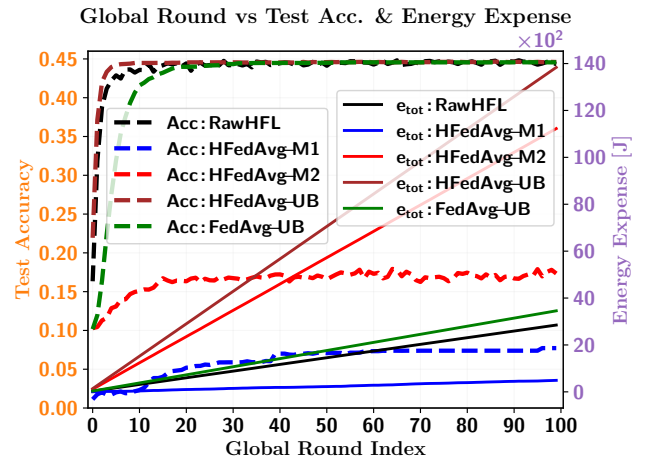


Fig. 9: Baseline comparisons: FL round vs. accuracy and energy expense ($v_u \in [0.1, 0.8]$)

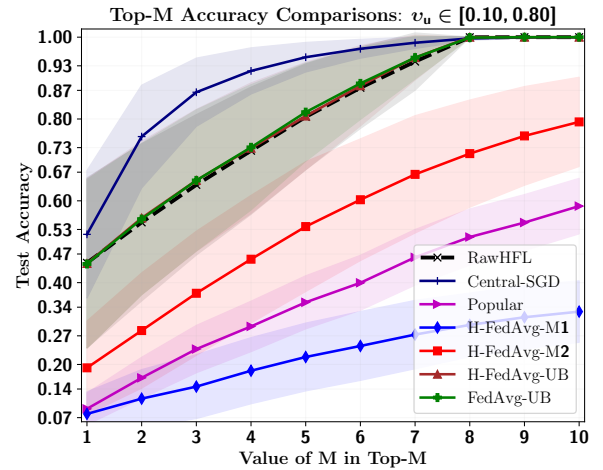


Fig. 10: Top- M accuracy comparisons: probability that requested content is in the Top- M predicted content ($v_u \in [0.1, 0.8]$)

TABLE III: Performance comparison: $K=400$, $E=4$, $t_{th}=150$ s, $v_u=0.7$

FL Algorithm	Test Accuracy	Energy Expense [J]
RawHFL- $ \mathcal{Z}_b =2$	0.7013 ± 0.0142	1508.33 ± 205.47
RawHFL- $ \mathcal{Z}_b =4$	0.7013 ± 0.0142	2848.16 ± 273.85
RawHFL- $ \mathcal{Z}_b =6$	0.7013 ± 0.0142	4137.94 ± 401.28
Central-SGD	0.7013 ± 0.0141	N/A
H-FedAvg-M1	0.1289 ± 0.0309	490.23 ± 1391.70
H-FedAvg-M2	0.3483 ± 0.0636	11226.51 ± 413.97
H-FedAvg-UB [38]	0.7013 ± 0.0142	13836.46 ± 519.91
FedAvg-UB [5]	0.7013 ± 0.0142	3455.56 ± 131.95
Top-Popular	0.0591 ± 0.0322	N/A

compared to the H-FedAvg-UB baseline, it is more energy efficient. Besides, when $|\mathcal{Z}_b|$ is high, FedAvg-UB may require less energy than RawHFL. However, recall that FedAvg-UB has $(|\mathcal{Z}_b| - 1)$ times higher communication overhead in the BS-CS backhaul links. Moreover, although centralized SGD outperforms the FL algorithms in all examined scenarios, the test accuracy gap with our proposed RawHFL depends on the value of the v_u . Particularly, this gap is higher when

TABLE IV: Performance comparison: $K=400$, $E=4$, $t_{th}=150$ s, $v_u \in [0.1, 0.8]$

FL Algorithm	Test Accuracy	Energy Expense [J]
RawHFL- $ \mathcal{U}_b =2$	0.4485 ± 0.2072	1508.33 ± 205.47
RawHFL- $ \mathcal{U}_b =4$	0.4485 ± 0.2075	2848.16 ± 273.85
RawHFL- $ \mathcal{U}_b =6$	0.4484 ± 0.2075	4137.94 ± 401.28
Central-SGD	0.5180 ± 0.1558	N/A
H-FedAvg-M1	0.0791 ± 0.0542	490.23 ± 1391.70
H-FedAvg-M2	0.1918 ± 0.1142	11226.51 ± 413.97
H-FedAvg-UB [38]	0.4468 ± 0.2069	13836.46 ± 519.91
FedAvg-UB [5]	0.4457 ± 0.2061	3455.56 ± 131.95
Top-Popular	0.0916 ± 0.0386	N/A

v_u is small and decreases as v_u increases. This is due to the fact that a higher v_u increases more personalized content requests from the client's preferred genre, leading to a clear trend in their datasets. However, a smaller v_u leads to more exploration of different genres, leading to irregular request patterns that are hard to predict. Since the centralized SGD can access all clients' training datasets, the severity of these irregularities can be predicted better with centralized SGD. Furthermore, it is worth noting that the performance gaps between the centralized SGD and the FL algorithms in the above results indicate the impact of the clients' non-IID data distributions. Moreover, since the non-IID data distribution problem typically requires special treatments and belongs to a different research direction [46], the solution to this problem in wireless video caching networks deserves a separate study, which we leave as our future works.

VI. CONCLUSION

Considering a realistic dataset acquisition method, this paper proposed a privacy-preserving RawHFL solution for predicting users' to-be-requested content in resource-constrained wireless video caching networks. Our theoretical analysis revealed that the convergence bound of the proposed algorithm depends on the FL and wireless networking parameters, as these parameters determine whether the ES receives the trained gradients from the clients. Besides, the formulated weighted utility function enabled energy-efficient training of the proposed RawHFL by jointly selecting clients, local training rounds, CPU frequencies and uplink wireless transmission power. Furthermore, our extensive simulation results indicate that more clients yield better test performances at the expense of higher energy costs. Moreover, our solution delivers nearly identical performance to the ideal case with significantly lower energy costs. Finally, we will leverage the prediction results of RawHFL in our future work and design an appropriate cache placement policy.

ACKNOWLEDGEMENT

The authors thank Prof. Minseok Choi, Omer Gokalp Serbetci and Yijing Zhang for helpful discussions.

The authors acknowledge the Center for Advanced Research Computing (CARC) at the University of Southern California for providing computing resources that have contributed to the research. URL: <https://carc.usc.edu>.

REFERENCES

- [1] M. F. Pervej and A. F. Molisch, "Resource-aware hierarchical federated learning for video caching in wireless networks," in *ICC 2024-IEEE International Conference on Communications*. IEEE, 2024, pp. 4723–4729.
- [2] F. Loh, F. Wamser, F. Poignée, S. Geißler, and T. Hoßfeld, "Youtube dataset on mobile streaming for internet traffic modeling and streaming analysis," *Scientific Data*, vol. 9, no. 1, p. 293, 2022.
- [3] N. Golrezaei, A. F. Molisch, A. G. Dimakis, and G. Caire, "Femto-caching and device-to-device collaboration: A new architecture for wireless video distribution," *IEEE Commun. Magaz.*, vol. 51, no. 4, pp. 142–149, 2013.
- [4] D. Liu, B. Chen, C. Yang, and A. F. Molisch, "Caching at the wireless edge: design aspects, challenges, and future directions," *IEEE Commun. Magaz.*, vol. 54, no. 9, pp. 22–28, 2016.
- [5] B. McMahan, E. Moore, D. Ramage, S. Hampson, and B. A. y Arcas, "Communication-efficient learning of deep networks from decentralized data," in *Proc. AISTATS*. PMLR, 2017, pp. 1273–1282. [Online]. Available: <https://proceedings.mlr.press/v54/mcmahan17a.html>
- [6] J. Wang, S. Wang, R.-R. Chen, and M. Ji, "Demystifying why local aggregation helps: Convergence analysis of hierarchical SGD," in *Proc. AAAI*, vol. 36, no. 8, 2022, pp. 8548–8556.
- [7] M. F. Pervej, R. Jin, and H. Dai, "Hierarchical federated learning in wireless networks: Pruning tackles bandwidth scarcity and system heterogeneity," *IEEE Trans. Wireless Commun.*, vol. 23, no. 9, pp. 11 417–11 432, 2024.
- [8] M. Javedankherad, Z. Zeinalpour-Yazdi, and F. Ashtiani, "Mobility-aware content caching using graph-coloring," *IEEE Trans. Vehicular Technol.*, vol. 71, no. 5, pp. 5666–5670, 2022.
- [9] D. Malak, F. V. Mutlu, J. Zhang, and E. M. Yeh, "Joint power control and caching for transmission delay minimization in wireless hetnets," *IEEE/ACM Trans. Network.*, 2023.
- [10] B. Qian, T. Ma, K. Yu, Y. Xu, Y. Wu, and H. Zhou, "3C resource sharing for personalized content delivery in B5G networks: A contract approach," *IEEE Internet Things J.*, 2023.
- [11] Q. Ning, M. Yang, C. Tang, and L. Huang, "Optimizing network performance through joint caching and recommendation policy for continuous user request behavior," *IEEE Trans. Network Serv. Manag.*, 2023.
- [12] M. W. Kang and Y. W. Chung, "Content caching based on popularity and priority of content using seq2seq LSTM in ICN," *IEEE Access*, vol. 11, pp. 16 831–16 842, 2023.
- [13] D. Li, H. Ding, H. Zhang, L. Wang, and D. Yuan, "Deep learning-enabled joint edge content caching and power allocation strategy in wireless networks," *IEEE Trans. Vehicular Technol.*, 2023.
- [14] T.-V. Nguyen, N.-N. Dao, W. Noh, S. Cho *et al.*, "User-aware and flexible proactive caching using LSTM and ensemble learning in IoT-MEC networks," *IEEE Internet Things J.*, vol. 9, no. 5, pp. 3251–3269, 2021.
- [15] P. Lin, Z. Ning, Z. Zhang, Y. Liu, F. R. Yu, and V. C. Leung, "Joint optimization of preference-aware caching and content migration in cost-efficient mobile edge networks," *IEEE Trans. Wireless Commun.*, 2023.
- [16] C. Fang, Z. Hu, X. Meng, S. Tu, Z. Wang, D. Zeng, W. Ni, S. Guo, and Z. Han, "DRL-driven joint task offloading and resource allocation for energy-efficient content delivery in cloud-edge cooperation networks," *IEEE Trans. Vehicular Technol.*, 2023.
- [17] X. Zhou, Z. Ke, and T. Qiu, "Recommendation-driven multi-cell cooperative caching: A multi-agent reinforcement learning approach," *IEEE Trans. Mobile Comput.*, 2023.
- [18] G. Xiong, S. Wang, G. Yan, and J. Li, "Reinforcement learning for dynamic dimensioning of cloud caches: A restless bandit approach," *IEEE/ACM Trans. Networ.*, 2023.
- [19] D. Qiao, S. Guo, D. Liu, S. Long, P. Zhou, and Z. Li, "Adaptive federated deep reinforcement learning for proactive content caching in edge computing," *IEEE Trans. Parallel Distrib. Syst.*, vol. 33, no. 12, pp. 4767–4782, 2022.
- [20] X. Wang, Y. Han, C. Wang, Q. Zhao, X. Chen, and M. Chen, "In-edge AI: Intelligentizing mobile edge computing, caching and communication by federated learning," *IEEE Network*, vol. 33, no. 5, pp. 156–165, 2019.
- [21] Y. Wang, K. Zheng, W. Ye, and Y. Tang, "Popularity-aware caching for vehicle clusters with federated deep reinforcement learning," *IEEE Commun. Let.*, 2023.
- [22] Y. Jiang, Y. Wu, F.-C. Zheng, M. Bennis, and X. You, "Federated learning-based content popularity prediction in fog radio access networks," *IEEE Trans. Wireless Commun.*, vol. 21, no. 6, pp. 3836–3849, 2021.

- [23] D. Li, H. Zhang, T. Li, H. Ding, and D. Yuan, "Community detection and attention-weighted federated learning based proactive edge caching for D2D-assisted wireless networks," *IEEE Trans. Wireless Commun.*, 2023.
- [24] S. Khanal, K. Thar, and E.-N. Huh, "Route-based proactive content caching using self-attention in hierarchical federated learning," *IEEE Access*, vol. 10, pp. 29 514–29 527, 2022.
- [25] N. Lin, Y. Wang, E. Zhang, K. Yu, L. Zhao, and M. Guizani, "Feedback delay-tolerant proactive caching scheme based on federated learning at the wireless edge," *IEEE Network Let.*, vol. 5, no. 1, pp. 26–30, 2023.
- [26] G. T. Maale, G. Sun, N. A. E. Kuadey, T. Kwantwi, R. Ou, and G. Liu, "Deepfesi: Deep federated echo state learning-based proactive content caching in UAV-assisted networks," *IEEE Trans. Vehicular Technol.*, 2023.
- [27] Y. Cao, S. Maghsudi, T. Ohtsuki, and T. Q. Quek, "Mobility-aware routing and caching in small cell networks using federated learning," *IEEE Trans. Commun.*, 2023.
- [28] B. Feng, C. Feng, D. Feng, Y. Wu, and X.-G. Xia, "Proactive content caching scheme in urban vehicular networks," *IEEE Trans. Commun.*, 2023.
- [29] P. Kairouz, H. B. McMahan, B. Avent, A. Bellet, M. Bennis, A. N. Bhagoji, K. Bonawitz, Z. Charles, G. Cormode, R. Cummings *et al.*, "Advances and open problems in federated learning," *Foundations and trends® in machine learning*, vol. 14, no. 1–2, pp. 1–210, 2021.
- [30] Y. Jee Cho, J. Wang, and G. Joshi, "Towards understanding biased client selection in federated learning," in *Proc. AISTAT.*, vol. 151. PMLR, 28–30 Mar 2022, pp. 10 351–10 375. [Online]. Available: <https://proceedings.mlr.press/v151/jee-cho22a.html>
- [31] W. Chen, S. Horváth, and P. Richtárik, "Optimal client sampling for federated learning," *Trans. on Machine Learning Research*, 2022. [Online]. Available: <https://openreview.net/forum?id=8GvRCWKHIL>
- [32] S. Wang and M. Ji, "A lightweight method for tackling unknown participation statistics in federated averaging," in *Proc. ICLR*, 2024. [Online]. Available: <https://openreview.net/forum?id=ZKEuFKfCKA>
- [33] H. Yang, M. Fang, and J. Liu, "Achieving linear speedup with partial worker participation in non-IID federated learning," in *Proc. ICLR*, 2021. [Online]. Available: <https://openreview.net/forum?id=jDdzh5ul-d>
- [34] M. F. Pervej, R. Jin, and H. Dai, "Resource constrained vehicular edge federated learning with highly mobile connected vehicles," *IEEE J. Sel. Areas Commun.*, vol. 41, no. 6, pp. 1825–1844, 2023.
- [35] J. Du, B. Jiang, C. Jiang, Y. Shi, and Z. Han, "Gradient and channel aware dynamic scheduling for over-the-air computation in federated edge learning systems," *IEEE J. Sel. Areas Commun.*, vol. 41, no. 4, pp. 1035–1050, 2023.
- [36] Z. Chen, W. Yi, and A. Nallanathan, "Exploring representativity in device scheduling for wireless federated learning," *IEEE Trans. Wireless Commun.*, vol. 23, no. 1, pp. 720–735, 2024.
- [37] Z. Ni, Z. Zhang, N. C. Luong, D. Niyato, D. I. Kim, and S. Feng, "Joint client scheduling and quantization optimization in energy harvesting-enabled federated learning networks," *IEEE Trans. Wireless Commun.*, 2024.
- [38] L. Liu, J. Zhang, S. Song, and K. B. Letaief, "Client-edge-cloud hierarchical federated learning," in *Proc. IEEE ICC*, 2020.
- [39] A. F. Molisch, *Wireless Communications: From Fundamentals to Beyond 5G*, 3rd ed. IEEE Press - Wiley, 2023.
- [40] "3rd generation partnership project; technical specification group radio access network; study on channel model for frequencies from 0.5 to 100 GHz," 3GPP TR 38.901 V16.1.0, Release 16, Dec. 2019.
- [41] S. O. Somuyiwa, A. György, and D. Gündüz, "A reinforcement-learning approach to proactive caching in wireless networks," *IEEE J. Sel. Areas Commun.*, vol. 36, no. 6, pp. 1331–1344, 2018.
- [42] B. Bharath, K. G. Nagananda, D. Gündüz, and H. V. Poor, "Caching with time-varying popularity profiles: A learning-theoretic perspective," *IEEE Trans. Commun.*, vol. 66, no. 9, pp. 3837–3847, 2018.
- [43] M. F. Pervej, R. Jin, S.-C. Lin, and H. Dai, "Efficient content delivery in user-centric and cache-enabled vehicular edge networks with deadline-constrained heterogeneous demands," *IEEE Trans. Vehicular Technol.*, vol. 73, no. 1, pp. 1129–1145, 2024.
- [44] M. F. Pervej *et al.*, "Mobility, communication and computation aware federated learning for internet of vehicles," in *Proc. IEEE Intel. Vehicles Symp.*, 2022.
- [45] S. Hosseinalipour, S. Wang, N. Michelusi, V. Aggarwal, C. G. Brinton, D. J. Love, and M. Chiang, "Parallel successive learning for dynamic distributed model training over heterogeneous wireless networks," *IEEE/ACM Trans. Network.*, pp. 1–16, 2023.
- [46] Z. Zhu, J. Hong, and J. Zhou, "Data-free knowledge distillation for heterogeneous federated learning," in *Proc. ICML*, vol. 139. PMLR, 18–24 Jul 2021, pp. 12 878–12 889. [Online]. Available: <https://proceedings.mlr.press/v139/zhu21b.html>
- [47] T. Zeng, O. Semiari, M. Chen, W. Saad, and M. Bennis, "Federated learning on the road autonomous controller design for connected and autonomous vehicles," *IEEE Trans. Wireless Commun.*, vol. 21, no. 12, pp. 10 407–10 423, 2022.
- [48] J. Du, C. Jiang, J. Wang, Y. Ren, and M. Debbah, "Machine learning for 6g wireless networks: Carrying forward enhanced bandwidth, massive access, and ultrareliable/low-latency service," *IEEE Vehicular Technol. Magaz.*, vol. 15, no. 4, pp. 122–134, 2020.
- [49] S. Diamond and S. Boyd, "CVXPY: A Python-embedded modeling language for convex optimization," *J. Machine Learn. Research*, vol. 17, no. 83, pp. 1–5, 2016.
- [50] Y. Sun, D. Xu, D. W. K. Ng, L. Dai, and R. Schober, "Optimal 3D-trajectory design and resource allocation for solar-powered UAV communication systems," *IEEE Trans. Commun.*, vol. 67, no. 6, pp. 4281–4298, 2019.

SUPPLEMENTARY MATERIAL

A. Key Equations

Recall that the UEs minimizes the following local loss function.

$$f_u(\mathbf{w}|\mathcal{D}_{u,\text{proc}}^t) := [1/D_{u,\text{proc}}^t] \sum_{(\mathbf{x}_u^a, \mathbf{y}_u^a) \in \mathcal{D}_{u,\text{proc}}^t} l(\mathbf{w}|\mathbf{x}_u^a, \mathbf{y}_u^a), \quad (41)$$

where $l(\mathbf{w}|\mathbf{x}_u^a, \mathbf{y}_u^a)$ is the loss associated with the a^{th} data sample. The UE minimizes (41) by taking $L_u^{k,e}$ SGD steps as

$$\mathbf{w}_u^{k,e,L_u^{k,e}} = \mathbf{w}_u^{k,e,0} - \eta \sum_{l=0}^{L_u^{k,e}-1} g_u(\mathbf{w}_u^{k,e,l}), \quad (42)$$

where η is the learning rate and $g_u(\mathbf{w}_u^{k,e,l})$ is the stochastic gradient.

Besides, the ESs want to minimize the following loss

$$f_b(\mathbf{w}|\cup_{u \in \mathcal{U}_b^{k,e}} \mathcal{D}_{u,\text{proc}}^t) := \sum_{u \in \mathcal{U}_b^{k,e}} \alpha_u f_u(\mathbf{w}|\mathcal{D}_{u,\text{proc}}^t), \quad (43)$$

where $\sum_{u \in \mathcal{U}_b^{k,e}} \alpha_u = 1$. Each ES follows the following aggregation rule.

$$\mathbf{w}_b^{k,e+1} = \mathbf{w}_b^{k,e} - \eta \sum_{u \in \mathcal{U}_b^{k,e}} \alpha_u [1_{u,\text{sc}}^{k,e}/P_{u,\text{sc}}^{k,e}] \tilde{g}_u^{k,e}, \quad (44)$$

where $\tilde{g}_u^{k,e} := \sum_{l=0}^{L_u^{k,e}-1} g_u(\mathbf{w}_u^{k,e,l})$ and $1_{u,\text{sc}}^{k,e}$ is defined as

$$1_{u,\text{sc}}^{k,e} = \begin{cases} 1, & \text{with probability } p_{u,\text{sc}}^{k,e}, \\ 0, & \text{otherwise,} \end{cases} \quad (45)$$

The central server wants to minimize the following loss function

$$f(\mathbf{w}^k|\cup_{b=0}^{B-1} \cup_{u \in \mathcal{U}_b^{k,e}} \mathcal{D}_{u,\text{proc}}^t) := \sum_{b=0}^{B-1} \alpha_b f_b(\mathbf{w}^k|\cup_{u \in \mathcal{U}_b^{k,e}} \mathcal{D}_{u,\text{proc}}^t), \quad (46)$$

where $\sum_{b=0}^{B-1} \alpha_b = 1$. Moreover, the central server uses the following aggregation rule.

$$\mathbf{w}^{k+1} = \sum_{b=0}^{B-1} \alpha_b \mathbf{w}_b^{k,E} = \mathbf{w}^k - \eta \sum_{e=0}^{E-1} \sum_{b=0}^{B-1} \alpha_b \sum_{u \in \mathcal{U}_b^{k,e}} \alpha_u [1_{u,\text{sc}}^{k,e}/P_{u,\text{sc}}^{k,e}] \tilde{g}_u^{k,e}. \quad (47)$$

In the following, we have used $f_u(\mathbf{w})$, $f_b(\mathbf{w})$ and $f(\mathbf{w})$ to represent $f_u(\mathbf{w}|\mathcal{D}_{u,\text{proc}}^t)$, $f_b(\mathbf{w}|\cup_{u \in \mathcal{U}_b^{k,e}} \mathcal{D}_{u,\text{proc}}^t)$ and $f(\mathbf{w}|\cup_{b=0}^{B-1} \cup_{u \in \mathcal{U}_b^{k,e}} \mathcal{D}_{u,\text{proc}}^t)$, respectively, for notational simplicity. Moreover, from the definition of the loss functions, it is easy to notice that $\nabla f_b(\mathbf{w}) = \sum_{u \in \mathcal{U}_b^{k,e}} \alpha_u \nabla f_u(\mathbf{w})$ and $\nabla f(\mathbf{w}) = \sum_{b=0}^{B-1} \alpha_b \nabla f_b(\mathbf{w}) = \sum_{b=0}^{B-1} \alpha_b \sum_{u \in \mathcal{U}_b^{k,e}} \alpha_u \nabla f_u(\mathbf{w})$.

B. Key Assumptions

We make the following assumptions for our theoretical analysis, which are standard in the literature [6], [7], [34], [45].

Assumption 6. β -smoothness: The loss functions in all nodes are β -smooth, i.e., $\|\nabla f(\mathbf{w}) - \nabla f(\mathbf{w}')\| \leq \beta \|\mathbf{w} - \mathbf{w}'\|$, where $\|\cdot\|$ is the L_2 norm.

Assumption 7. Unbiased SGD: mini-batch gradients are unbiased, i.e., $\mathbb{E}_{\xi \sim \mathcal{D}_{u,\text{proc}}} [g_u(\mathbf{w})] = \nabla f_u(\mathbf{w})$, where $\mathbb{E}[\cdot]$ is the expectation operator, and ξ is client's randomly sampled mini-batch.

Assumption 8. Bounded variance: variance of the gradients is bounded, i.e., $\|g_u(\mathbf{w}) - \nabla f_u(\mathbf{w})\|^2 \leq \sigma^2$.

Assumption 9. Independence: a) the stochastic gradients are independent of each other in different episodes and b) accumulated gradient offloading is independent of client selection and each other in each edge round e .

Assumption 10. Bounded divergence: divergence between the a) local and edge and b) edge and global loss functions are bounded, i.e., for all u , b and \mathbf{w}

$$\sum_{u \in \mathcal{U}_b^{k,e}} \alpha_u \|\nabla f_u(\mathbf{w}) - \nabla f_b(\mathbf{w})\|^2 \leq \varepsilon_0^2, \quad (48)$$

$$\sum_{b=0}^{B-1} \alpha_b \left\| \sum_{u \in \mathcal{U}_b^{k,e}} \alpha_u \nabla \tilde{f}_u(\mathbf{w}) - \sum_{b'=0}^{B-1} \alpha_{b'} \sum_{u' \in \mathcal{U}_{b'}^{k,e}} \alpha_{u'} \nabla \tilde{f}_{u'}(\mathbf{w}) \right\|^2 \leq \varepsilon_1^2, \quad (49)$$

where $\nabla \tilde{f}_u(\mathbf{w}) := \sum_{l=0}^{L_u^{k,e}-1} \nabla f_u(\mathbf{w})$.

APPENDIX A
PROOF OF THEOREM 1

Theorem 1. Suppose $\eta < \min\left\{\frac{1}{2\sqrt{5}\beta L}, \frac{1}{\beta EL}\right\}$ and the above assumptions hold. Then, the average global gradient norm from K global rounds of RawHFL is upper-bounded as

$$\begin{aligned} \frac{1}{K} \sum_{k=0}^{K-1} \mathbb{E}[\|\nabla f(\mathbf{w}^k)\|^2] &\leq \frac{2}{\eta K} \sum_{k=0}^{K-1} \frac{1}{\Omega^k} \left\{ \mathbb{E}[f(\mathbf{w}^k)] - \mathbb{E}[f(\mathbf{w}^{k+1})] \right\} + \frac{2\beta\eta L\sigma^2}{K} \sum_{k=0}^{K-1} \frac{N_1^k}{\Omega^k} + \frac{18E\beta^2\varepsilon_0^2\eta^2L^3}{K} \sum_{k=0}^{K-1} \frac{N_2}{\Omega^k} + \\ &\frac{20L\beta^2\varepsilon_1^2\eta^2E^3}{K} \sum_{k=0}^{K-1} \frac{1}{\Omega^k} + \frac{2\beta\eta L}{K} \sum_{k=0}^{K-1} \frac{1}{\Omega^k} \sum_{e=0}^{E-1} \sum_{b=0}^{B-1} \alpha_b \sum_{u \in \mathcal{Q}_b^{k,e}} \alpha_u N_u [(1/p_{u,sc}^{k,e}) - 1] \sum_{l=0}^{L_u^{k,e}-1} \mathbb{E}[\|g_u(\mathbf{w}_u^{k,e,l})\|^2], \end{aligned} \quad (50)$$

where the expectations depend on clients' randomly selected mini-batches and $1_{u,sc}^{k,e}$'s. Besides, $\Omega^k := \sum_{e=0}^{E-1} \sum_{b=0}^{B-1} \alpha_b \sum_{u \in \mathcal{Q}_b^{k,e}} \alpha_u L_u^{k,e}$, $N_1^k := 60\beta^3\eta^3E^3L^3 + 3\beta\eta EL + \sum_{e=0}^{E-1} \sum_{b=0}^{B-1} \alpha_b (\alpha_b + 4EL\beta\eta) \sum_{u \in \mathcal{Q}_b^{k,e}} (\alpha_u)^2$, $N_2 := 1 + 20\beta^2\eta^2E^2L^2$ and $N_u := E + 3\beta\eta L + 4\beta\eta E (\alpha_u + 15E\beta^2\eta^2L^3)$.

Proof. From our aggregation rule in (47), we write the following

$$\begin{aligned} f(\mathbf{w}^{k+1}) &= f\left(\mathbf{w}^k - \eta \sum_{e=0}^{E-1} \sum_{b=0}^{B-1} \alpha_b \sum_{u \in \mathcal{Q}_b^{k,e}} \alpha_u \frac{1_{u,sc}^{k,e}}{p_{u,sc}} g_u^{k,e}\right) \\ &\stackrel{(a)}{\leq} f(\mathbf{w}^k) + \left\langle \nabla f(\mathbf{w}^k), -\eta \sum_{e=0}^{E-1} \sum_{b=0}^{B-1} \alpha_b \sum_{u \in \mathcal{Q}_b^{k,e}} \alpha_u \frac{1_{u,sc}^{k,e}}{p_{u,sc}} g_u^{k,e} \right\rangle + \frac{\beta\eta^2}{2} \left\| \sum_{e=0}^{E-1} \sum_{b=0}^{B-1} \alpha_b \sum_{u \in \mathcal{Q}_b^{k,e}} \alpha_u \frac{1_{u,sc}^{k,e}}{p_{u,sc}} g_u^{k,e} \right\|^2 \\ &= f(\mathbf{w}^k) - \eta \left\langle \nabla f(\mathbf{w}^k), \sum_{e=0}^{E-1} \sum_{b=0}^{B-1} \alpha_b \sum_{u \in \mathcal{Q}_b^{k,e}} \alpha_u \frac{1_{u,sc}^{k,e}}{p_{u,sc}} \sum_{l=0}^{L_u^{k,e}-1} g_u(\mathbf{w}_u^{k,e,l}) \right\rangle + \frac{\beta\eta^2}{2} \left\| \sum_{e=0}^{E-1} \sum_{b=0}^{B-1} \alpha_b \sum_{u \in \mathcal{Q}_b^{k,e}} \alpha_u \frac{1_{u,sc}^{k,e}}{p_{u,sc}} g_u^{k,e} \right\|^2, \end{aligned} \quad (51)$$

where (a) stems from β -smoothness property, i.e., $f(\mathbf{y}) \leq f(\mathbf{x}) + \langle \nabla f(\mathbf{x}), \mathbf{y} - \mathbf{x} \rangle + \frac{\beta}{2} \|\mathbf{y} - \mathbf{x}\|^2$.

Now, taking expectation over both sides of (51), we get

$$\begin{aligned} \mathbb{E}[f(\mathbf{w}^{k+1})] &\leq \underbrace{\mathbb{E}[f(\mathbf{w}^k)] - \eta \sum_{e=0}^{E-1} \sum_{b=0}^{B-1} \alpha_b \sum_{u \in \mathcal{Q}_b^{k,e}} \alpha_u \sum_{l=0}^{L_u^{k,e}-1} \mathbb{E}\left[\left\langle \nabla f(\mathbf{w}^k), \frac{1_{u,sc}^{k,e}}{p_{u,sc}} g_u(\mathbf{w}_u^{k,e,l}) \right\rangle\right]}_{T_1} + \\ &\underbrace{\frac{\beta\eta^2}{2} \mathbb{E}\left[\left\| \sum_{e=0}^{E-1} \sum_{b=0}^{B-1} \alpha_b \sum_{u \in \mathcal{Q}_b^{k,e}} \alpha_u \frac{1_{u,sc}^{k,e}}{p_{u,sc}} g_u^{k,e} \right\|^2\right]}_{T_2}, \end{aligned} \quad (52)$$

where $\mathbb{E}[\cdot]$ depends on $1_{u,sc}^{k,e}$'s and clients mini-batches.

Now, we simplify the T_1 term as

$$\begin{aligned} T_1 &\stackrel{(a)}{=} -\eta \sum_{e=0}^{E-1} \sum_{b=0}^{B-1} \alpha_b \sum_{u \in \mathcal{Q}_b^{k,e}} \alpha_u \sum_{l=0}^{L_u^{k,e}-1} \left\langle \nabla f(\mathbf{w}^k), \frac{\mathbb{E}[1_{u,sc}^{k,e}]}{p_{u,sc}} \mathbb{E}[g_u(\mathbf{w}_u^{k,e,l})] \right\rangle \\ &\stackrel{(b)}{=} -\eta \sum_{e=0}^{E-1} \sum_{b=0}^{B-1} \alpha_b \sum_{u \in \mathcal{Q}_b^{k,e}} \alpha_u \sum_{l=0}^{L_u^{k,e}-1} \left\langle \nabla f(\mathbf{w}^k), \nabla f_u(\mathbf{w}_u^{k,e,l}) \right\rangle \\ &= -\frac{\eta}{2} \sum_{e=0}^{E-1} \sum_{b=0}^{B-1} \alpha_b \sum_{u \in \mathcal{Q}_b^{k,e}} \alpha_u \sum_{l=0}^{L_u^{k,e}-1} \left[\|\nabla f(\mathbf{w}^k)\|^2 + \|\nabla f_u(\mathbf{w}_u^{k,e,l})\|^2 - \|\nabla f(\mathbf{w}^k) - \nabla f_u(\mathbf{w}_u^{k,e,l})\|^2 \right] \\ &= \frac{\eta}{2} \sum_{e=0}^{E-1} \sum_{b=0}^{B-1} \alpha_b \sum_{u \in \mathcal{Q}_b^{k,e}} \alpha_u \sum_{l=0}^{L_u^{k,e}-1} \|\nabla f(\mathbf{w}^k) - \nabla f_u(\mathbf{w}_u^{k,e,l})\|^2 - \frac{\eta}{2} \sum_{e=0}^{E-1} \sum_{b=0}^{B-1} \alpha_b \sum_{u \in \mathcal{Q}_b^{k,e}} \alpha_u L_u^{k,e} \|\nabla f(\mathbf{w}^k)\|^2 - \\ &\frac{\eta}{2} \sum_{e=0}^{E-1} \sum_{b=0}^{B-1} \alpha_b \sum_{u \in \mathcal{Q}_b^{k,e}} \alpha_u \sum_{l=0}^{L_u^{k,e}-1} \|\nabla f_u(\mathbf{w}_u^{k,e,l})\|^2, \end{aligned} \quad (53)$$

where (a) appears from the independence of successful offloading of $\hat{g}_u^{k,e}$'s and stochastic gradients. Besides, (b) stems from the fact that $\mathbb{E}[1_{u,\text{sc}}^{k,e}] = p_{u,\text{sc}}^{k,e}$ and $\mathbb{E}[g_u(\mathbf{w}_u^{k,e,l})] = \nabla f_u(\mathbf{w}_u^{k,e,l})$.

We also simplify the T_2 term as follows:

$$\begin{aligned}
T_2 &\stackrel{(a)}{=} \frac{\beta \eta^2}{2} \mathbb{E} \left[\left\| \sum_{e=0}^{E-1} \sum_{b=0}^{B-1} \alpha_b \sum_{u \in \mathcal{U}_b^{k,e}} \alpha_u \frac{1_{u,\text{sc}}^{k,e}}{p_{u,\text{sc}}^{k,e}} \hat{g}_u^{k,e} - \mathbb{E} \left[\sum_{e=0}^{E-1} \sum_{b=0}^{B-1} \alpha_b \sum_{u \in \mathcal{U}_b^{k,e}} \alpha_u \frac{1_{u,\text{sc}}^{k,e}}{p_{u,\text{sc}}^{k,e}} \hat{g}_u^{k,e} \right] \right\|^2 \right] + \\
&\quad \frac{\beta \eta^2}{2} \left(\mathbb{E} \left[\sum_{e=0}^{E-1} \sum_{b=0}^{B-1} \alpha_b \sum_{u \in \mathcal{U}_b^{k,e}} \alpha_u \frac{1_{u,\text{sc}}^{k,e}}{p_{u,\text{sc}}^{k,e}} \hat{g}_u^{k,e} \right] \right)^2 \\
&= \frac{\beta \eta^2}{2} \mathbb{E} \left[\left\| \sum_{e=0}^{E-1} \sum_{b=0}^{B-1} \alpha_b \sum_{u \in \mathcal{U}_b^{k,e}} \alpha_u \frac{1_{u,\text{sc}}^{k,e}}{p_{u,\text{sc}}^{k,e}} \hat{g}_u^{k,e} - \sum_{e=0}^{E-1} \sum_{b=0}^{B-1} \alpha_b \sum_{u \in \mathcal{U}_b^{k,e}} \alpha_u \sum_{l=0}^{L_u^{k,e}-1} \nabla f_u(\mathbf{w}_u^{k,e,l}) \right\|^2 \right] + \\
&\quad \frac{\beta \eta^2}{2} \left\| \sum_{e=0}^{E-1} \sum_{b=0}^{B-1} \alpha_b \sum_{u \in \mathcal{U}_b^{k,e}} \alpha_u \sum_{l=0}^{L_u^{k,e}-1} \nabla f_u(\mathbf{w}_u^{k,e,l}) \right\|^2 \\
&\stackrel{(b)}{\leq} \frac{\beta \eta^2}{2} \mathbb{E} \left[\left\| \sum_{e=0}^{E-1} \sum_{b=0}^{B-1} \alpha_b \sum_{u \in \mathcal{U}_b^{k,e}} \alpha_u \frac{1_{u,\text{sc}}^{k,e}}{p_{u,\text{sc}}^{k,e}} \sum_{l=0}^{L_u^{k,e}-1} g_u(\mathbf{w}_u^{k,e,l}) \pm \sum_{e=0}^{E-1} \sum_{b=0}^{B-1} \alpha_b \sum_{u \in \mathcal{U}_b^{k,e}} \alpha_u \sum_{l=0}^{L_u^{k,e}-1} g_u(\mathbf{w}_u^{k,e,l}) - \right. \right. \\
&\quad \left. \left. \sum_{e=0}^{E-1} \sum_{b=0}^{B-1} \alpha_b \sum_{u \in \mathcal{U}_b^{k,e}} \alpha_u \sum_{l=0}^{L_u^{k,e}-1} \nabla f_u(\mathbf{w}_u^{k,e,l}) \right\|^2 \right] + \frac{\beta E \eta^2}{2} \sum_{e=0}^{E-1} \sum_{b=0}^{B-1} \alpha_b \sum_{u \in \mathcal{U}_b^{k,e}} \alpha_u \sum_{l=0}^{L_u^{k,e}-1} \left\| \nabla f_u(\mathbf{w}_u^{k,e,l}) \right\|^2 \\
&\stackrel{(c)}{\leq} \frac{\beta \eta^2}{2} \mathbb{E} \left[\left\| \sum_{e=0}^{E-1} \sum_{b=0}^{B-1} \alpha_b \sum_{u \in \mathcal{U}_b^{k,e}} \alpha_u \sum_{l=0}^{L_u^{k,e}-1} g_u(\mathbf{w}_u^{k,e,l}) \left(\frac{1_{u,\text{sc}}^{k,e}}{p_{u,\text{sc}}^{k,e}} - 1 \right) + \sum_{e=0}^{E-1} \sum_{b=0}^{B-1} \alpha_b \sum_{u \in \mathcal{U}_b^{k,e}} \alpha_u \sum_{l=0}^{L_u^{k,e}-1} \left(g_u(\mathbf{w}_u^{k,e,l}) - \nabla f_u(\mathbf{w}_u^{k,e,l}) \right) \right\|^2 \right] \\
&\quad + \frac{\beta E L \eta^2}{2} \sum_{e=0}^{E-1} \sum_{b=0}^{B-1} \alpha_b \sum_{u \in \mathcal{U}_b^{k,e}} \alpha_u \sum_{l=0}^{L_u^{k,e}-1} \left\| \nabla f_u(\mathbf{w}_u^{k,e,l}) \right\|^2 \\
&\leq \beta \eta^2 \mathbb{E} \left[\left\| \sum_{e=0}^{E-1} \sum_{b=0}^{B-1} \alpha_b \sum_{u \in \mathcal{U}_b^{k,e}} \alpha_u \sum_{l=0}^{L_u^{k,e}-1} g_u(\mathbf{w}_u^{k,e,l}) \left(\frac{1_{u,\text{sc}}^{k,e}}{p_{u,\text{sc}}^{k,e}} - 1 \right) \right\|^2 \right] + \frac{\beta E L \eta^2}{2} \sum_{e=0}^{E-1} \sum_{b=0}^{B-1} \alpha_b \sum_{u \in \mathcal{U}_b^{k,e}} \alpha_u \sum_{l=0}^{L_u^{k,e}-1} \left\| \nabla f_u(\mathbf{w}_u^{k,e,l}) \right\|^2 + \\
&\quad \beta \eta^2 \mathbb{E} \left[\left\| \sum_{e=0}^{E-1} \sum_{b=0}^{B-1} \alpha_b \sum_{u \in \mathcal{U}_b^{k,e}} \alpha_u \sum_{l=0}^{L_u^{k,e}-1} \left(g_u(\mathbf{w}_u^{k,e,l}) - \nabla f_u(\mathbf{w}_u^{k,e,l}) \right) \right\|^2 \right] \\
&\leq \beta E \eta^2 \sum_{e=0}^{E-1} \sum_{b=0}^{B-1} \alpha_b \sum_{u \in \mathcal{U}_b^{k,e}} \alpha_u \sum_{l=0}^{L_u^{k,e}-1} \mathbb{E} \left[\left\| g_u(\mathbf{w}_u^{k,e,l}) \left(\frac{1_{u,\text{sc}}^{k,e}}{p_{u,\text{sc}}^{k,e}} - 1 \right) \right\|^2 \right] + \frac{\beta E L \eta^2}{2} \sum_{e=0}^{E-1} \sum_{b=0}^{B-1} \alpha_b \sum_{u \in \mathcal{U}_b^{k,e}} \alpha_u \sum_{l=0}^{L_u^{k,e}-1} \left\| \nabla f_u(\mathbf{w}_u^{k,e,l}) \right\|^2 + \\
&\quad \beta \eta^2 \mathbb{E} \left[\left\| \sum_{b=0}^{B-1} \sum_{e=0}^{E-1} \sum_{u \in \mathcal{U}_b^{k,e}} \alpha_u \sum_{l=0}^{L_u^{k,e}-1} \left(g_u(\mathbf{w}_u^{k,e,l}) - \nabla f_u(\mathbf{w}_u^{k,e,l}) \right) \right\|^2 \right] \\
&\stackrel{(d)}{=} \beta E \eta^2 \sum_{e=0}^{E-1} \sum_{b=0}^{B-1} \alpha_b \sum_{u \in \mathcal{U}_b^{k,e}} \alpha_u \sum_{l=0}^{L_u^{k,e}-1} \mathbb{E} \left[\left\| g_u(\mathbf{w}_u^{k,e,l}) \right\|^2 \right] \times \mathbb{E} \left[\left(\frac{1_{u,\text{sc}}^{k,e}}{p_{u,\text{sc}}^{k,e}} - 1 \right)^2 \right] + \\
&\quad \frac{\beta E L \eta^2}{2} \sum_{e=0}^{E-1} \sum_{b=0}^{B-1} \alpha_b \sum_{u \in \mathcal{U}_b^{k,e}} \alpha_u \sum_{l=0}^{L_u^{k,e}-1} \left\| \nabla f_u(\mathbf{w}_u^{k,e,l}) \right\|^2 + \beta \eta^2 \mathbb{E} \left\{ \sum_{b=0}^{B-1} (\alpha_b)^2 \left\| \sum_{e=0}^{E-1} \sum_{u \in \mathcal{U}_b^{k,e}} \alpha_u \sum_{l=0}^{L_u^{k,e}-1} \left(g_u(\mathbf{w}_u^{k,e,l}) - \nabla f_u(\mathbf{w}_u^{k,e,l}) \right) \right\|^2 \right. \\
&\quad \left. + \sum_{b=0}^{B-1} \alpha_b \left[\sum_{e=0}^{E-1} \sum_{u \in \mathcal{U}_b^{k,e}} \alpha_u \sum_{l=0}^{L_u^{k,e}-1} \left(g_u(\mathbf{w}_u^{k,e,l}) - \nabla f_u(\mathbf{w}_u^{k,e,l}) \right) \right] \times \sum_{b'=1, b' \neq b}^B \alpha_{b'} \left[\sum_{e=0}^{E-1} \sum_{u \in \mathcal{U}_{b'}^{k,e}} \alpha_u \sum_{l=0}^{L_u^{k,e}-1} \left(g_u(\mathbf{w}_u^{k,e,l}) - \nabla f_u(\mathbf{w}_u^{k,e,l}) \right) \right] \right\} \\
&\stackrel{(e)}{=} \beta E \eta^2 \sum_{e=0}^{E-1} \sum_{b=0}^{B-1} \alpha_b \sum_{u \in \mathcal{U}_b^{k,e}} \alpha_u \sum_{l=0}^{L_u^{k,e}-1} \left[\frac{1}{p_{u,\text{sc}}^{k,e}} - 1 \right] \mathbb{E} \left[\left\| g_u(\mathbf{w}_u^{k,e,l}) \right\|^2 \right] + \frac{\beta E L \eta^2}{2} \sum_{e=0}^{E-1} \sum_{b=0}^{B-1} \alpha_b \sum_{u \in \mathcal{U}_b^{k,e}} \alpha_u \sum_{l=0}^{L_u^{k,e}-1} \left\| \nabla f_u(\mathbf{w}_u^{k,e,l}) \right\|^2 +
\end{aligned}$$

$$\begin{aligned}
& \beta \eta^2 \sum_{b=0}^{B-1} (\alpha_b)^2 \mathbb{E} \left[\left\| \sum_{e=0}^{E-1} \sum_{u \in \mathcal{U}_b^{k,e}} \alpha_u \sum_{l=0}^{L_u^{k,e}-1} \left(g_u(\mathbf{w}_u^{k,e,l}) - \nabla f_u(\mathbf{w}_u^{k,e,l}) \right) \right\|^2 \right] \\
\stackrel{(f)}{=} & \beta E \eta^2 \sum_{e=0}^{E-1} \sum_{b=0}^{B-1} \alpha_b \sum_{u \in \mathcal{U}_b^{k,e}} \alpha_u L_u^{k,e} \sum_{l=0}^{L_u^{k,e}-1} \left[\frac{1}{\mathbb{P}_{u,sc}^{k,e}} - 1 \right] \mathbb{E} \left[\left\| g_u(\mathbf{w}_u^{k,e,l}) \right\|^2 \right] + \frac{\beta E L \eta^2}{2} \sum_{e=0}^{E-1} \sum_{b=0}^{B-1} \alpha_b \sum_{u \in \mathcal{U}_b^{k,e}} \alpha_u \sum_{l=0}^{L_u^{k,e}-1} \left\| \nabla f_u(\mathbf{w}_u^{k,e,l}) \right\|^2 + \\
& \beta \eta^2 \sum_{e=0}^{E-1} \sum_{b=0}^{B-1} (\alpha_b)^2 \sum_{u \in \mathcal{U}_b^{k,e}} (\alpha_u)^2 \sum_{l=0}^{L_u^{k,e}-1} \mathbb{E} \left[\left\| g_u(\mathbf{w}_u^{k,e,l}) - \nabla f_u(\mathbf{w}_u^{k,e,l}) \right\|^2 \right] \\
\stackrel{(g)}{\leq} & \beta E \eta^2 \sum_{e=0}^{E-1} \sum_{b=0}^{B-1} \alpha_b \sum_{u \in \mathcal{U}_b^{k,e}} \alpha_u L_u^{k,e} \sum_{l=0}^{L_u^{k,e}-1} \left[\frac{1}{\mathbb{P}_{u,sc}^{k,e}} - 1 \right] \mathbb{E} \left[\left\| g_u(\mathbf{w}_u^{k,e,l}) \right\|^2 \right] + \frac{\beta E L \eta^2}{2} \sum_{e=0}^{E-1} \sum_{b=0}^{B-1} \alpha_b \sum_{u \in \mathcal{U}_b^{k,e}} \alpha_u \sum_{l=0}^{L_u^{k,e}-1} \left\| \nabla f_u(\mathbf{w}_u^{k,e,l}) \right\|^2 + \\
& \beta \eta^2 \sum_{e=0}^{E-1} \sum_{b=0}^{B-1} (\alpha_b)^2 \sum_{u \in \mathcal{U}_b^{k,e}} (\alpha_u)^2 \sum_{l=0}^{L_u^{k,e}-1} \sigma^2 \\
= & \beta \eta^2 \sigma^2 \sum_{e=0}^{E-1} \sum_{b=0}^{B-1} (\alpha_b)^2 \sum_{u \in \mathcal{U}_b^{k,e}} (\alpha_u)^2 L_u^{k,e} + \beta E \eta^2 \sum_{e=0}^{E-1} \sum_{b=0}^{B-1} \alpha_b \sum_{u \in \mathcal{U}_b^{k,e}} \alpha_u L_u^{k,e} \sum_{l=0}^{L_u^{k,e}-1} \left[\frac{1}{\mathbb{P}_{u,sc}^{k,e}} - 1 \right] \mathbb{E} \left[\left\| g_u(\mathbf{w}_u^{k,e,l}) \right\|^2 \right] + \\
& \frac{\beta E L \eta^2}{2} \sum_{e=0}^{E-1} \sum_{b=0}^{B-1} \alpha_b \sum_{u \in \mathcal{U}_b^{k,e}} \alpha_u \sum_{l=0}^{L_u^{k,e}-1} \left\| \nabla f_u(\mathbf{w}_u^{k,e,l}) \right\|^2, \tag{54}
\end{aligned}$$

where (a) comes from the definition of variance. (b) stems from the fact that $\|\sum_{j=1}^J \mathbf{x}_j\|^2 \leq J \sum_{j=1}^J \|\mathbf{x}_j\|^2$, and from the convexity of $\|\cdot\|$ and Jensen inequality $\|\sum_{j=1}^J \alpha_j \mathbf{x}_j\|^2 \leq \sum_{j=1}^J \alpha_j \|\mathbf{x}_j\|^2$. Besides, the notation $\pm \mathbf{x}$ is used to indicate that $(+\mathbf{x} - \mathbf{x})$ for brevity. In (c), we use the fact that $1 \leq L_u^{k,e} \leq L$ in the last term. Furthermore, we get (d) using the fact that $1_{u,sc}^{k,e}$ and $g_u(\mathbf{w}_u^{k,e,l})$ are independent. (e) is true since $\mathbb{E}[T_1] = 0$ from the unbiased mini-batch gradient assumption, i.e., $\mathbb{E}[g_u(\mathbf{w}_u^{k,e,l})] = \nabla f_u(\mathbf{w}_u^{k,e,l})$. Moreover, in (f), we follow similar steps as in (d) and (e). Finally, (g) is obtained from the bounded variance assumption of the gradients.

Now, plugging T_1 and T_2 into (52), we get

$$\begin{aligned}
\mathbb{E} [f(\mathbf{w}^{k+1})] & \leq \mathbb{E}[f(\mathbf{w}^k)] + \frac{\eta}{2} \sum_{e=0}^{E-1} \sum_{b=0}^{B-1} \alpha_b \sum_{u \in \mathcal{U}_b^{k,e}} \alpha_u \sum_{l=0}^{L_u^{k,e}-1} \left\| \nabla f(\mathbf{w}^k) - \nabla f_u(\mathbf{w}_u^{k,e,l}) \right\|^2 - \frac{\eta}{2} \sum_{e=0}^{E-1} \sum_{b=0}^{B-1} \alpha_b \sum_{u \in \mathcal{U}_b^{k,e}} \alpha_u L_u^{k,e} \left\| \nabla f(\mathbf{w}^k) \right\|^2 - \\
& \frac{\eta}{2} \sum_{e=0}^{E-1} \sum_{b=0}^{B-1} \alpha_b \sum_{u \in \mathcal{U}_b^{k,e}} \alpha_u \sum_{l=0}^{L_u^{k,e}-1} \left\| \nabla f_u(\mathbf{w}_u^{k,e,l}) \right\|^2 + \beta \eta^2 \sigma^2 \sum_{e=0}^{E-1} \sum_{b=0}^{B-1} (\alpha_b)^2 \sum_{u \in \mathcal{U}_b^{k,e}} (\alpha_u)^2 L_u^{k,e} + \\
& \beta E \eta^2 \sum_{e=0}^{E-1} \sum_{b=0}^{B-1} \alpha_b \sum_{u \in \mathcal{U}_b^{k,e}} \alpha_u L_u^{k,e} \sum_{l=0}^{L_u^{k,e}-1} \left[\frac{1}{\mathbb{P}_{u,sc}^{k,e}} - 1 \right] \mathbb{E} \left[\left\| g_u(\mathbf{w}_u^{k,e,l}) \right\|^2 \right] + \frac{\beta E L \eta^2}{2} \sum_{e=0}^{E-1} \sum_{b=0}^{B-1} \alpha_b \sum_{u \in \mathcal{U}_b^{k,e}} \alpha_u \sum_{l=0}^{L_u^{k,e}-1} \left\| \nabla f_u(\mathbf{w}_u^{k,e,l}) \right\|^2 \\
= & \mathbb{E}[f(\mathbf{w}^k)] + \beta \eta^2 \sigma^2 \sum_{e=0}^{E-1} \sum_{b=0}^{B-1} (\alpha_b)^2 \sum_{u \in \mathcal{U}_b^{k,e}} (\alpha_u)^2 L_u^{k,e} + \beta E \eta^2 \sum_{e=0}^{E-1} \sum_{b=0}^{B-1} \alpha_b \sum_{u \in \mathcal{U}_b^{k,e}} \alpha_u L_u^{k,e} \sum_{l=0}^{L_u^{k,e}-1} \left[\frac{1}{\mathbb{P}_{u,sc}^{k,e}} - 1 \right] \mathbb{E} \left[\left\| g_u(\mathbf{w}_u^{k,e,l}) \right\|^2 \right] + \\
& \frac{\eta}{2} \sum_{e=0}^{E-1} \sum_{b=0}^{B-1} \alpha_b \sum_{u \in \mathcal{U}_b^{k,e}} \alpha_u \sum_{l=0}^{L_u^{k,e}-1} \left\| \nabla f(\mathbf{w}^k) - \nabla f_u(\mathbf{w}_u^{k,e,l}) \right\|^2 - \frac{\eta}{2} \sum_{e=0}^{E-1} \sum_{b=0}^{B-1} \alpha_b \sum_{u \in \mathcal{U}_b^{k,e}} \alpha_u L_u^{k,e} \left\| \nabla f(\mathbf{w}^k) \right\|^2 - \\
& \frac{\eta}{2} (1 - \beta \eta E L) \sum_{e=0}^{E-1} \sum_{b=0}^{B-1} \alpha_b \sum_{u \in \mathcal{U}_b^{k,e}} \alpha_u \sum_{l=0}^{L_u^{k,e}-1} \left\| \nabla f_u(\mathbf{w}_u^{k,e,l}) \right\|^2, \tag{55}
\end{aligned}$$

where the last term is non-negative when $\eta \leq \frac{1}{\beta E L}$, as $\|\cdot\| \geq 0$.

To that end, as we are after an upper-bound, we drop the last term using $\eta \leq \frac{1}{\beta E L}$. Then we divide both sides by $\frac{\eta}{2}$, rearrange the terms and take expectations on both sides, which yields

$$\sum_{e=0}^{E-1} \sum_{b=0}^{B-1} \alpha_b \sum_{u \in \mathcal{U}_b^{k,e}} \alpha_u L_u^{k,e} \mathbb{E} \left[\left\| \nabla f(\mathbf{w}^k) \right\|^2 \right] \leq \frac{2(\mathbb{E}[f(\mathbf{w}^k)] - \mathbb{E}[f(\mathbf{w}^{k+1})])}{\eta} + 2\beta \eta \sigma^2 \sum_{e=0}^{E-1} \sum_{b=0}^{B-1} (\alpha_b)^2 \sum_{u \in \mathcal{U}_b^{k,e}} (\alpha_u)^2 L_u^{k,e} +$$

$$2\beta\eta E \sum_{e=0}^{E-1} \sum_{b=0}^{B-1} \alpha_b \sum_{u \in \mathcal{U}_b^{k,e}} \alpha_u L_u^{k,e} \sum_{l=0}^{L_u^{k,e}-1} \left[\frac{1}{\mathbb{P}_{u,sc}^{k,e}} - 1 \right] \mathbb{E} \left[\left\| g_u(\mathbf{w}_u^{k,e,l}) \right\|^2 \right] + \underbrace{\sum_{e=0}^{E-1} \sum_{b=0}^{B-1} \alpha_b \sum_{u \in \mathcal{U}_b^{k,e}} \alpha_u \sum_{l=0}^{L_u^{k,e}-1} \mathbb{E} \left[\left\| \nabla f(\mathbf{w}^k) - \nabla f_u(\mathbf{w}_u^{k,e,l}) \right\|^2 \right]}_{T_3}. \quad (56)$$

We now bound the T_3 term as

$$\begin{aligned} T_3 &\stackrel{(a)}{=} \sum_{e=0}^{E-1} \sum_{b=0}^{B-1} \alpha_b \sum_{u \in \mathcal{U}_b^{k,e}} \alpha_u \sum_{l=0}^{L_u^{k,e}-1} \mathbb{E} \left[\left\| \sum_{b'=0}^{B-1} \alpha_{b'} \sum_{u' \in \mathcal{U}_{b'}^{k,e}} \alpha_{u'} \nabla f_{u'}(\mathbf{w}^k) - \nabla f_u(\mathbf{w}_u^{k,e,l}) \right\|^2 \right] \\ &\stackrel{(b)}{=} \sum_{e=0}^{E-1} \sum_{b=0}^{B-1} \alpha_b \sum_{u \in \mathcal{U}_b^{k,e}} \alpha_u \sum_{l=0}^{L_u^{k,e}-1} \mathbb{E} \left[\left\| \sum_{b'=0}^{B-1} \alpha_{b'} \sum_{u' \in \mathcal{U}_{b'}^{k,e}} \alpha_{u'} \left[\nabla f_{u'}(\mathbf{w}^k) - \nabla f_{u'}(\mathbf{w}_u^{k,e,l}) \right] \right\|^2 \right] \\ &\stackrel{(c)}{\leq} \sum_{e=0}^{E-1} \sum_{b=0}^{B-1} \alpha_b \sum_{u \in \mathcal{U}_b^{k,e}} \alpha_u \sum_{l=0}^{L_u^{k,e}-1} \mathbb{E} \left[\left\| \nabla f_u(\mathbf{w}^k) \pm \nabla f_u(\mathbf{w}_b^{k,e}) - \nabla f_u(\mathbf{w}_u^{k,e,l}) \right\|^2 \right] \\ &\stackrel{(d)}{\leq} 2 \sum_{e=0}^{E-1} \sum_{b=0}^{B-1} \alpha_b \sum_{u \in \mathcal{U}_b^{k,e}} \alpha_u \sum_{l=0}^{L_u^{k,e}-1} \mathbb{E} \left[\left\| \nabla f_u(\mathbf{w}^k) - \nabla f_u(\mathbf{w}_b^{k,e}) \right\|^2 \right] + 2 \sum_{e=0}^{E-1} \sum_{b=0}^{B-1} \alpha_b \sum_{u \in \mathcal{U}_b^{k,e}} \alpha_u \sum_{l=0}^{L_u^{k,e}-1} \mathbb{E} \left[\left\| \nabla f_u(\mathbf{w}_b^{k,e}) - \nabla f_u(\mathbf{w}_u^{k,e,l}) \right\|^2 \right] \\ &\stackrel{(e)}{\leq} 2\beta^2 \sum_{e=0}^{E-1} \sum_{b=0}^{B-1} \alpha_b \sum_{u \in \mathcal{U}_b^{k,e}} \alpha_u \sum_{l=0}^{L_u^{k,e}-1} \mathbb{E} \left[\left\| \mathbf{w}_b^{k,e} - \mathbf{w}_u^{k,e,l} \right\|^2 \right] + 2\beta^2 \sum_{e=0}^{E-1} \sum_{b=0}^{B-1} \alpha_b \sum_{u \in \mathcal{U}_b^{k,e}} \alpha_u L_u^{k,e} \mathbb{E} \left[\left\| \mathbf{w}^k - \mathbf{w}_b^{k,e} \right\|^2 \right] \\ &\stackrel{(f)}{\leq} 2\beta^2 \sum_{e=0}^{E-1} \sum_{b=0}^{B-1} \alpha_b \sum_{u \in \mathcal{U}_b^{k,e}} \alpha_u \sum_{l=0}^{L_u^{k,e}-1} \mathbb{E} \left[\left\| \mathbf{w}_b^{k,e} - \mathbf{w}_u^{k,e,l} \right\|^2 \right] + 2L\beta^2 \sum_{e=0}^{E-1} \sum_{b=0}^{B-1} \alpha_b \mathbb{E} \left[\left\| \mathbf{w}^k - \mathbf{w}_b^{k,e} \right\|^2 \right], \end{aligned} \quad (57)$$

where, in step (a), we use the fact that $\nabla f(\mathbf{w}^k) = \sum_{b'=0}^{B-1} \alpha_{b'} \sum_{u' \in \mathcal{U}_{b'}^{k,e}} \alpha_{u'} \nabla f_{u'}(\mathbf{w}^k)$ by definition of the global loss function in (46). Besides, we write (b) because $\sum_{u \in \mathcal{U}_b^{k,e}} \alpha_u = 1$ and $\sum_{b=0}^{B-1} \alpha_b = 1$. Furthermore, (c) stems from Jensen inequality and (d) appears from the fact $\|\sum_{j=1}^J \mathbf{x}_j\|^2 \leq J \sum_{j=1}^J \|\mathbf{x}_j\|^2$. Moreover, we get to (e) by using β -smoothness assumption. Finally, we write (f) since $1 \leq L_u^{k,e} \leq L$ and $\|\cdot\| \geq 0$.

Now, plugging T_3 into (56) and averaging over K global rounds, we get

$$\begin{aligned} \frac{1}{K} \sum_{k=0}^{K-1} \mathbb{E} \left[\left\| \nabla f(\mathbf{w}^k) \right\|^2 \right] &\leq \frac{2}{\eta K} \sum_{k=0}^{K-1} \left[\frac{\mathbb{E}[f(\mathbf{w}^k)] - \mathbb{E}[f(\mathbf{w}^{k+1})]}{\Omega^k} \right] + \frac{2\beta\eta\sigma^2}{K} \sum_{k=0}^{K-1} \left[\frac{\sum_{e=0}^{E-1} \sum_{b=0}^{B-1} (\alpha_b)^2 \sum_{u \in \mathcal{U}_b^{k,e}} (\alpha_u)^2 L_u^{k,e}}{\Omega^k} \right] + \\ &\frac{2\beta\eta E}{K} \sum_{k=0}^{K-1} \frac{1}{\Omega^k} \sum_{e=0}^{E-1} \sum_{b=0}^{B-1} \alpha_b \sum_{u \in \mathcal{U}_b^{k,e}} \alpha_u L_u^{k,e} \sum_{l=0}^{L_u^{k,e}-1} \left[\frac{1}{\mathbb{P}_{u,sc}^{k,e}} - 1 \right] \mathbb{E} \left[\left\| g_u(\mathbf{w}_u^{k,e,l}) \right\|^2 \right] + \\ &\frac{2L\beta^2}{K} \sum_{k=0}^{K-1} \frac{1}{\Omega^k} \sum_{e=0}^{E-1} \sum_{b=0}^{B-1} \alpha_b \mathbb{E} \left[\left\| \mathbf{w}^k - \mathbf{w}_b^{k,e} \right\|^2 \right] + \frac{2\beta^2}{K} \sum_{k=0}^{K-1} \frac{1}{\Omega^k} \sum_{e=0}^{E-1} \sum_{b=0}^{B-1} \alpha_b \sum_{u \in \mathcal{U}_b^{k,e}} \alpha_u \sum_{l=0}^{L_u^{k,e}-1} \mathbb{E} \left[\left\| \mathbf{w}_b^{k,e} - \mathbf{w}_u^{k,e,l} \right\|^2 \right]. \end{aligned} \quad (58)$$

where $\Omega^k := \sum_{e=0}^{E-1} \sum_{b=0}^{B-1} \alpha_b \sum_{u \in \mathcal{U}_b^{k,e}} \alpha_u L_u^{k,e}$.

Lemma 1. When learning rate $\eta < \min \left\{ \frac{1}{\beta EL}, \frac{1}{3\sqrt{2}\beta L} \right\}$, the mean square error between the local model and the ES model is upper-bounded as

$$\begin{aligned} \frac{1}{K} \sum_{k=0}^{K-1} \frac{1}{\Omega^k} \sum_{e=0}^{E-1} \sum_{b=0}^{B-1} \alpha_b \sum_{u \in \mathcal{U}_b^{k,e}} \alpha_u \sum_{l=0}^{L_u^{k,e}-1} \mathbb{E} \left[\left\| \mathbf{w}_b^{k,e} - \mathbf{w}_u^{k,e,l} \right\|^2 \right] &\leq \frac{3EL^2\eta^2\sigma^2}{K} \sum_{k=0}^{K-1} \frac{1}{\Omega^k} + \frac{9E\varepsilon_0^2\eta^2L^3}{K} \sum_{k=0}^{K-1} \frac{1}{\Omega^k} + \\ &\frac{3L^2\eta^2}{K} \sum_{k=0}^{K-1} \frac{1}{\Omega^k} \sum_{e=0}^{E-1} \sum_{b=0}^{B-1} \alpha_b \sum_{u \in \mathcal{U}_b^{k,e}} \alpha_u \left[\frac{1}{\mathbb{P}_{u,sc}^{k,e}} - 1 \right] \sum_{l=0}^{L_u^{k,e}-1} \mathbb{E} \left[\left\| g_u(\mathbf{w}_u^{k,e,l}) \right\|^2 \right]. \end{aligned} \quad (59)$$

Proof. The proof is left to Appendix B-A. ■

Lemma 2. When learning rate $\eta < \min\left\{\frac{1}{2\sqrt{5}\beta L}, \frac{1}{\beta EL}\right\}$, the mean square error between the edge model at the ES and the global model at the central server is upper-bounded as

$$\begin{aligned} & \frac{1}{K} \sum_{k=0}^{K-1} \frac{1}{\Omega^k} \sum_{e=0}^{E-1} \sum_{b=0}^{B-1} \alpha_b \mathbb{E} \left[\left\| \mathbf{w}^k - \mathbf{w}_b^{k,e} \right\|^2 \right] \\ & \leq \frac{4E\eta^2\sigma^2}{K} \sum_{k=0}^{K-1} \frac{1}{\Omega^k} \sum_{e=0}^{E-1} \sum_{b=0}^{B-1} \alpha_b \sum_{u \in \mathcal{U}_b^{k,e}} (\alpha_u)^2 L_u^{k,e} + \frac{60\beta^2\sigma^2 E^3 L^3 \eta^4}{K} \sum_{k=0}^{K-1} \frac{1}{\Omega^k} + \frac{180\beta^2 \varepsilon_0^2 E^3 L^4 \eta^4}{K} \sum_{k=0}^{K-1} \frac{1}{\Omega^k} + \frac{10\varepsilon_1^2 \eta^2 E^3}{K} \sum_{k=0}^{K-1} \frac{1}{\Omega^k} + \\ & \quad \frac{4E\eta^2}{K} \sum_{k=0}^{K-1} \frac{1}{\Omega^k} \sum_{e=0}^{E-1} \sum_{b=0}^{B-1} \alpha_b \sum_{u \in \mathcal{U}_b^{k,e}} \alpha_u (\alpha_u + 15E\beta^2\eta^2 L^3) \left[\frac{1}{p_{u,sc}^{k,e}} - 1 \right] \sum_{l=0}^{L_u^{k,e}-1} \mathbb{E} \left[\left\| g_u(\mathbf{w}_u^{k,e,l}) \right\|^2 \right]. \end{aligned} \quad (60)$$

Proof. The proof is left to Appendix B-B. ■

Final Results: Using Lemma 1 and Lemma 2, we write

$$\begin{aligned} & \frac{1}{K} \sum_{k=0}^{K-1} \mathbb{E} \left[\left\| \nabla f(\mathbf{w}^k) \right\|^2 \right] \leq \frac{2}{\eta K} \sum_{k=0}^{K-1} \left[\frac{\mathbb{E}[f(\mathbf{w}^k)] - \mathbb{E}[f(\mathbf{w}^{k+1})]}{\Omega^k} \right] + \frac{2\beta\eta\sigma^2}{K} \sum_{k=0}^{K-1} \left[\frac{\sum_{e=0}^{E-1} \sum_{b=0}^{B-1} (\alpha_b)^2 \sum_{u \in \mathcal{U}_b^{k,e}} (\alpha_u)^2 L_u^{k,e}}{\Omega^k} \right] + \\ & \quad \frac{2\beta\eta E}{K} \sum_{k=0}^{K-1} \frac{1}{\Omega^k} \sum_{e=0}^{E-1} \sum_{b=0}^{B-1} \alpha_b \sum_{u \in \mathcal{U}_b^{k,e}} \alpha_u L_u^{k,e} \sum_{l=0}^{L_u^{k,e}-1} \left[\frac{1}{p_{u,sc}^{k,e}} - 1 \right] \mathbb{E} \left[\left\| g_u(\mathbf{w}_u^{k,e,l}) \right\|^2 \right] + \\ & \quad \frac{8EL\beta^2\eta^2\sigma^2}{K} \sum_{k=0}^{K-1} \frac{1}{\Omega^k} \sum_{e=0}^{E-1} \sum_{b=0}^{B-1} \alpha_b \sum_{u \in \mathcal{U}_b^{k,e}} (\alpha_u)^2 L_u^{k,e} + \frac{120\sigma^2 E^3 \beta^4 \eta^4 L^4}{K} \sum_{k=0}^{K-1} \frac{1}{\Omega^k} + \frac{360\varepsilon_0^2 E^3 \beta^4 \eta^4 L^5}{K} \sum_{k=0}^{K-1} \frac{1}{\Omega^k} + \frac{20L\beta^2 \varepsilon_1^2 \eta^2 E^3}{K} \sum_{k=0}^{K-1} \frac{1}{\Omega^k} + \\ & \quad \frac{8EL\beta^2\eta^2}{K} \sum_{k=0}^{K-1} \frac{1}{\Omega^k} \sum_{e=0}^{E-1} \sum_{b=0}^{B-1} \alpha_b \sum_{u \in \mathcal{U}_b^{k,e}} \alpha_u (\alpha_u + 15E\beta^2\eta^2 L^3) \left[\frac{1}{p_{u,sc}^{k,e}} - 1 \right] \sum_{l=0}^{L_u^{k,e}-1} \mathbb{E} \left[\left\| g_u(\mathbf{w}_u^{k,e,l}) \right\|^2 \right] + \frac{6E\beta^2\eta^2\sigma^2 L^2}{K} \sum_{k=0}^{K-1} \frac{1}{\Omega^k} + \\ & \quad \frac{18E\beta^2\varepsilon_0^2\eta^2 L^3}{K} \sum_{k=0}^{K-1} \frac{1}{\Omega^k} + \frac{6\beta^2 L^2 \eta^2}{K} \sum_{k=0}^{K-1} \frac{1}{\Omega^k} \sum_{e=0}^{E-1} \sum_{b=0}^{B-1} \alpha_b \sum_{u \in \mathcal{U}_b^{k,e}} \alpha_u \left[\frac{1}{p_{u,sc}^{k,e}} - 1 \right] \sum_{l=0}^{L_u^{k,e}-1} \mathbb{E} \left[\left\| g_u(\mathbf{w}_u^{k,e,l}) \right\|^2 \right] \\ & \leq \frac{2}{\eta K} \sum_{k=0}^{K-1} \frac{1}{\Omega^k} \left(\mathbb{E}[f(\mathbf{w}^k)] - \mathbb{E}[f(\mathbf{w}^{k+1})] \right) + \frac{2\beta\eta L\sigma^2}{K} \sum_{k=0}^{K-1} \frac{1}{\Omega^k} \left[60\beta^3\eta^3 E^3 L^3 + 3\beta\eta EL + \sum_{e=0}^{E-1} \sum_{b=0}^{B-1} \alpha_b (\alpha_b + 4EL\beta\eta) \sum_{u \in \mathcal{U}_b^{k,e}} (\alpha_u)^2 \right] + \\ & \quad \frac{18E\beta^2\varepsilon_0^2\eta^2 L^3}{K} \sum_{k=0}^{K-1} \frac{1}{\Omega^k} [1 + 20\beta^2\eta^2 E^2 L^2] + \frac{20L\beta^2\varepsilon_1^2\eta^2 E^3}{K} \sum_{k=0}^{K-1} \frac{1}{\Omega^k} + \frac{2\beta\eta L}{K} \sum_{k=0}^{K-1} \frac{1}{\Omega^k} \sum_{e=0}^{E-1} \sum_{b=0}^{B-1} \alpha_b \sum_{u \in \mathcal{U}_b^{k,e}} \alpha_u [E + 3\beta\eta L + \\ & \quad 4\beta\eta E (\alpha_u + 15E\beta^2\eta^2 L^3)] \sum_{l=0}^{L_u^{k,e}-1} \left[\frac{1}{p_{u,sc}^{k,e}} - 1 \right] \mathbb{E} \left[\left\| g_u(\mathbf{w}_u^{k,e,l}) \right\|^2 \right] \\ & = \frac{2}{\eta K} \sum_{k=0}^{K-1} \frac{1}{\Omega^k} \left(\mathbb{E}[f(\mathbf{w}^k)] - \mathbb{E}[f(\mathbf{w}^{k+1})] \right) + \frac{2\beta\eta L\sigma^2}{K} \sum_{k=0}^{K-1} \frac{N_1^k}{\Omega^k} + \frac{18E\beta^2\varepsilon_0^2\eta^2 L^3}{K} \sum_{k=0}^{K-1} \frac{N_2}{\Omega^k} + \frac{20L\beta^2\varepsilon_1^2\eta^2 E^3}{K} \sum_{k=0}^{K-1} \frac{1}{\Omega^k} + \\ & \quad \frac{2\beta\eta L}{K} \sum_{k=0}^{K-1} \frac{1}{\Omega^k} \sum_{e=0}^{E-1} \sum_{b=0}^{B-1} \alpha_b \sum_{u \in \mathcal{U}_b^{k,e}} \alpha_u N_u \left[\frac{1}{p_{u,sc}^{k,e}} - 1 \right] \sum_{l=0}^{L_u^{k,e}-1} \mathbb{E} \left[\left\| g_u(\mathbf{w}_u^{k,e,l}) \right\|^2 \right], \end{aligned} \quad (61)$$

where $N_1^k := 60\beta^3\eta^3 E^3 L^3 + 3\beta\eta EL + \sum_{e=0}^{E-1} \sum_{b=0}^{B-1} \alpha_b (\alpha_b + 4EL\beta\eta) \sum_{u \in \mathcal{U}_b^{k,e}} (\alpha_u)^2$, $N_2 := [1 + 20\beta^2\eta^2 E^2 L^2]$ and $N_u := E + 3\beta\eta L + 4\beta\eta E (\alpha_u + 15E\beta^2\eta^2 L^3)$.

This concludes the proof of Theorem 1. ■

APPENDIX B

MISSING PROOF OF LEMMA 1 AND LEMMA 2

A. Proof of Lemma 1

$$\frac{1}{K} \sum_{k=0}^{K-1} \frac{1}{\Omega^k} \sum_{e=0}^{E-1} \sum_{b=0}^{B-1} \alpha_b \sum_{u \in \mathcal{U}_b^{k,e}} \alpha_u \sum_{l=0}^{L_u^{k,e}-1} \mathbb{E} \left[\left\| \mathbf{w}_b^{k,e} - \mathbf{w}_u^{k,e,l} \right\|^2 \right]$$

$$\begin{aligned}
&\stackrel{(a)}{=} \frac{\eta^2}{K} \sum_{k=0}^{K-1} \frac{1}{\Omega^k} \sum_{e=0}^{E-1} \sum_{b=0}^{B-1} \alpha_b \sum_{u \in \mathcal{U}_b^{k,e}} \alpha_u \sum_{l=0}^{L_u^{k,e}-1} \mathbb{E} \left[\left\| \sum_{l'=0}^{l-1} g(\mathbf{w}_u^{k,e,l'}) - \sum_{u' \in \mathcal{U}_b} \alpha_{u'} \frac{1^{k,e}}{P_{u',sc}^{k,e}} \sum_{l'=0}^{l-1} g(\mathbf{w}_{u'}^{k,e,l'}) \right\|^2 \right] \\
&= \frac{\eta^2}{K} \sum_{k=0}^{K-1} \frac{1}{\Omega^k} \sum_{e=0}^{E-1} \sum_{b=0}^{B-1} \alpha_b \sum_{u \in \mathcal{U}_b^{k,e}} \alpha_u \sum_{l=0}^{L_u^{k,e}-1} \mathbb{E} \left[\left\| \sum_{l'=0}^{l-1} g(\mathbf{w}_u^{k,e,l'}) \pm \sum_{l'=0}^{l-1} \nabla f_u(\mathbf{w}_u^{k,e,l'}) - \sum_{u' \in \mathcal{U}_b} \alpha_{u'} \frac{1^{k,e}}{P_{u',sc}^{k,e}} \sum_{l'=0}^{l-1} g(\mathbf{w}_{u'}^{k,e,l'}) \right. \right. \\
&\quad \left. \left. \pm \sum_{u' \in \mathcal{U}_b} \alpha_{u'} \sum_{l'=0}^{l-1} g(\mathbf{w}_{u'}^{k,e,l'}) \pm \sum_{u' \in \mathcal{U}_b} \alpha_{u'} \sum_{l'=0}^{l-1} \nabla f_{u'}(\mathbf{w}_{u'}^{k,e,l'}) \right\|^2 \right] \\
&\leq \frac{3\eta^2}{K} \sum_{k=0}^{K-1} \frac{1}{\Omega^k} \sum_{e=0}^{E-1} \sum_{b=0}^{B-1} \alpha_b \sum_{u \in \mathcal{U}_b^{k,e}} \alpha_u \sum_{l=0}^{L_u^{k,e}-1} \mathbb{E} \left[\left\| \sum_{l'=0}^{l-1} \left[g(\mathbf{w}_u^{k,e,l'}) - \nabla f_u(\mathbf{w}_u^{k,e,l'}) \right] - \right. \right. \\
&\quad \left. \left. \sum_{u' \in \mathcal{U}_b} \alpha_{u'} \sum_{l'=0}^{l-1} \left[g(\mathbf{w}_{u'}^{k,e,l'}) - \nabla f_{u'}(\mathbf{w}_{u'}^{k,e,l'}) \right] \right\|^2 \right] + \\
&\quad \frac{3\eta^2}{K} \sum_{k=0}^{K-1} \frac{1}{\Omega^k} \sum_{e=0}^{E-1} \sum_{b=0}^{B-1} \alpha_b \sum_{u \in \mathcal{U}_b^{k,e}} \alpha_u \sum_{l=0}^{L_u^{k,e}-1} \mathbb{E} \left[\left\| \sum_{l'=0}^{l-1} \nabla f_u(\mathbf{w}_u^{k,e,l'}) - \sum_{u' \in \mathcal{U}_b} \alpha_{u'} \sum_{l'=0}^{l-1} \nabla f_{u'}(\mathbf{w}_{u'}^{k,e,l'}) \right\|^2 \right] + \\
&\quad \frac{3\eta^2}{K} \sum_{k=0}^{K-1} \frac{1}{\Omega^k} \sum_{e=0}^{E-1} \sum_{b=0}^{B-1} \alpha_b \sum_{u \in \mathcal{U}_b^{k,e}} \alpha_u \sum_{l=0}^{L_u^{k,e}-1} \mathbb{E} \left[\left\| \sum_{u' \in \mathcal{U}_b} \alpha_{u'} \sum_{l'=0}^{l-1} g(\mathbf{w}_{u'}^{k,e,l'}) \left[1 - \frac{1^{k,e}}{P_{u',sc}^{k,e}} \right] \right\|^2 \right], \tag{62}
\end{aligned}$$

where we get (a) due to the fact that the client received the same model from the ES during the synchronization time. Besides, the change in the ES' model is captured for all $0 \leq l' \leq l-1$ SGD rounds, and the aggregation rule follows (44) to indicate whether these gradients are received at the ES.

The first term of (62) is upper bounded as

$$\begin{aligned}
&\frac{3\eta^2}{K} \sum_{k=0}^{K-1} \frac{1}{\Omega^k} \sum_{e=0}^{E-1} \sum_{b=0}^{B-1} \alpha_b \sum_{u \in \mathcal{U}_b^{k,e}} \alpha_u \sum_{l=0}^{L_u^{k,e}-1} \mathbb{E} \left[\left\| \sum_{l'=0}^{l-1} \left[\left(g(\mathbf{w}_u^{k,e,l'}) - \nabla f_u(\mathbf{w}_u^{k,e,l'}) \right) - \sum_{u' \in \mathcal{U}_b^{k,e}} \alpha_{u'} \left(g(\mathbf{w}_{u'}^{k,e,l'}) - \nabla f_{u'}(\mathbf{w}_{u'}^{k,e,l'}) \right) \right] \right\|^2 \right] \\
&= \frac{3\eta^2}{K} \sum_{k=0}^{K-1} \frac{1}{\Omega^k} \sum_{e=0}^{E-1} \sum_{b=0}^{B-1} \alpha_b \sum_{u \in \mathcal{U}_b^{k,e}} \alpha_u \sum_{l=0}^{L_u^{k,e}-1} \mathbb{E} \left[\sum_{l'=0}^{l-1} \left\| \left(g(\mathbf{w}_u^{k,e,l'}) - \nabla f_u(\mathbf{w}_u^{k,e,l'}) \right) - \sum_{u' \in \mathcal{U}_b^{k,e}} \alpha_{u'} \left(g(\mathbf{w}_{u'}^{k,e,l'}) - \nabla f_{u'}(\mathbf{w}_{u'}^{k,e,l'}) \right) \right\|^2 \right] + \\
&\quad \sum_{l'=0}^{l-1} \left\{ \left(g(\mathbf{w}_u^{k,e,l'}) - \nabla f_u(\mathbf{w}_u^{k,e,l'}) \right) - \sum_{u' \in \mathcal{U}_b^{k,e}} \alpha_{u'} \left(g(\mathbf{w}_{u'}^{k,e,l'}) - \nabla f_{u'}(\mathbf{w}_{u'}^{k,e,l'}) \right) \right\} \times \sum_{l''=0, l'' \neq l'}^{l-1} \left\{ \left(g(\mathbf{w}_u^{k,e,l''}) - \nabla f_u(\mathbf{w}_u^{k,e,l''}) \right) - \right. \\
&\quad \left. \sum_{u' \in \mathcal{U}_b^{k,e}} \alpha_{u'} \left(g(\mathbf{w}_{u'}^{k,e,l''}) - \nabla f_{u'}(\mathbf{w}_{u'}^{k,e,l''}) \right) \right\} \\
&\stackrel{(a)}{=} \frac{3\eta^2}{K} \sum_{k=0}^{K-1} \frac{1}{\Omega^k} \sum_{e=0}^{E-1} \sum_{b=0}^{B-1} \alpha_b \sum_{u \in \mathcal{U}_b^{k,e}} \alpha_u \sum_{l=0}^{L_u^{k,e}-1} \sum_{l'=0}^{l-1} \mathbb{E} \left[\left\| \left(g(\mathbf{w}_u^{k,e,l'}) - \nabla f_u(\mathbf{w}_u^{k,e,l'}) \right) - \sum_{u' \in \mathcal{U}_b^{k,e}} \alpha_{u'} \left(g(\mathbf{w}_{u'}^{k,e,l'}) - \nabla f_{u'}(\mathbf{w}_{u'}^{k,e,l'}) \right) \right\|^2 \right] \\
&\stackrel{(b)}{\leq} \frac{3L\eta^2}{K} \sum_{k=0}^{K-1} \frac{1}{\Omega^k} \sum_{e=0}^{E-1} \sum_{b=0}^{B-1} \alpha_b \sum_{u \in \mathcal{U}_b^{k,e}} \alpha_u \sum_{l=0}^{L_u^{k,e}-1} \mathbb{E} \left[\left\| \left(g_u(\mathbf{w}_u^{k,e,l}) - \nabla f_u(\mathbf{w}_u^{k,e,l}) \right) - \sum_{u' \in \mathcal{U}_b^{k,e}} \alpha_{u'} \left(g(\mathbf{w}_{u'}^{k,e,l}) - \nabla f_{u'}(\mathbf{w}_{u'}^{k,e,l}) \right) \right\|^2 \right] \\
&\stackrel{(c)}{=} \frac{3L\eta^2}{K} \sum_{k=0}^{K-1} \frac{1}{\Omega^k} \sum_{e=0}^{E-1} \sum_{b=0}^{B-1} \sum_{l=0}^{L_u^{k,e}-1} \alpha_u \mathbb{E} \left[\left\| g_u(\mathbf{w}_u^{k,e,l}) - \nabla f_u(\mathbf{w}_u^{k,e,l}) \right\|^2 \right] - \\
&\quad \frac{3L\eta^2}{K} \sum_{k=0}^{K-1} \frac{1}{\Omega^k} \sum_{e=0}^{E-1} \sum_{b=0}^{B-1} \sum_{l=0}^{L_u^{k,e}-1} \mathbb{E} \left[\left\| \sum_{u' \in \mathcal{U}_b^{k,e}} \alpha_{u'} \left(g(\mathbf{w}_{u'}^{k,e,l}) - \nabla f_{u'}(\mathbf{w}_{u'}^{k,e,l}) \right) \right\|^2 \right] \\
&\stackrel{(d)}{\leq} \frac{3L\eta^2}{K} \sum_{k=0}^{K-1} \frac{1}{\Omega^k} \sum_{e=0}^{E-1} \sum_{b=0}^{B-1} \sum_{l=0}^{L_u^{k,e}-1} \alpha_u \sigma^2 - \frac{3L\eta^2}{K} \sum_{k=0}^{K-1} \frac{1}{\Omega^k} \sum_{e=0}^{E-1} \sum_{b=0}^{B-1} \sum_{l=0}^{L_u^{k,e}-1} \sum_{u' \in \mathcal{U}_b^{k,e}} (\alpha_{u'})^2 \mathbb{E} \left[\left\| g(\mathbf{w}_{u'}^{k,e,l}) - \nabla f_{u'}(\mathbf{w}_{u'}^{k,e,l}) \right\|^2 \right]
\end{aligned}$$

$$\begin{aligned}
&\stackrel{(e)}{\leq} \frac{3EL^2\eta^2\sigma^2}{K} \sum_{k=0}^{K-1} \frac{1}{\Omega^k} - \frac{3L^2\eta^2\sigma^2}{K} \sum_{k=0}^{K-1} \frac{1}{\Omega^k} \sum_{e=0}^{E-1} \sum_{b=0}^{B-1} \alpha_b \\
&\leq \frac{3EL^2\eta^2\sigma^2}{K} \sum_{k=0}^{K-1} \frac{1}{\Omega^k}, \tag{63}
\end{aligned}$$

where (a) stems from time independence of the mini-batch gradients and $\mathbb{E}[g_u(\mathbf{w}_u^{k,e,l})] = \nabla f_u(\mathbf{w}_u^{k,e,l})$, which makes the expectation of the cross product terms 0. Besides, we used the fact that $l \leq L_u^{k,e}$ and $1 \leq L_u^{k,e} \leq L$ in (b). In (c), $\sum_{j=1}^J \alpha_j \|\mathbf{x}_j - \bar{\mathbf{x}}\|^2 = \sum_{j=1}^J \alpha_j \|\mathbf{x}_j\|^2 - \|\bar{\mathbf{x}}\|^2$, where $\bar{\mathbf{x}} = \sum_{j=1}^J \alpha_j \mathbf{x}_j$. In (d) and (e), we use the bounded variance of the SGD assumptions and independence of SGDs in different epochs.

For the second term of (62), we write

$$\begin{aligned}
&\frac{3\eta^2}{K} \sum_{k=0}^{K-1} \frac{1}{\Omega^k} \sum_{e=0}^{E-1} \sum_{b=0}^{B-1} \alpha_b \sum_{u \in \mathcal{U}_b^{k,e}} \alpha_u \sum_{l=0}^{L_u^{k,e}-1} \mathbb{E} \left[\left\| \sum_{l'=0}^{l-1} \left(\nabla f_u(\mathbf{w}_u^{k,e,l'}) - \sum_{u' \in \mathcal{U}_b} \alpha_{u'} \nabla f_{u'}(\mathbf{w}_{u'}^{k,e,l'}) \right) \right\|^2 \right] \\
&\leq \frac{3L\eta^2}{K} \sum_{k=0}^{K-1} \frac{1}{\Omega^k} \sum_{e=0}^{E-1} \sum_{b=0}^{B-1} \alpha_b \sum_{u \in \mathcal{U}_b^{k,e}} \alpha_u \sum_{l=0}^{L_u^{k,e}-1} \sum_{l'=0}^{l-1} \mathbb{E} \left[\left\| \nabla f_u(\mathbf{w}_u^{k,e,l'}) - \sum_{u' \in \mathcal{U}_b} \alpha_{u'} \nabla f_{u'}(\mathbf{w}_{u'}^{k,e,l'}) \right\|^2 \right] \\
&\leq \frac{3L^2\eta^2}{K} \sum_{k=0}^{K-1} \frac{1}{\Omega^k} \sum_{e=0}^{E-1} \sum_{b=0}^{B-1} \alpha_b \sum_{u \in \mathcal{U}_b^{k,e}} \alpha_u \sum_{l=0}^{L_u^{k,e}-1} \mathbb{E} \left[\left\| \nabla f_u(\mathbf{w}_u^{k,e,l}) \pm \nabla f_u(\mathbf{w}_b^{k,e}) \pm \sum_{u' \in \mathcal{U}_b} \alpha_{u'} \nabla f_{u'}(\mathbf{w}_b^{k,e}) - \sum_{u' \in \mathcal{U}_b} \alpha_{u'} \nabla f_{u'}(\mathbf{w}_{u'}^{k,e,l}) \right\|^2 \right] \\
&\leq \frac{9L^2\eta^2}{K} \sum_{k=0}^{K-1} \frac{1}{\Omega^k} \sum_{e=0}^{E-1} \sum_{b=0}^{B-1} \alpha_b \sum_{u \in \mathcal{U}_b^{k,e}} \alpha_u \sum_{l=0}^{L_u^{k,e}-1} \mathbb{E} \left[\left\| \nabla f_u(\mathbf{w}_u^{k,e,l}) - \nabla f_u(\mathbf{w}_b^{k,e}) \right\|^2 \right] + \\
&\quad \frac{9L^2\eta^2}{K} \sum_{k=0}^{K-1} \frac{1}{\Omega^k} \sum_{e=0}^{E-1} \sum_{b=0}^{B-1} \alpha_b \sum_{u \in \mathcal{U}_b^{k,e}} \alpha_u \sum_{l=0}^{L_u^{k,e}-1} \mathbb{E} \left[\left\| \nabla f_u(\mathbf{w}_b^{k,e}) - \sum_{u' \in \mathcal{U}_b} \alpha_{u'} \nabla f_{u'}(\mathbf{w}_b^{k,e}) \right\|^2 \right] + \\
&\quad \frac{9L^2\eta^2}{K} \sum_{k=0}^{K-1} \frac{1}{\Omega^k} \sum_{e=0}^{E-1} \sum_{b=0}^{B-1} \alpha_b \sum_{u \in \mathcal{U}_b^{k,e}} \alpha_u \sum_{l=0}^{L_u^{k,e}-1} \mathbb{E} \left[\left\| \sum_{u' \in \mathcal{U}_b} \alpha_{u'} \nabla f_{u'}(\mathbf{w}_b^{k,e}) - \sum_{u' \in \mathcal{U}_b} \alpha_{u'} \nabla f_{u'}(\mathbf{w}_{u'}^{k,e,l}) \right\|^2 \right] \\
&\leq \frac{9L^2\beta^2\eta^2}{K} \sum_{k=0}^{K-1} \frac{1}{\Omega^k} \sum_{e=0}^{E-1} \sum_{b=0}^{B-1} \alpha_b \sum_{u \in \mathcal{U}_b^{k,e}} \alpha_u \sum_{l=0}^{L_u^{k,e}-1} \mathbb{E} \left[\left\| \mathbf{w}_b^{k,e} - \mathbf{w}_u^{k,e,l} \right\|^2 \right] + \\
&\quad \frac{9L^2\eta^2}{K} \sum_{k=0}^{K-1} \frac{1}{\Omega^k} \sum_{e=0}^{E-1} \sum_{b=0}^{B-1} \alpha_b \sum_{u \in \mathcal{U}_b^{k,e}} \alpha_u \sum_{l=0}^{L_u^{k,e}-1} \mathbb{E} \left[\left\| \nabla f_u(\mathbf{w}_b^{k,e}) - \nabla f_b(\mathbf{w}_b^{k,e}) \right\|^2 \right] + \\
&\quad \frac{9L^2\beta^2\eta^2}{K} \sum_{k=0}^{K-1} \frac{1}{\Omega^k} \sum_{e=0}^{E-1} \sum_{b=0}^{B-1} \alpha_b \sum_{u \in \mathcal{U}_b^{k,e}} \alpha_u \sum_{l=0}^{L_u^{k,e}-1} \mathbb{E} \left[\left\| \mathbf{w}_b^{k,e} - \mathbf{w}_u^{k,e,l} \right\|^2 \right] \\
&\leq \frac{18L^2\beta^2\eta^2}{K} \sum_{k=0}^{K-1} \frac{1}{\Omega^k} \sum_{e=0}^{E-1} \sum_{b=0}^{B-1} \alpha_b \sum_{u \in \mathcal{U}_b^{k,e}} \alpha_u \sum_{l=0}^{L_u^{k,e}-1} \mathbb{E} \left[\left\| \mathbf{w}_b^{k,e} - \mathbf{w}_u^{k,e,l} \right\|^2 \right] + \frac{9L^2\eta^2}{K} \sum_{k=0}^{K-1} \frac{1}{\Omega^k} \sum_{e=0}^{E-1} \sum_{b=0}^{B-1} \alpha_b \sum_{u \in \mathcal{U}_b^{k,e}} \alpha_u \sum_{l=0}^{L_u^{k,e}-1} \varepsilon_0^2 \\
&\leq \frac{9E\varepsilon_0^2\eta^2L^3}{K} \sum_{k=0}^{K-1} \frac{1}{\Omega^k} + \frac{18L^2\beta^2\eta^2}{K} \sum_{k=0}^{K-1} \frac{1}{\Omega^k} \sum_{e=0}^{E-1} \sum_{b=0}^{B-1} \alpha_b \sum_{u \in \mathcal{U}_b^{k,e}} \alpha_u \sum_{l=0}^{L_u^{k,e}-1} \mathbb{E} \left[\left\| \mathbf{w}_b^{k,e} - \mathbf{w}_u^{k,e,l} \right\|^2 \right]. \tag{64}
\end{aligned}$$

For the third term of (62), we write

$$\begin{aligned}
&\frac{3\eta^2}{K} \sum_{k=0}^{K-1} \frac{1}{\Omega^k} \sum_{e=0}^{E-1} \sum_{b=0}^{B-1} \alpha_b \sum_{u \in \mathcal{U}_b^{k,e}} \alpha_u \sum_{l=0}^{L_u^{k,e}-1} \mathbb{E} \left[\left\| \sum_{u' \in \mathcal{U}_b} \alpha_{u'} \sum_{l'=0}^{l-1} g(\mathbf{w}_{u'}^{k,e,l'}) \left[1 - \frac{1_{u',sc}^{k,e}}{P_{u',sc}^{k,e}} \right] \right\|^2 \right] \\
&\leq \frac{3L\eta^2}{K} \sum_{k=0}^{K-1} \frac{1}{\Omega^k} \sum_{e=0}^{E-1} \sum_{b=0}^{B-1} \alpha_b \sum_{u \in \mathcal{U}_b^{k,e}} \alpha_u \sum_{l=0}^{L_u^{k,e}-1} \sum_{l'=0}^{l-1} \mathbb{E} \left[\left\| g(\mathbf{w}_u^{k,e,l'}) \left[1 - \frac{1_{u,sc}^{k,e}}{P_{u,sc}^{k,e}} \right] \right\|^2 \right] \\
&\leq \frac{3L^2\eta^2}{K} \sum_{k=0}^{K-1} \frac{1}{\Omega^k} \sum_{e=0}^{E-1} \sum_{b=0}^{B-1} \alpha_b \sum_{u \in \mathcal{U}_b^{k,e}} \alpha_u \sum_{l=0}^{L_u^{k,e}-1} \mathbb{E} \left[\left\| g_u(\mathbf{w}_u^{k,e,l}) \left[1 - \frac{1_{u,sc}^{k,e}}{P_{u,sc}^{k,e}} \right] \right\|^2 \right]
\end{aligned}$$

$$= \frac{3L^2\eta^2}{K} \sum_{k=0}^{K-1} \frac{1}{\Omega^k} \sum_{e=0}^{E-1} \sum_{b=0}^{B-1} \alpha_b \sum_{u \in \mathcal{U}_b^{k,e}} \alpha_u \left[\frac{1}{\mathbb{P}_{u,\text{sc}}^{k,e}} - 1 \right] \sum_{l=0}^{L_u^{k,e}-1} \mathbb{E} \left[\left\| g_u(\mathbf{w}_u^{k,e,l}) \right\|^2 \right] \quad (65)$$

To this end, plugging (63), (64) and (65) into (62), and rearranging the terms, we get

$$\begin{aligned} & \frac{1}{K} \sum_{k=0}^{K-1} \frac{1}{\Omega^k} \sum_{e=0}^{E-1} \sum_{b=0}^{B-1} \alpha_b \sum_{u \in \mathcal{U}_b^{k,e}} \alpha_u \sum_{l=0}^{L_u^{k,e}-1} \mathbb{E} \left[\left\| \mathbf{w}_b^{k,e} - \mathbf{w}_u^{k,e,l} \right\|^2 \right] \\ & \leq \frac{\frac{3EL^2\eta^2\sigma^2}{K} \sum_{k=0}^{K-1} \frac{1}{\Omega^k} + \frac{9E\varepsilon_0^2\eta^2L^3}{K} \sum_{k=0}^{K-1} \frac{1}{\Omega^k} + \frac{3L^2\eta^2}{K} \sum_{k=0}^{K-1} \frac{1}{\Omega^k} \sum_{e=0}^{E-1} \sum_{b=0}^{B-1} \alpha_b \sum_{u \in \mathcal{U}_b^{k,e}} \alpha_u \left[\frac{1}{\mathbb{P}_{u,\text{sc}}^{k,e}} - 1 \right] \sum_{l=0}^{L_u^{k,e}-1} \mathbb{E} \left[\left\| g_u(\mathbf{w}_u^{k,e,l}) \right\|^2 \right]}{1 - 18\beta^2\eta^2L^2} \end{aligned} \quad (66)$$

Notice that, when learning rate $\eta < \frac{1}{3\sqrt{2}\beta L}$, we have $0 < (1 - 18\beta^2\eta^2L^2) < 1$. Besides, we can assume that $\eta < \min \left\{ \frac{1}{3\sqrt{2}\beta L}, \frac{1}{\beta EL} \right\}$ to satisfy all assumptions for the learning rate. As such, we write the upper bound as

$$\begin{aligned} & \frac{1}{K} \sum_{k=0}^{K-1} \frac{1}{\Omega^k} \sum_{e=0}^{E-1} \sum_{b=0}^{B-1} \alpha_b \sum_{u \in \mathcal{U}_b^{k,e}} \alpha_u \sum_{l=0}^{L_u^{k,e}-1} \mathbb{E} \left[\left\| \mathbf{w}_b^{k,e} - \mathbf{w}_u^{k,e,l} \right\|^2 \right] \\ & \leq \frac{3EL^2\eta^2\sigma^2}{K} \sum_{k=0}^{K-1} \frac{1}{\Omega^k} + \frac{9E\varepsilon_0^2\eta^2L^3}{K} \sum_{k=0}^{K-1} \frac{1}{\Omega^k} + \frac{3L^2\eta^2}{K} \sum_{k=0}^{K-1} \frac{1}{\Omega^k} \sum_{e=0}^{E-1} \sum_{b=0}^{B-1} \alpha_b \sum_{u \in \mathcal{U}_b^{k,e}} \alpha_u \left[\frac{1}{\mathbb{P}_{u,\text{sc}}^{k,e}} - 1 \right] \sum_{l=0}^{L_u^{k,e}-1} \mathbb{E} \left[\left\| g_u(\mathbf{w}_u^{k,e,l}) \right\|^2 \right]. \end{aligned} \quad (67)$$

This concludes the proof of Lemma 1.

B. Proof of Lemma 2

$$\begin{aligned} & \frac{1}{K} \sum_{k=0}^{K-1} \frac{1}{\Omega^k} \sum_{e=0}^{E-1} \sum_{b=0}^{B-1} \alpha_b \mathbb{E} \left[\left\| \mathbf{w}^k - \mathbf{w}_b^{k,e} \right\|^2 \right] \\ & = \frac{\eta^2}{K} \sum_{k=0}^{K-1} \frac{1}{\Omega^k} \sum_{e=0}^{E-1} \sum_{b=0}^{B-1} \alpha_b \mathbb{E} \left[\left\| \sum_{e'=0}^{e-1} \sum_{u \in \mathcal{U}_b^{k,e'}} \alpha_u \frac{1_{u,\text{sc}}^{k,e'}}{\mathbb{P}_{u,\text{sc}}^{k,e'}} \mathbf{g}_u^{k,e'} - \sum_{e'=0}^{e-1} \sum_{b'=0}^{B-1} \alpha_{b'} \sum_{u' \in \mathcal{U}_{b'}^{k,e'}} \alpha_{u'} \frac{1_{u',\text{sc}}^{k,e'}}{\mathbb{P}_{u',\text{sc}}^{k,e'}} \mathbf{g}_{u'}^{k,e'} \right\|^2 \right] \\ & = \frac{\eta^2}{K} \sum_{k=0}^{K-1} \frac{1}{\Omega^k} \sum_{e=0}^{E-1} \sum_{b=0}^{B-1} \alpha_b \mathbb{E} \left[\left\| \sum_{e'=0}^{e-1} \left\{ \sum_{u \in \mathcal{U}_b^{k,e'}} \alpha_u \sum_{l=0}^{L_u^{k,e'}-1} \left(\frac{1_{u,\text{sc}}^{k,e'}}{\mathbb{P}_{u,\text{sc}}^{k,e'}} g_u(\mathbf{w}_u^{k,e',l}) \pm \nabla f_u(\mathbf{w}_u^{k,e',l}) \right) - \right. \right. \right. \\ & \quad \left. \left. \left. \sum_{b'=0}^B \alpha_{b'} \sum_{u' \in \mathcal{U}_{b'}^{k,e'}} \alpha_{u'} \sum_{l=0}^{L_{u'}^{k,e'}-1} \left(\frac{1_{u',\text{sc}}^{k,e'}}{\mathbb{P}_{u',\text{sc}}^{k,e'}} g(\mathbf{w}_{u'}^{k,e',l}) \pm \nabla f_{u'}(\mathbf{w}_{u'}^{k,e',l}) \right) \right\} \right\|^2 \right] \\ & \leq \frac{2\eta^2}{K} \sum_{k=0}^{K-1} \frac{1}{\Omega^k} \sum_{e=0}^{E-1} \sum_{b=0}^{B-1} \alpha_b \mathbb{E} \left[\left\| \sum_{e'=0}^{e-1} \left\{ \sum_{u \in \mathcal{U}_b^{k,e'}} \alpha_u \sum_{l=0}^{L_u^{k,e'}-1} \left(\frac{1_{u,\text{sc}}^{k,e'}}{\mathbb{P}_{u,\text{sc}}^{k,e'}} g_u(\mathbf{w}_u^{k,e',l}) - \nabla f_u(\mathbf{w}_u^{k,e',l}) \right) - \right. \right. \right. \\ & \quad \left. \left. \left. \sum_{b'=0}^B \alpha_{b'} \sum_{u' \in \mathcal{U}_{b'}^{k,e'}} \alpha_{u'} \sum_{l=0}^{L_{u'}^{k,e'}-1} \left(\frac{1_{u',\text{sc}}^{k,e'}}{\mathbb{P}_{u',\text{sc}}^{k,e'}} g(\mathbf{w}_{u'}^{k,e',l}) - \nabla f_{u'}(\mathbf{w}_{u'}^{k,e',l}) \right) \right\} \right\|^2 \right] + \\ & \quad \frac{2\eta^2}{K} \sum_{k=0}^{K-1} \frac{1}{\Omega^k} \sum_{e=0}^{E-1} \sum_{b=0}^{B-1} \alpha_b \mathbb{E} \left[\left\| \sum_{e'=0}^{e-1} \left\{ \sum_{u \in \mathcal{U}_b^{k,e'}} \alpha_u \sum_{l=0}^{L_u^{k,e'}-1} \nabla f_u(\mathbf{w}_u^{k,e',l}) - \sum_{b'=0}^B \alpha_{b'} \sum_{u' \in \mathcal{U}_{b'}^{k,e'}} \alpha_{u'} \sum_{l=0}^{L_{u'}^{k,e'}-1} \nabla f_{u'}(\mathbf{w}_{u'}^{k,e',l}) \right\} \right\|^2 \right], \end{aligned} \quad (68)$$

The first part of (68) is simplified as

$$\frac{2\eta^2}{K} \sum_{k=0}^{K-1} \frac{1}{\Omega^k} \sum_{e=0}^{E-1} \sum_{b=0}^{B-1} \alpha_b \mathbb{E} \left[\left\| \sum_{e'=0}^{e-1} \left\{ \sum_{u \in \mathcal{U}_b^{k,e'}} \alpha_u \sum_{l=0}^{L_u^{k,e'}-1} \left(\frac{1_{u,\text{sc}}^{k,e'}}{\mathbb{P}_{u,\text{sc}}^{k,e'}} g_u(\mathbf{w}_u^{k,e',l}) - \nabla f_u(\mathbf{w}_u^{k,e',l}) \right) - \right. \right. \right.$$

$$\begin{aligned}
& \left. \sum_{b'=0}^B \alpha_{b'} \sum_{u' \in \mathcal{Q}_b^{k,e'}} \alpha_{u'} \sum_{l=0}^{L_{u'}^{k,e'}-1} \left(\frac{1_{u',sc}^{k,e'}}{P_{u',sc}} g(\mathbf{w}_{u'}^{k,e',l}) - \nabla f_{u'}(\mathbf{w}_{u'}^{k,e',l}) \right) \right\| \Bigg\|^2 \\
\stackrel{(a)}{=} & \frac{2\eta^2}{K} \sum_{k=0}^{K-1} \frac{1}{\Omega^k} \sum_{e=0}^{E-1} \sum_{b=0}^{B-1} \alpha_b \mathbb{E} \left[\left\| \sum_{e'=0}^{e-1} \left\{ \sum_{u \in \mathcal{Q}_b^{k,e'}} \alpha_u \sum_{l=0}^{L_u^{k,e'}-1} \left(\frac{1_{u,sc}^{k,e'}}{P_{u,sc}} g_u(\mathbf{w}_u^{k,e',l}) - \nabla f_u(\mathbf{w}_u^{k,e',l}) \right) \right\} \right\|^2 \right] - \\
& \frac{2\eta^2}{K} \sum_{k=0}^{K-1} \frac{1}{\Omega^k} \sum_{e=0}^{E-1} \mathbb{E} \left[\left\| \sum_{e'=0}^{e-1} \left\{ \sum_{b=0}^B \sum_{u \in \mathcal{Q}_b^{k,e'}} \alpha_u \sum_{l=0}^{L_u^{k,e'}-1} \left(\frac{1_{u,sc}^{k,e'}}{P_{u,sc}} g_u(\mathbf{w}_u^{k,e',l}) - \nabla f_u(\mathbf{w}_u^{k,e',l}) \right) \right\} \right\|^2 \right] \\
\stackrel{(b)}{=} & \frac{2\eta^2}{K} \sum_{k=0}^{K-1} \frac{1}{\Omega^k} \sum_{e=0}^{E-1} \sum_{b=0}^{B-1} \alpha_b \sum_{e'=0}^{e-1} \mathbb{E} \left[\left\| \sum_{u \in \mathcal{Q}_b^{k,e'}} \alpha_u \sum_{l=0}^{L_u^{k,e'}-1} \left(\frac{1_{u,sc}^{k,e'}}{P_{u,sc}} g_u(\mathbf{w}_u^{k,e',l}) - \nabla f_u(\mathbf{w}_u^{k,e',l}) \right) \right\|^2 \right] - \\
& \frac{2\eta^2}{K} \sum_{k=0}^{K-1} \frac{1}{\Omega^k} \sum_{e=0}^{E-1} \sum_{e'=0}^{e-1} \mathbb{E} \left[\left\| \sum_{b=0}^B \sum_{u \in \mathcal{Q}_b^{k,e'}} \alpha_u \sum_{l=0}^{L_u^{k,e'}-1} \left(\frac{1_{u,sc}^{k,e'}}{P_{u,sc}} g_u(\mathbf{w}_u^{k,e',l}) - \nabla f_u(\mathbf{w}_u^{k,e',l}) \right) \right\|^2 \right] \\
\stackrel{(c)}{\leq} & \frac{2E\eta^2}{K} \sum_{k=0}^{K-1} \frac{1}{\Omega^k} \sum_{e=0}^{E-1} \sum_{b=0}^{B-1} \alpha_b \mathbb{E} \left[\left\| \sum_{u \in \mathcal{Q}_b^{k,e}} \alpha_u \sum_{l=0}^{L_u^{k,e}-1} \left(\frac{1_{u,sc}^{k,e}}{P_{u,sc}} g_u(\mathbf{w}_u^{k,e,l}) - \nabla f_u(\mathbf{w}_u^{k,e,l}) \right) \right\|^2 \right] - \\
& \frac{2E\eta^2}{K} \sum_{k=0}^{K-1} \frac{1}{\Omega^k} \sum_{e=0}^{E-1} \mathbb{E} \left[\left\| \sum_{b=0}^B \sum_{u \in \mathcal{Q}_b^{k,e}} \alpha_u \sum_{l=0}^{L_u^{k,e}-1} \left(\frac{1_{u,sc}^{k,e}}{P_{u,sc}} g_u(\mathbf{w}_u^{k,e,l}) - \nabla f_u(\mathbf{w}_u^{k,e,l}) \right) \right\|^2 \right] \\
\stackrel{(d)}{=} & \frac{2E\eta^2}{K} \sum_{k=0}^{K-1} \frac{1}{\Omega^k} \sum_{e=0}^{E-1} \sum_{b=0}^{B-1} \alpha_b \sum_{u \in \mathcal{Q}_b^{k,e}} (\alpha_u)^2 \sum_{l=0}^{L_u^{k,e}-1} \mathbb{E} \left[\left\| \frac{1_{u,sc}^{k,e}}{P_{u,sc}} g_u(\mathbf{w}_u^{k,e,l}) - \nabla f_u(\mathbf{w}_u^{k,e,l}) \right\|^2 \right] - \\
& \frac{2E\eta^2}{K} \sum_{k=0}^{K-1} \frac{1}{\Omega^k} \sum_{e=0}^{E-1} \sum_{b=0}^B (\alpha_b)^2 \sum_{u \in \mathcal{Q}_b^{k,e}} (\alpha_u)^2 \sum_{l=0}^{L_u^{k,e}-1} \mathbb{E} \left[\left\| \frac{1_{u,sc}^{k,e}}{P_{u,sc}} g_u(\mathbf{w}_u^{k,e,l}) - \nabla f_{u'}(\mathbf{w}_u^{k,e,l}) \right\|^2 \right] \\
= & \frac{2E\eta^2}{K} \sum_{k=0}^{K-1} \frac{1}{\Omega^k} \sum_{e=0}^{E-1} \sum_{b=0}^{B-1} \alpha_b \sum_{u \in \mathcal{Q}_b^{k,e}} (\alpha_u)^2 \sum_{l=0}^{L_u^{k,e}-1} \mathbb{E} \left[\left\| \frac{1_{u,sc}^{k,e}}{P_{u,sc}} g_u(\mathbf{w}_u^{k,e,l}) \pm g_u(\mathbf{w}_u^{k,e,l}) - \nabla f_u(\mathbf{w}_u^{k,e,l}) \right\|^2 \right] - \\
& \frac{2E\eta^2}{K} \sum_{k=0}^{K-1} \frac{1}{\Omega^k} \sum_{e=0}^{E-1} \sum_{b=0}^B (\alpha_b)^2 \sum_{u \in \mathcal{Q}_b^{k,e}} (\alpha_u)^2 \sum_{l=0}^{L_u^{k,e}-1} \mathbb{E} \left[\left\| \frac{1_{u,sc}^{k,e}}{P_{u,sc}} g_u(\mathbf{w}_u^{k,e,l}) \pm g_u(\mathbf{w}_u^{k,e,l}) - \nabla f_u(\mathbf{w}_u^{k,e,l}) \right\|^2 \right] \\
\stackrel{(e)}{\leq} & \frac{4E\eta^2}{K} \sum_{k=0}^{K-1} \frac{1}{\Omega^k} \sum_{e=0}^{E-1} \sum_{b=0}^{B-1} \alpha_b \sum_{u \in \mathcal{Q}_b^{k,e}} (\alpha_u)^2 \sum_{l=0}^{L_u^{k,e}-1} \mathbb{E} \left[\left\| \left(\frac{1_{u,sc}^{k,e}}{P_{u,sc}} - 1 \right) g_u(\mathbf{w}_u^{k,e,l}) \right\|^2 \right] + \\
& \frac{4E\eta^2}{K} \sum_{k=0}^{K-1} \frac{1}{\Omega^k} \sum_{e=0}^{E-1} \sum_{b=0}^{B-1} \alpha_b \sum_{u \in \mathcal{Q}_b^{k,e}} (\alpha_u)^2 \sum_{l=0}^{L_u^{k,e}-1} \mathbb{E} \left[\left\| g_u(\mathbf{w}_u^{k,e,l}) - \nabla f_u(\mathbf{w}_u^{k,e,l}) \right\|^2 \right] - \\
& \frac{4E\eta^2}{K} \sum_{k=0}^{K-1} \frac{1}{\Omega^k} \sum_{e=0}^{E-1} \sum_{b=0}^B (\alpha_b)^2 \sum_{u \in \mathcal{Q}_b^{k,e}} (\alpha_u)^2 \sum_{l=0}^{L_u^{k,e}-1} \mathbb{E} \left[\left\| \left(\frac{1_{u,sc}^{k,e}}{P_{u,sc}} - 1 \right) g_u(\mathbf{w}_u^{k,e,l}) \right\|^2 \right] - \\
& \frac{4E\eta^2}{K} \sum_{k=0}^{K-1} \frac{1}{\Omega^k} \sum_{e=0}^{E-1} \sum_{b=0}^B (\alpha_b)^2 \sum_{u \in \mathcal{Q}_b^{k,e}} (\alpha_u)^2 \sum_{l=0}^{L_u^{k,e}-1} \mathbb{E} \left[\left\| g_u(\mathbf{w}_u^{k,e,l}) - \nabla f_u(\mathbf{w}_u^{k,e,l}) \right\|^2 \right] \\
\stackrel{(f)}{\leq} & \frac{4E\eta^2\sigma^2}{K} \sum_{k=0}^{K-1} \frac{1}{\Omega^k} \sum_{e=0}^{E-1} \sum_{b=0}^{B-1} \alpha_b \sum_{u \in \mathcal{Q}_b^{k,e}} (\alpha_u)^2 L_u^{k,e} + \frac{4E\eta^2}{K} \sum_{k=0}^{K-1} \frac{1}{\Omega^k} \sum_{e=0}^{E-1} \sum_{b=0}^{B-1} \alpha_b \sum_{u \in \mathcal{Q}_b^{k,e}} (\alpha_u)^2 \left[\frac{1}{P_{u,sc}^{k,e}} - 1 \right] \sum_{l=0}^{L_u^{k,e}-1} \mathbb{E} \left[\left\| g_u(\mathbf{w}_u^{k,e,l}) \right\|^2 \right] - \\
& \frac{4E\eta^2\sigma^2}{K} \sum_{k=0}^{K-1} \frac{1}{\Omega^k} \sum_{e=0}^{E-1} \sum_{b=0}^B (\alpha_b)^2 \sum_{u \in \mathcal{Q}_b^{k,e}} (\alpha_u)^2 L_u^{k,e} - \frac{4E\eta^2}{K} \sum_{k=0}^{K-1} \frac{1}{\Omega^k} \sum_{e=0}^{E-1} \sum_{b=0}^B (\alpha_b)^2 \sum_{u \in \mathcal{Q}_b^{k,e}} (\alpha_u)^2 \left[\frac{1}{P_{u,sc}^{k,e}} - 1 \right] \sum_{l=0}^{L_u^{k,e}-1} \mathbb{E} \left[\left\| g_u(\mathbf{w}_u^{k,e,l}) \right\|^2 \right]
\end{aligned}$$

$$\leq \frac{4E\eta^2\sigma^2}{K} \sum_{k=0}^{K-1} \frac{1}{\Omega^k} \sum_{e=0}^{E-1} \sum_{b=0}^{B-1} \alpha_b \sum_{u \in \mathcal{Q}_b^{k,e}} (\alpha_u)^2 L_u^{k,e} + \frac{4E\eta^2}{K} \sum_{k=0}^{K-1} \frac{1}{\Omega^k} \sum_{e=0}^{E-1} \sum_{b=0}^{B-1} \alpha_b \sum_{u \in \mathcal{Q}_b^{k,e}} (\alpha_u)^2 \left[\frac{1}{\mathbb{P}_{u,\text{sc}}} - 1 \right] \sum_{l=0}^{L_u^{k,e}-1} \mathbb{E} \left[\left\| g_u(\mathbf{w}_u^{k,e,l}) \right\|^2 \right], \quad (69)$$

where (a) stems from the fact that $\sum_{j=1}^J \alpha_j \|\mathbf{x}_j - \bar{\mathbf{x}}\|^2 = \sum_{j=1}^J \alpha_j \|\mathbf{x}_j\|^2 - \|\bar{\mathbf{x}}\|^2$, where $\bar{\mathbf{x}} = \sum_{j=1}^J \alpha_j \mathbf{x}_j$. Besides, (b) appears from the independent mini-batch gradients and $\mathbb{E}[g_u(\mathbf{w}_u^{k,e,l})] = \nabla f_u(\mathbf{w}_u^{k,e,l})$ assumptions, which make the expectation of the cross product terms 0. Besides, (c) is true since $(e-1) - e' \leq E$. Furthermore, we use the independent mini-batch gradients and $\mathbb{E}[g_u(\mathbf{w}_u^{k,e,l})] = \nabla f_u(\mathbf{w}_u^{k,e,l})$ assumptions in step (d). In (e), we use the fact that $\|\sum_{j=1}^J \mathbf{x}_j\|^2 \leq J \sum_{j=1}^J \|\mathbf{x}_j\|^2$. Moreover, (f) appears from bounded variance of the gradients. Finally, we drop the negative second term of (f) in the last inequality.

The second part of (68) is simplified as

$$\begin{aligned} & \frac{2\eta^2}{K} \sum_{k=0}^{K-1} \frac{1}{\Omega^k} \sum_{e=0}^{E-1} \sum_{b=0}^{B-1} \alpha_b \mathbb{E} \left[\left\| \sum_{e'=0}^{e-1} \left\{ \sum_{u \in \mathcal{Q}_b^{k,e'}} \alpha_u \sum_{l=0}^{L_u^{k,e'}-1} \nabla f_u(\mathbf{w}_u^{k,e',l}) - \sum_{b'=0}^B \alpha_{b'} \sum_{u' \in \mathcal{Q}_{b'}^{k,e'}} \alpha_{u'} \sum_{l=0}^{L_{u'}^{k,e'}-1} \nabla f_{u'}(\mathbf{w}_{u'}^{k,e',l}) \right\} \right\|^2 \right] \\ & \stackrel{(a)}{\leq} \frac{2E\eta^2}{K} \sum_{k=0}^{K-1} \frac{1}{\Omega^k} \sum_{e=0}^{E-1} \sum_{b=0}^{B-1} \alpha_b \sum_{e'=0}^{e-1} \mathbb{E} \left[\left\| \sum_{u \in \mathcal{Q}_b^{k,e'}} \alpha_u \sum_{l=0}^{L_u^{k,e'}-1} \nabla f_u(\mathbf{w}_u^{k,e',l}) - \sum_{b'=0}^B \alpha_{b'} \sum_{u' \in \mathcal{Q}_{b'}^{k,e'}} \alpha_{u'} \sum_{l=0}^{L_{u'}^{k,e'}-1} \nabla f_{u'}(\mathbf{w}_{u'}^{k,e',l}) \right\|^2 \right] \\ & \stackrel{(b)}{\leq} \frac{2\eta^2 E^2}{K} \sum_{k=0}^{K-1} \frac{1}{\Omega^k} \sum_{e=0}^{E-1} \sum_{b=0}^{B-1} \alpha_b \mathbb{E} \left[\left\| \sum_{u \in \mathcal{Q}_b^{k,e}} \alpha_u \sum_{l=0}^{L_u^{k,e}-1} \nabla f_u(\mathbf{w}_u^{k,e,l}) - \sum_{b'=0}^B \alpha_{b'} \sum_{u' \in \mathcal{Q}_{b'}^{k,e}} \alpha_{u'} \sum_{l=0}^{L_{u'}^{k,e}-1} \nabla f_{u'}(\mathbf{w}_{u'}^{k,e,l}) \right\|^2 \right] \\ & = \frac{2\eta^2 E^2}{K} \sum_{k=0}^{K-1} \frac{1}{\Omega^k} \sum_{e=0}^{E-1} \sum_{b=0}^{B-1} \alpha_b \mathbb{E} \left[\left\| \sum_{u \in \mathcal{Q}_b^{k,e}} \alpha_u \sum_{l=0}^{L_u^{k,e}-1} [\nabla f_u(\mathbf{w}_u^{k,e,l}) - \nabla f_u(\mathbf{w}_b^{k,e})] + \sum_{u \in \mathcal{Q}_b^{k,e}} \alpha_u \sum_{l=0}^{L_u^{k,e}-1} [\nabla f_u(\mathbf{w}_b^{k,e}) - \nabla f_u(\mathbf{w}^k)] + \right. \right. \\ & \quad \left. \sum_{u \in \mathcal{Q}_b^{k,e}} \alpha_u \sum_{l=0}^{L_u^{k,e}-1} \nabla f_u(\mathbf{w}^k) - \sum_{b'=0}^B \alpha_{b'} \sum_{u' \in \mathcal{Q}_{b'}^{k,e}} \alpha_{u'} \sum_{l=0}^{L_{u'}^{k,e}-1} \nabla f_{u'}(\mathbf{w}^k) + \sum_{b'=0}^B \alpha_{b'} \sum_{u' \in \mathcal{Q}_{b'}^{k,e}} \alpha_{u'} \sum_{l=0}^{L_{u'}^{k,e}-1} [\nabla f_{u'}(\mathbf{w}^k) - \nabla f_{u'}(\mathbf{w}_{b'}^{k,e})] + \right. \\ & \quad \left. \sum_{b'=0}^B \alpha_{b'} \sum_{u' \in \mathcal{Q}_{b'}^{k,e}} \alpha_{u'} \sum_{l=0}^{L_{u'}^{k,e}-1} [\nabla f_{u'}(\mathbf{w}_{b'}^{k,e}) - \nabla f_{u'}(\mathbf{w}_{u'}^{k,e,l})] \right\|^2 \right] \\ & \stackrel{(c)}{\leq} \frac{10\eta^2 E^2}{K} \sum_{k=0}^{K-1} \frac{1}{\Omega^k} \sum_{e=0}^{E-1} \sum_{b=0}^{B-1} \alpha_b \mathbb{E} \left[\left\| \sum_{u \in \mathcal{Q}_b^{k,e}} \alpha_u \sum_{l=0}^{L_u^{k,e}-1} [\nabla f_u(\mathbf{w}_u^{k,e,l}) - \nabla f_u(\mathbf{w}_b^{k,e})] \right\|^2 \right] + \\ & \quad \frac{10\eta^2 E^2}{K} \sum_{k=0}^{K-1} \frac{1}{\Omega^k} \sum_{e=0}^{E-1} \sum_{b=0}^{B-1} \alpha_b \mathbb{E} \left[\left\| \sum_{u \in \mathcal{Q}_b^{k,e}} \alpha_u \sum_{l=0}^{L_u^{k,e}-1} [\nabla f_u(\mathbf{w}_b^{k,e}) - \nabla f_u(\mathbf{w}^k)] \right\|^2 \right] + \\ & \quad \frac{10\eta^2 E^2}{K} \sum_{k=0}^{K-1} \frac{1}{\Omega^k} \sum_{e=0}^{E-1} \sum_{b=0}^{B-1} \alpha_b \mathbb{E} \left[\left\| \sum_{u \in \mathcal{Q}_b^{k,e}} \alpha_u \sum_{l=0}^{L_u^{k,e}-1} \nabla f_u(\mathbf{w}^k) - \sum_{b'=0}^B \alpha_{b'} \sum_{u' \in \mathcal{Q}_{b'}^{k,e}} \alpha_{u'} \sum_{l=0}^{L_{u'}^{k,e}-1} \nabla f_{u'}(\mathbf{w}^k) \right\|^2 \right] + \\ & \quad \frac{10\eta^2 E^2}{K} \sum_{k=0}^{K-1} \frac{1}{\Omega^k} \sum_{e=0}^{E-1} \sum_{b=0}^{B-1} \alpha_b \mathbb{E} \left[\left\| \sum_{b'=0}^B \alpha_{b'} \sum_{u' \in \mathcal{Q}_{b'}^{k,e}} \alpha_{u'} \sum_{l=0}^{L_{u'}^{k,e}-1} [\nabla f_{u'}(\mathbf{w}^k) - \nabla f_{u'}(\mathbf{w}_{b'}^{k,e})] \right\|^2 \right] + \\ & \quad \frac{10\eta^2 E^2}{K} \sum_{k=0}^{K-1} \frac{1}{\Omega^k} \sum_{e=0}^{E-1} \sum_{b=0}^{B-1} \alpha_b \mathbb{E} \left[\left\| \sum_{b'=0}^B \alpha_{b'} \sum_{u' \in \mathcal{Q}_{b'}^{k,e}} \alpha_{u'} \sum_{l=0}^{L_{u'}^{k,e}-1} [\nabla f_{u'}(\mathbf{w}_{b'}^{k,e}) - \nabla f_{u'}(\mathbf{w}_{u'}^{k,e,l})] \right\|^2 \right] \\ & \stackrel{(d)}{\leq} \frac{10\eta^2 E^2}{K} \sum_{k=0}^{K-1} \frac{1}{\Omega^k} \sum_{e=0}^{E-1} \sum_{b=0}^{B-1} \alpha_b \sum_{u \in \mathcal{Q}_b^{k,e}} \alpha_u \mathbb{E} \left[\left\| \sum_{l=0}^{L_u^{k,e}-1} [\nabla f_u(\mathbf{w}_u^{k,e,l}) - \nabla f_u(\mathbf{w}_b^{k,e})] \right\|^2 \right] + \\ & \quad \frac{10\eta^2 E^2}{K} \sum_{k=0}^{K-1} \frac{1}{\Omega^k} \sum_{e=0}^{E-1} \sum_{b=0}^{B-1} \alpha_b \sum_{u \in \mathcal{Q}_b^{k,e}} \alpha_u \mathbb{E} \left[\left\| \sum_{l=0}^{L_u^{k,e}-1} [\nabla f_u(\mathbf{w}_b^{k,e}) - \nabla f_u(\mathbf{w}^k)] \right\|^2 \right] + \end{aligned}$$

$$\begin{aligned}
& \frac{10\eta^2 E^2}{K} \sum_{k=0}^{K-1} \frac{1}{\Omega^k} \sum_{e=0}^{E-1} \sum_{b=0}^{B-1} \alpha_b \mathbb{E} \left[\left\| \sum_{u \in \mathcal{U}_b^{k,e}} \alpha_u \nabla \tilde{f}_u(\mathbf{w}^k) - \sum_{b'=0}^B \alpha_{b'} \sum_{u' \in \mathcal{U}_{b'}^{k,e}} \alpha_{u'} \nabla \tilde{f}_{u'}(\mathbf{w}^k) \right\|^2 \right] + \\
& \frac{10\eta^2 E^2}{K} \sum_{k=0}^{K-1} \frac{1}{\Omega^k} \sum_{e=0}^{E-1} \sum_{b=0}^{B-1} \alpha_b \sum_{u \in \mathcal{U}_b^{k,e}} \alpha_u \mathbb{E} \left[\left\| \sum_{l=0}^{L_u^{k,e}-1} [\nabla f_u(\mathbf{w}^k) - \nabla f_u(\mathbf{w}_b^{k,e})] \right\|^2 \right] + \\
& \frac{10\eta^2 E^2}{K} \sum_{k=0}^{K-1} \frac{1}{\Omega^k} \sum_{e=0}^{E-1} \sum_{b=0}^{B-1} \alpha_b \sum_{u \in \mathcal{U}_b^{k,e}} \alpha_u \mathbb{E} \left[\left\| \sum_{l=0}^{L_u^{k,e}-1} [\nabla f_u(\mathbf{w}_b^{k,e}) - \nabla f_u(\mathbf{w}_u^{k,e,l})] \right\|^2 \right] \\
\stackrel{(e)}{\leq} & \frac{10L\eta^2 E^2}{K} \sum_{k=0}^{K-1} \frac{1}{\Omega^k} \sum_{e=0}^{E-1} \sum_{b=0}^{B-1} \alpha_b \sum_{u \in \mathcal{U}_b^{k,e}} \alpha_u \sum_{l=0}^{L_u^{k,e}-1} \mathbb{E} \left[\left\| \nabla f_u(\mathbf{w}_u^{k,e,l}) - \nabla f_u(\mathbf{w}_b^{k,e}) \right\|^2 \right] + \\
& \frac{10L\eta^2 E^2}{K} \sum_{k=0}^{K-1} \frac{1}{\Omega^k} \sum_{e=0}^{E-1} \sum_{b=0}^{B-1} \alpha_b \sum_{u \in \mathcal{U}_b^{k,e}} \alpha_u \sum_{l=0}^{L_u^{k,e}-1} \mathbb{E} \left[\left\| \nabla f_u(\mathbf{w}_b^{k,e}) - \nabla f_u(\mathbf{w}^k) \right\|^2 \right] + \frac{10\eta^2 E^2}{K} \sum_{k=0}^{K-1} \frac{1}{\Omega^k} \sum_{e=0}^{E-1} \sum_{b=0}^{B-1} \alpha_b \cdot \varepsilon_1^2 + \\
& \frac{10L\eta^2 E^2}{K} \sum_{k=0}^{K-1} \frac{1}{\Omega^k} \sum_{e=0}^{E-1} \sum_{b=0}^{B-1} \alpha_b \sum_{u \in \mathcal{U}_b^{k,e}} \alpha_u \sum_{l=0}^{L_u^{k,e}-1} \mathbb{E} \left[\left\| \nabla f_u(\mathbf{w}^k) - \nabla f_u(\mathbf{w}_b^{k,e}) \right\|^2 \right] + \\
& \frac{10L\eta^2 E^2}{K} \sum_{k=0}^{K-1} \frac{1}{\Omega^k} \sum_{e=0}^{E-1} \sum_{b=0}^{B-1} \alpha_b \sum_{u \in \mathcal{U}_b^{k,e}} \alpha_u \sum_{l=0}^{L_u^{k,e}-1} \mathbb{E} \left[\left\| \nabla f_u(\mathbf{w}_b^{k,e}) - \nabla f_u(\mathbf{w}_u^{k,e,l}) \right\|^2 \right] \\
\stackrel{(f)}{\leq} & \frac{10\varepsilon_1^2 \eta^2 E^3}{K} \sum_{k=0}^{K-1} \frac{1}{\Omega^k} + \frac{20L\beta^2 \eta^2 E^2}{K} \sum_{k=0}^{K-1} \frac{1}{\Omega^k} \sum_{e=0}^{E-1} \sum_{b=0}^{B-1} \alpha_b \sum_{u \in \mathcal{U}_b^{k,e}} \alpha_u \sum_{l=0}^{L_u^{k,e}-1} \mathbb{E} \left[\left\| \mathbf{w}_b^{k,e} - \mathbf{w}_u^{k,e,l} \right\|^2 \right] + \\
& \frac{20\beta^2 \eta^2 E^2 L^2}{K} \sum_{k=0}^{K-1} \frac{1}{\Omega^k} \sum_{e=0}^{E-1} \sum_{b=0}^{B-1} \alpha_b \mathbb{E} \left[\left\| \mathbf{w}^k - \mathbf{w}_b^{k,e} \right\|^2 \right] \\
\stackrel{(g)}{\leq} & \frac{10\varepsilon_1^2 \eta^2 E^3}{K} \sum_{k=0}^{K-1} \frac{1}{\Omega^k} + \frac{20\beta^2 \eta^2 E^2 L^2}{K} \sum_{k=0}^{K-1} \frac{1}{\Omega^k} \sum_{e=0}^{E-1} \sum_{b=0}^{B-1} \alpha_b \mathbb{E} \left[\left\| \mathbf{w}^k - \mathbf{w}_b^{k,e} \right\|^2 \right] + 20L\beta^2 \eta^2 E^2 \times \left[\frac{3EL^2 \eta^2 \sigma^2}{K} \sum_{k=0}^{K-1} \frac{1}{\Omega^k} + \right. \\
& \left. \frac{9E\varepsilon_0^2 \eta^2 L^3}{K} \sum_{k=0}^{K-1} \frac{1}{\Omega^k} + \frac{3L^2 \eta^2}{K} \sum_{k=0}^{K-1} \frac{1}{\Omega^k} \sum_{e=0}^{E-1} \sum_{b=0}^{B-1} \alpha_b \sum_{u \in \mathcal{U}_b^{k,e}} \alpha_u \left[\frac{1}{\text{Pu,sc}} - 1 \right] \sum_{l=0}^{L_u^{k,e}-1} \mathbb{E} \left[\left\| g_u(\mathbf{w}_u^{k,e,l}) \right\|^2 \right] \right] \\
= & \frac{180\beta^2 \varepsilon_0^2 E^3 L^4 \eta^4}{K} \sum_{k=0}^{K-1} \frac{1}{\Omega^k} + \frac{10\varepsilon_1^2 \eta^2 E^3}{K} \sum_{k=0}^{K-1} \frac{1}{\Omega^k} + \frac{60\beta^2 \sigma^2 E^3 L^3 \eta^4}{K} \sum_{k=0}^{K-1} \frac{1}{\Omega^k} + \\
& \frac{60\beta^2 E^2 L^3 \eta^4}{K} \sum_{k=0}^{K-1} \frac{1}{\Omega^k} \sum_{e=0}^{E-1} \sum_{b=0}^{B-1} \alpha_b \sum_{u \in \mathcal{U}_b^{k,e}} \alpha_u \left[\frac{1}{\text{Pu,sc}} - 1 \right] \sum_{l=0}^{L_u^{k,e}-1} \mathbb{E} \left[\left\| g_u(\mathbf{w}_u^{k,e,l}) \right\|^2 \right] + \\
& \frac{20\beta^2 \eta^2 E^2 L^2}{K} \sum_{k=0}^{K-1} \frac{1}{\Omega^k} \sum_{e=0}^{E-1} \sum_{b=0}^{B-1} \alpha_b \mathbb{E} \left[\left\| \mathbf{w}^k - \mathbf{w}_b^{k,e} \right\|^2 \right], \tag{70}
\end{aligned}$$

where (a) and c stem from the fact that $\|\sum_{j=1}^J \mathbf{x}_j\|^2 \leq J \sum_{j=1}^J \|\mathbf{x}_j\|^2$. Besides, we used $(e-1) - e' \leq E$ in step (a) and step (b). In (d), we use the fact that $\|\sum_{j=1}^J \alpha_j \mathbf{x}_j\|^2 \leq \sum_{j=1}^J \alpha_j \|\mathbf{x}_j\|^2$ and the definition of $\nabla \tilde{f}_u(\mathbf{w}^k) := \sum_{l=0}^{L_u^{k,e}-1} \nabla f_u(\mathbf{w}^k)$. Furthermore, $\|\sum_{j=1}^J \mathbf{x}_j\|^2 \leq J \sum_{j=1}^J \|\mathbf{x}_j\|^2$ and the bounded divergence assumption in (49) yield (e). Moreover, the inequality in (f) stems from the β -smoothness property. Finally, we use Lemma 1 in step (g).

Now, plugging (69) and (70) into (68), we get

$$\begin{aligned}
& (1 - 20\beta^2 \eta^2 E^2 L^2) \frac{1}{K} \sum_{k=0}^{K-1} \frac{1}{\Omega^k} \sum_{e=0}^{E-1} \sum_{b=0}^{B-1} \alpha_b \mathbb{E} \left[\left\| \mathbf{w}^k - \mathbf{w}_b^{k,e} \right\|^2 \right] \\
\leq & \frac{4E\eta^2 \sigma^2}{K} \sum_{k=0}^{K-1} \frac{1}{\Omega^k} \sum_{e=0}^{E-1} \sum_{b=0}^{B-1} \alpha_b \sum_{u \in \mathcal{U}_b^{k,e}} (\alpha_u)^2 L_u^{k,e} + \frac{60\beta^2 \sigma^2 E^3 L^3 \eta^4}{K} \sum_{k=0}^{K-1} \frac{1}{\Omega^k} + \frac{180\beta^2 \varepsilon_0^2 E^3 L^4 \eta^4}{K} \sum_{k=0}^{K-1} \frac{1}{\Omega^k} + \frac{10\varepsilon_1^2 \eta^2 E^3}{K} \sum_{k=0}^{K-1} \frac{1}{\Omega^k} +
\end{aligned}$$

$$\frac{4E\eta^2}{K} \sum_{k=0}^{K-1} \frac{1}{\Omega^k} \sum_{e=0}^{E-1} \sum_{b=0}^{B-1} \alpha_b \sum_{u \in \mathcal{Q}_b^{k,e}} \alpha_u (\alpha_u + 15E\beta^2\eta^2L^3) \left[\frac{1}{\mathbf{p}_{u,sc}^{k,e}} - 1 \right] \sum_{l=0}^{L_u^{k,e}-1} \mathbb{E} \left[\left\| g_u(\mathbf{w}_u^{k,e,l}) \right\|^2 \right]. \quad (71)$$

It is worth noting that when $\eta < \frac{1}{2\sqrt{5}\beta EL}$, we have $0 < (1 - 20\beta^2\eta^2E^2L^2) < 1$. In order to satisfy the previous assumptions on the learning rate, we let $\eta < \min \left\{ \frac{1}{2\sqrt{5}\beta L}, \frac{1}{\beta EL} \right\}$. As such, we re-write (71) as follows:

$$\begin{aligned} & \frac{1}{K} \sum_{k=0}^{K-1} \frac{1}{\Omega^k} \sum_{e=0}^{E-1} \sum_{b=0}^{B-1} \alpha_b \mathbb{E} \left[\left\| \mathbf{w}^k - \mathbf{w}_b^{k,e} \right\|^2 \right] \\ & \leq \frac{4E\eta^2\sigma^2}{K} \sum_{k=0}^{K-1} \frac{1}{\Omega^k} \sum_{e=0}^{E-1} \sum_{b=0}^{B-1} \alpha_b \sum_{u \in \mathcal{Q}_b^{k,e}} (\alpha_u)^2 L_u^{k,e} + \frac{60\beta^2\sigma^2E^3L^3\eta^4}{K} \sum_{k=0}^{K-1} \frac{1}{\Omega^k} + \frac{180\beta^2\epsilon_0^2E^3L^4\eta^4}{K} \sum_{k=0}^{K-1} \frac{1}{\Omega^k} + \frac{10\epsilon_1^2\eta^2E^3}{K} \sum_{k=0}^{K-1} \frac{1}{\Omega^k} + \\ & \quad \frac{4E\eta^2}{K} \sum_{k=0}^{K-1} \frac{1}{\Omega^k} \sum_{e=0}^{E-1} \sum_{b=0}^{B-1} \alpha_b \sum_{u \in \mathcal{Q}_b^{k,e}} \alpha_u (\alpha_u + 15E\beta^2\eta^2L^3) \left[\frac{1}{\mathbf{p}_{u,sc}^{k,e}} - 1 \right] \sum_{l=0}^{L_u^{k,e}-1} \mathbb{E} \left[\left\| g_u(\mathbf{w}_u^{k,e,l}) \right\|^2 \right]. \end{aligned} \quad (72)$$

This concludes the proof of Lemma 2.